

**The Estimation of *Eucalyptus* Plantation Forest Structural
Attributes using Medium and High Spatial Resolution Satellite
Imagery**

by

Michael T. Gebreslasie

Submitted in fulfilment of the academic requirements for the degree of

Doctor of Philosophy in Applied Environmental Science

Faculty of Science and Agriculture, University of KwaZulu-Natal Pietermaritzburg,
South Africa

December 2008

Preface

The work undertaken in this study was carried out at the School of Environmental Sciences, Faculty of Science and Agriculture, University of KwaZulu-Natal, Pietermaritzburg, in association with the Forestry and Forest Products Research Centre, a joint venture between the CSIR Natural Resources and the Environment Operating Unit and the University of KwaZulu-Natal with financial support from MONDI-SA Company. This research was completed under the supervision of the following academic staff:

Professor F.B. Ahmed, Head of School of Environmental Sciences, University of KwaZulu-Natal, Durban.

Dr. J.A.N. van Aardt, Associate Professor, Rochester Institute of Technology, Centre for Imaging Science; Laboratory for Imaging Algorithms and Systems, Rochester, NY, USA

The duration of this study was from August 2005 to December 2008.

The contents of this work have not been submitted in any form to another University and, except where the work of others is acknowledged in the text, the results are the author's own investigation.

Michael T. Gebreslasie
December 2008

We certify that the above statement is correct:

Professor. F.B. Ahmed

Dr. J.A.N.

Declaration 1- Plagiarism

I, Michael T. Gebreslasie declare that:

1. The research reported in this thesis, except where otherwise indicated, is my original research.
2. This thesis has not been submitted for any degree or examination at any other university.
3. This thesis does not contain other persons' data, pictures, graphs or other information, unless specifically acknowledged as being sourced from other persons.
4. This thesis does not contain other persons' writing, unless specifically acknowledged as being sourced from other researchers. Where other written sources have been quoted, then:
 - a. Their words have been re-written but the general information attributed to them has been referenced
 - b. Where their exact words have been used, then their writing has been placed in italics and inside quotation marks, and referenced.
5. This thesis does not contain text, graphics or tables copied and pasted from the Internet, unless specifically acknowledged, and the source being detailed in the thesis and in the References sections.

Signed.....

Declaration 2 - Publications

1. Roberts W., Gebreslasie, M, Gebrmaiam, S., Ahmed, F. B., van Aardt, J. (2007) Forest Structural Assessment using Remote Sensing Technologies: An Overview of the current state of the art. *Southern Hemisphere Forestry Journal* 2007, 69(3): 183–203.
2. Gebreslasie, M., Ahmed, F. B., and van Aardt, J. (2008) Estimating plot-level forest structural attributes using high spectral resolution ASTER satellite data in even-aged *Eucalyptus* plantations, in KwaZulu-Natal, South Africa. *Southern Forests: A Journal of Forest Science* 71(3): 227-236
3. Gebreslasie, M., Ahmed, F. B., and van Aardt, J. (2008) Image-based reflectance conversion of ASTER and IKONOS imagery as precursor to structural assessment of plantation forests in KwaZulu-Natal, South Africa. *Southern Forests: A journal of Forest Science* (Submitted)
4. Gebreslasie, M., Ahmed, F. B., and van Aardt, J. (2008) Extracting structural attributes from IKONOS imagery for *Eucalyptus* plantation forests in KwaZulu-Natal, South Africa, using image texture analysis and artificial neural networks *International Journal of Remote Sensing* (Submitted)
5. Gebreslasie, M., Ahmed, F. B., and van Aardt, J. (2008) Individual tree detection based on variable and fixed window size local maxima filtering applied to IKONOS imagery for even-aged *Eucalyptus* plantation forests *International Journal of Remote Sensing* (Submitted)

The first publication is a review paper; it covers Optical Remote Sensing systems, Active Remote Sensing systems and Fusion of the two Remote Sensing systems for the assessment of forest structural attribute was co-authored by (PhD students) Mr Gebreslasie, Mr Gebremariam and Mr Roberts, respectively. The contribution of Professor Ahmed was as a supervisor to provide lawful commands and guidance as well as proofreading of the article. The contribution of Dr van Aardt, who joined the team as a co-supervisor at a late stage was only proofreading at this part.

The conceptual development and analysis of data for the last four publications as well as the write-up was completely accomplished by the author of this thesis. The contribution of my supervisor Professor Ahmed and my co-supervisor Dr van Aardt was providing hints and comments as well as proofreading of the manuscripts.

Signed.....

Acknowledgements

First and foremost I would like to express my warmest thanks and gratitude to Professor Fethi Ahmed for his professional and personal support throughout my postgraduate studies. I am also deeply thankful to my co-supervisor Dr Jan van Aardt, for his consistent encouragement and inspirations during my research.

Particular thanks are due to my colleagues, Solomon Gebremariam, Wesley Roberts, Thamsanqa Mzinyane, Wesley Naidoo, and Sasha Naidoo; their support during the field data collection and all the discussions and valuable hints are gratefully acknowledged.

My appreciation is also extended to the Remote Sensing Co-operative steering committee members: Ms. Felicity (Flic) Blakeway and Dr Tammy Bush (CSIR), Dr Mark Norris-Rogers, Johan Wiese and Bill Esler (MONDI-SA), and Professor Fethi Ahmed (University of KwaZulu Natal). I appreciate their guidance, support, and constructive challenges raised during my studies. They all contributed to my research being the most enriching professional experience I have had this far.

This study was financed by the Council for Scientific and Industrial Research, MONDI-SA, and University of KwaZulu-Natal. I also respectfully acknowledge Dr Tammy Bush for her support in terms of the administrative issues related to my Ph.D. studies.

I have been fortunate to have outstanding friends in Riyad Ismail and Geraldine Coertze I relied on them for input, helping with solving statistical mysteries, and proofreading.

Finally, my deepest appreciation goes to my sister Luwam for her support. Most importantly, I cannot thank my parents, Teweldemedhin Gebreslasie and Hiriti Haile, enough for everything they meant to me throughout my life.

Abstract

Sustaining the socioeconomic and ecological benefits of South African plantation forests is challenging. A more systematic and rapid forest inventory system is required by forest managers. This study investigates the utility of medium (ASTER 15 m) and high (IKONOS 1-4 m) spatial resolution satellite imageries in an effort to improve the remote capture of structural attributes of even-aged *Eucalyptus* plantations grown in the warm temperate climatic zone of southern KwaZulu-Natal, South Africa.

The conversion of image data to surface reflectance is a pre-requisite for the establishment of relationships between satellite remote sensing data and ground collected forest structural data. In this study image-based atmospheric correction methods applied on ASTER and IKONOS imagery were evaluated for the purpose of retrieving surface reflectance of plantation forests. Multiple linear regression and canonical correlation analyses were used to develop models for the prediction of plantation forest structural attributes from ASTER data. Artificial neural networks and multiple linear regression were also used to develop models for the assessment of plantation forests structural attributes from IKONOS data. The plantation forest structural attributes considered in this study included: stems per hectare, diameter at breast height, mean tree height, basal area, and volume. In addition, location based stems per hectare were determined using high spatial resolution panchromatic IKONOS data where variable and fixed window sizes of local maxima were employed.

The image-based dark object subtraction (DOS) model was better suited for atmospheric correction of ASTER and IKONOS imagery of the study area. The medium spatial resolution data were not amenable to estimating even-aged *Eucalyptus* forest structural attributes. It is still encouraging that up to 64 % of variation could be explained by using medium spatial resolution data. The results from high spatial resolution data showed a promising result where the ARMSE% values obtained for stems per hectare, diameter at breast height, tree height, basal area and volume are 7.9, 5.1, 5.8, 8.7 and 8.7, respectively. Results such as these bode well for the application of high spatial resolution imagery to forest structural assessment. The results from the location based estimation of

stems per hectare illustrated that a variable window size approach developed in this study is highly accurate. The overall accuracy using a variable window size was 85% (RMSE of 189 trees per hectare).

The overall findings presented in this study are encouraging and show that high spatial resolution imagery was successful in predicting even-aged *Eucalyptus* forest structural attributes in the warm temperate climates of South Africa, with acceptable accuracy.

Table of Contents

Page

Preface.....	i
Declaration 1- Plagiarism	ii
Declaration 2 - Publications.....	iii
Acknowledgements.....	v
Abstract.....	vi
Table of Contents.....	viii
List of Figures.....	x
List of Tables	xii
Abbreviations.....	xiii
CHAPTER 1.....	1
GENERAL INTRODUCTION.....	1
1.1 Introduction.....	1
1.2 Objectives of the study.....	5
1.3 Outline of the thesis	5
1.4 References.....	6
CHAPTER 2.....	12
LITERATURE REVIEW	12
2.1 Introduction.....	13
2.2 Properties of Optical Remote Sensing.....	13
2.3 Forest attributes extraction approaches using optical remote sensing.....	16
2.3.1 Medium spatial resolution and forest structural attributes.....	16
2.3.2 High spatial resolution and forest structural attributes	18
2.4 References.....	21
CHAPTER 3.....	30
STUDY AREA.....	30
3.1 Introduction.....	30
3.2 Climate.....	30
3.3 Geology and soils.....	32
3.4 Topography.....	33
3.5 Land Use	33
3.6 References.....	33
CHAPTER 4.....	34
Image-based reflectance conversion of ASTER and IKONOS imagery as precursor to structural assessment of plantation forests in KwaZulu-Natal, South Africa.....	34
Abstract.....	35
4.1 Introduction.....	35
4.2 Materials and Methods.....	38
4.2.1 Study Site.....	38
4.2.2 Remote sensing data	39
4.2.3 Atmospheric Correction Methods.....	39
4.2.3.1 Apparent reflectance model	40
4.2.3.2 Dark object subtraction model.....	41

4.2.3.3 Cosine of atmospheric transmittance model	42
4.3 Accuracy Assessment of Atmospheric Corrections.....	43
4.4 Results and Discussion	44
4.4.1 Visual Assessment	44
4.4.2 Classification.....	47
4.4.3 Conclusions.....	48
4.4.4 Acknowledgements.....	49
4.4.5 References.....	49
CHAPTER 5	52
Estimating plot-level forest structural attributes using high spectral resolution ASTER satellite data in even-aged <i>Eucalyptus</i> plantation forests, in KwaZulu-Natal, South Africa.....	52
Abstract.....	53
5.1 Introduction.....	53
5.2 Materials and Methods.....	56
5.2.1 Study Area	56
5.2.2 Field measurements	57
5.2.3 Remote sensing data and processing.....	58
5.2.4 Spectral data extraction.....	60
5.2.5 Statistical analysis.....	61
5.2.6 Model evaluation	62
5.3 Results and Discussion	63
5.3.1 Canonical correlation analysis	65
5.3.2 Models for young plantation stands.....	66
5.3.3 Models for mature plantation stands.....	66
5.4 Conclusions.....	68
5.5 Acknowledgements.....	69
5.7 References.....	70
CHAPTER 6	75
Extracting structural attributes from high spatial resolution IKONOS imagery using image texture analysis and artificial neural networks in even- aged <i>Eucalyptus</i> plantation forests in KwaZulu-Natal, South Africa,	75
6.1 Introduction.....	76
6.2 Materials	80
6.2.1 Study site.....	80
6.2.1 Field data.....	81
6.2.2 Remote sensing data	82
6.3 Methods.....	83
6.3.1 Texture feature extraction	83
6.3.2 Statistical analyses	85
6.3.3 Multiple linear regressions.....	85
6.3.4 Artificial neural network.....	86
6.3.5 Performance assessment	88
6.4 Results.....	89
6.4.1 General.....	89
6.4.2 Multiple linear regression models.....	91

6.4.3 Artificial neural network models	96
6.4.4 Comparison of the MLR and ANN.....	102
6.5 Discussions	103
6.5.1 Forest attribute estimation from multispectral IKONOS imagery.....	103
6.5.2 Forest attribute estimation from panchromatic IKONOS imagery.....	104
6.5.3 Comparison between multispectral and panchromatic IKONOS imagery	105
6.5.4 Comparison between a multiple linear regression and artificial neural network	105
6.6. Conclusions.....	106
6.7 Acknowledgements.....	107
6.8 References.....	107
CHAPTER 7	113
Individual tree detection based on variable and fixed window size local maxima filtering applied to IKONOS imagery for even-aged <i>Eucalyptus</i> plantation forests in KwaZulu-Natal, South Africa	113
7.1 Introduction.....	114
7.2 Materials and Methods.....	117
7.2.1 Study area.....	117
7.2.2 Field data.....	118
7.2.3 Remote sensing data	119
7.2.4 Tree detection procedures.....	120
7.2.4.1 Gaussian image smoothing.....	121
7.2.4.2 Threshold definition.....	122
7.2.4.3 Variable Window size.....	122
7.2.6 Accuracy assessment of tree detection	124
7.3 Results and Discussion	125
7.4 Conclusions.....	129
7.5 Acknowledgements.....	130
7.6 References.....	131
CHAPTER 8	135
Conclusions and Recommendations.....	135

Appendices

Appendix 2.1: Examples of medium resolution studies using passive optical remote sensing.....	137
Appendix 2.2: Examples of high resolution studies using passive optical remote sensing	138
Appendix 4.1 ASTER data after atmospheric correction using AR, DOS, and COST ..	139
Appendix 4.2 IKONOS data after atmospheric correction using AR, DOS, and COST	140
Appendix 5.1 Correlation coefficients between plantation attributes and ASTER spectral information.....	141
Appendix 5.2 Correlation coefficients between plantation attributes and ASTER spectral information for young and mature plantation stands	140
Appendix 6.1 Description of the selected statistical texture features	142

List of Figures

Page

Chapter 2	
Figure 2.1 Spectral Reflectance Curve	14
Chapter 3	
Figure 3.1 Map showing the location of the study area	31
Figure 3.2 Climatology of the Richmond area and surrounds. Schulze <i>et al.</i> 1997	32
Chapter 4	
Figure 4.1 Map showing the location of the study sites	38
Chapter 5	
Figure 5.2 Scatter-plot of the ASTER red band and NIR band reflectance and estimated soil line.....	61
Figure 5.3 ASTER VNIR spectral response curves observed between ages 4-9 years	64
Chapter 6	
Figure 6.1 Map showing the location of the study sites	81
Figure 6.2 A schematic representation of the ANN.....	87
Figure 6.3 Illustration of the IKONOS bands effect for the estimation of forest structural attributes.....	89
Figure 6.4 Illustration of the window size effect for the estimation of forest structural attributes.....	90
Figure 6.5 Illustration of the statistical texture order and pixel displacement parameter effect on the estimation of forest structural attributes	91
Figure 6.7 Comparison of models developed from multispectral and panchromatic IKONOS imagery	96
Figure 6.8 Selection of optimal number of nodes in the hidden layer.....	97
Figure 6.9 Comparison of models developed using statistical texture features computed from multispectral and panchromatic IKONOS imagery	102
Figure 6.10 Comparison of models developed using multiple linear regression and artificial neural network statistical methods for the estimation of forest structural attributes.....	103
Chapter 7	
Figure 7.2 Diagram of the processing and analysis flow used in this study.....	121
Figure 7.3 Illustration of a theoretical semivariogram diagram (Goovaert 1997).....	123
Figure 7.4 Estimated SPHA, as a function of forest stands age, at different numbers of classes for natural break classification.....	125
Figure 7.5 Estimated SPHA, as a function of forest stands age, using VWS and FWS window size inputs to local maxima filtering.....	128

List of Tables	Page
 Chapter 4	
Table 4.1 ASTER and IKONOS band dependent parameters	40
Table 4.2 Julian day for IKONOS and ASTER	41
Table 4.3 Comparative data of supervised image classification accuracies for all three reflectance conversion approaches	48
 Chapter 5	
Table 5.1 Descriptive statistics of tree-level plantation structural attributes.....	58
Table 5.2 Coefficients used for volume estimation	58
Table 5.3 Characteristics of the ASTER VNIR and SWIR subsystems	59
Table 5.4 Spectral vegetation indices examined in this study	60
Table 5.5 Regression models, coefficients of determination (R^2), and RSME values for young plantation stands (n = 44).....	66
Table 5.6 Regression models, coefficients of determination, RMSE and RMSE% for mature plantation attributes (n = 40).....	67
 Chapter 6	
Table 6.1 Coefficients used for volume estimation	82
Table 6.2 IKONOS image characteristics.....	83
Table 6.4 Best regression model for each forest structural variable, based on multi-spectral IKONOS imagery and GLCM $\delta=1$ (n=37)	92
Table 6.5 Best regression model for each forest structural variable, based on panchromatic IKONOS imagery and GLCM $\delta=1$ (n=37)	93
Table 6.6 The ANN-MLP profile for prediction of the various structural parameters using multi-spectral and panchromatic imagery.....	97
Table 6.7 Connection weights and thresholds of ANN-MLP models for forest structural attributes using multi-spectral IKONOS imagery.....	98
Table 6.8 Connection weights and thresholds of ANN-MLP models for forest structural attributes using panchromatic IKONOS imagery	99
Table 6.9 ANN model performance for forest structural attribute estimation using multi-spectral and panchromatic IKONOS imagery	101
 Chapter 7	
Table 7.1 Descriptive statistics of tree-level plantation structural attributes.....	119
Table 7.2 IKONOS image characteristics.....	119
Table 7.3 Results of SPHA estimation using VWS and FWS as inputs to local maxima filtering at different plantation stand ages	126
Table 7.4 Overall accuracies for SPHA estimation using local maxima filtering based on the VWS and FWS approaches to window size selection	129

Abbreviations

%	Percentage
°	Degree
°C	Degree Centigrade
µm	Micrometer
Adjusted R ²	Coefficient of determination
ANN	Artificial Neural Network
ARM	Apparent Reflectance Model
ARMSE%	Absolute Root Mean Square Error (percentile).
ASTER	Advanced Space-borne Thermal Emission and Reflection Radiometer
BA	Basal Area
cm	Centimeter
CCA	Canonical Correlation Analysis
COST	Cosine of Atmospheric Transmittance
CSIR	Council for Scientific and Industrial Research
DBH	Diameter at Breast Height
DN	Digital Number
DOS	Dark Object Subtraction
DEM	Digital Elevation Model
DTM	Digital Terrain Model
DVI	Difference Vegetation Index
DWAF	Department of Water Affairs and Forestry
ETM+	Enhanced Thematic Mapper
EMR	Electro Magnetic Radiation
ERDAS	Earth Resources Data Analysis System
ESRI	Environmental Systems Research Institute
FAO	Food and Agriculture Organisation
FFP	Forestry and Forests Product
GCP	Ground Control Points

GDP	Gross Domestic Product
GIS	Geographic Information Systems
GLCM	Grey Level Co-occurrence Matrix
GLOM	Grey Level Occurrence Matrix
GMT	Greenwich Mean Time
GPS	Global Positioning Systems
ha	Hectare
LAI	Leaf Area Index
LiDAR	Light Detection and Ranging
m	Meter
m ²	Square metre
m ³	Cubic metre
MIR	Mid-infrared
MLR	Multiple Linear Regression
MSAVI	Modified Soil Adjusted Vegetation Index
NIR	Near-Infrared
NDVI	Normalized Difference Vegetation Index
PCA	Principal Component Analysis
PVI	Perpendicular Vegetation Index
<i>r</i>	Coefficient of correlation
R	Rand (South Africa Money)
RADAR	Radio Detection and Ranging
RMSE	Root Mean Square Error
RSR	Reduced Simple Ratio
SPOT	System Probatoire d'Observation de la Terre
SPHA	Stems per Hectare
SR	Simple Ratio
TOA	Top of Atmosphere
TIDA	Tree Identification and Delineation Algorithm
TSAVI	Transformed Soil Adjusted Vegetations Index

UNCED

United Nations Conference on Environment and
Development

δ

Standard Deviation

CHAPTER 1

GENERAL INTRODUCTION

1.1 Introduction

Forests have played a vital role in the economic and social development of South Africa (Department of Water Affairs and Forestry; DWAF, 2005). Plantation forests were introduced in South Africa in the late 19th Century, when the indigenous forests could not support the increasing industrial demand (Chamshama and Nwonwu, 2004). The development of plantation forests in South Africa is primarily aimed at benefiting the economy of the country (Tewari, 2001). A forestry product report by Chamberlain et al. (2005) indicated that the contribution of plantation forests to the South Africa GDP is R 12.2 billion. The authors furthermore illustrated that the country's economy also benefits through round-wood (saw-logs) exports, earning foreign exchange to the value of about R 270 million. Plantation forests supply domestic fuel-wood, as well as providing the raw material for downstream activities such as pulp milling, paper manufacturing, sawmilling, mining timber, pole manufacturing, fibreboard manufacture, charcoal, and woodchip production. All of these activities benefit the country's economy and many such benefits have been noted to have occurred in areas where economic alternatives are limited. Further to this, it should be noted that many of the social benefits of plantation forests are inextricably tied to the economic benefits, as in the case of employment and recreation privileges.

Over and above the socioeconomic benefits, ecological benefits of plantation forests have also been acknowledged by many regional and international institutions (Nambiar, 1999; Landsberg and Coops, 1999; Franklin, 2001; DWAF, 2005; FAO, 2005). Forests in general contribute to temperature and humidity moderation and absorb CO₂ (Brown, 2002; Goodale et al., 2002; Grace et al., 2002; Dong et al., 2003; Beedlow et al., 2004). Carbon is stored in both above and below ground biomass as well as dead wood and litter (Chen et al., 2006; Peichl and Arain, 2006; Quaife et al., 2008). In some situations forests can also increase fog condensation, thus replenishing soil moisture (Frahm and Grandstein, 1991; Kidron, 2005; Eugster et al., 2006). Finally, planting trees and re-

establishing vegetative cover also provide a means to reverse desertification and support agricultural production and community livelihoods (FAO, 2005).

The subject of interest becomes not so much a question of what the benefits of plantation forests are, but more of how to maximize, or perhaps optimize these benefits to satisfy as many interest groups as possible. Sustaining the multiple benefits and functions of all types of forests and woodlands is one of the main challenges that forest management faces today. In South Africa, as in other countries, there has been a general shift in forest management practice towards the concept of sustainability since the Rio Earth Summit (UNCED, 1992). As a result, the South African government stipulated a forest act, the main notion of which is: “to ensure that South Africa’s forests are protected, used, developed, conserved, managed and controlled in a sustainable and equitable manner, for the benefit of all” (National Forest Act, 1998).

Ensuring the implementation of sustainable forest management practice requires reliable, up to date, and synoptic spatial information regarding the status, trends, and structural characteristics of forest resources (Holmgren and Thuresson, 1998; Wulder, 1998; Nambiar, 1999; Franklin, 2001; Boyd and Danson, 2005; FAO, 2005; Duvemo and Lämäs, 2006; Barth et al., 2006). In addition to forest structural parameters being useful for ecosystem monitoring and management, current and accurate spatial information is instrumental for effective policies and planning implementation, as well as prioritizing interventions such as allocation of forest operations (Loveland et al., 2000; Holmgren and Persson, 2002; Mather, 2005; Valerie and Sherri, 2005). This information can also help to value forest resources for effective investment and forestry certification as well as raise the profile of the sector (Holmgren and Thuresson, 1998; Frost et al., 2003; Duvemo and Lämäs, 2006).

Currently in South Africa, the acquisitions of forest status and structural characteristics are often based upon field observations at sample locations throughout plantation stands. A plantation forest stand, sometimes also called plantation forest compartment, is the basic unit of data collection and plantation management operations, and typically represents a homogeneous forest region between approximately 1-35 ha in size. The

homogeneity of a plantation stand is defined by the site index, the age of the growing stock, the distribution of tree species, and other relevant stand characteristics (Esler, 2005).

The current state-of-the-art in terms of the South Africa forest inventory system relies heavily on the delineation of plantation stands by overhead digitizing from digital colour infrared aerial photographs, at a scale of 1:10000. During the field inventory, pre-delineated plantation stand borders are checked using GPS data and possible errors are corrected. Stand-level forest structural parameters, such as stems per hectare, tree height, and diameter at breast height are enumerated from sample plots, which typically represent 5 % of the plantation stand, whereas basal area and merchantable volume are computed from the enumerated parameters (Esler, 2004). The information content and inventory cycle of the current systems are satisfactory, considering the fact that the current approach to forest inventory is designed to provide forest information for decision making related mainly to cuttings and harvesting operations. In this kind of field inventory, the accuracy of forest structural attribute assessment is highly dependent on the skills of the forester. The relative estimation error of stem volume obtained from field stand-level inventories usually varies between 10 % and 15 % (Esler, 2004). More importantly, field-based forest surveying has limitations with regard to high costs and low spatial coverage and frequency (Wulder, 1998; Franklin, 2001; Wulder and Franklin, 2007; Duvemo and Lämäs, 2006).

In order to achieve the goals set by the South African forest act, it is clear that a more systematic and rapid approach to forest inventory is required. This goal has led to much research in the field of cost-effective, rapid, accurate, and precise forest inventory approaches. Efforts have focused mainly on supplementing field-based forest surveys with information from aerial and satellite remote sensing (Holmgren and Thuresson, 1998; Wulder, 1998; Franklin, 2001; Boyd and Danson 2005). An important development over the last ten years, scientific advances in remote sensing have produced a number of techniques that can retrieve information for various management areas ranging from strategic to operational forestry. Relatively new remote sensing systems such as ASTER, IKONOS, QuickBird, Radar, Lidar, can cover large areas in a fraction of the time

required by field workers. In addition, such systems offer a sampling intensity that approaches full coverage as opposed to current selective or targeted sampling through field plots. Data are acquired in digital form and can be processed to information by a computer, while integration with other datasets in a GIS is also possible (Running et al., 2000). Additionally, data may be processed in an automated fashion, minimizing subjectivity in the interpretation of the images (Wulder, 1998; Boyd and Danson, 2005). These are important advances, as it is generally acknowledged that remote sensing can provide information that is not currently part of an existing forest inventory.

Accordingly, a great deal of progress has been made in the development of remote sensing applications for the collection of forest resource information, e.g., Lu et al. (2004, forest above ground biomass estimation using Landsat TM); Ingram et al. (2005, forest height, diameter at breast height and stems per hectare using Landsat ETM+); Heiskanen (2006, forest biomass and leaf area index using ASTER data); Kayitakire et al. (2006, diameter at breast height, basal area, volume, stems per hectare and tree height using IKONOS data); Sivanpillai et al. (2006, forest stand age and stems per hectare using Landsat ETM+). These remote sensing studies used different types of satellite systems that have been launched over the past 30 years. In general, satellite remote sensing can be used to provide three types of forest information:

1. Information on the spatial extent of forest cover, which can be used to assess the spatial dynamics of forest cover.
2. Information related forest type and species composition.
3. Structural and chemical characteristics of forests.

Chiefly, this study is concerned with optical, passive satellite remote sensing methods and their application to the estimation of forest structural attributes.

The dependence between forest structural attributes and remotely sensed reflectance can be modelled either physically or empirically. Thus far empirical models have been more successful. Double sampling (e.g., Poso et al., 1999) and linear regression models (e.g., Franklin, 2001; Lu et al., 2004; Kayitakire et al., 2006) constitute classical approaches,

but nonparametric regression methods, e.g., k-nearest neighbours estimation and artificial neural network methods, have recently become popular both in research and practice (e.g., Hyypä et al., 2000; Franco-Lopez et al., 2001; Tomppo et al., 2002; Holmström and Fransson, 2003; Jensen and Binford, 2004; Mäkelä and Pekkarinen, 2004; Tomppo, 2005; Gebreslasie *et al.* (In press)). The successful exploitation of remote sensing relies on defining the link between the remotely sensed data and field surveyed variables of interest. Therefore, novel approaches are needed for up-scaling field observations to match the reflectance values for calibration and validation of remote sensing models.

1.2 Objectives of the study

This study contributes to the current body of knowledge in terms of the application of optical, passive remote sensing to the estimation of forest structural attributes in the plantation forests of a warm-temperate climatic zone in KwaZulu-Natal, South Africa. The forest structural attributes under investigation were stems per hectare, diameter at breast height, mean tree height, basal area, and volume. The specific objectives provide a general outline of the study approach for the specific research area and are as follows:

1. To investigate image-based atmospheric correction methods for ASTER and IKONOS imagery in a plantation forest context.
2. To examine the potential of medium spatial and high spectral resolution remote sensing imagery for the estimation of forest structural attributes.
3. To analyse the potential of high spatial resolution remote sensing imagery for the estimation of forest structural attributes
4. To develop an algorithm for the estimation of stems per hectare based on high spatial resolution satellite imagery.

1.3 Outline of the thesis

The thesis contains eight chapters, five of which were prepared in a peer-reviewed publication format with the intention of submitting to peer-reviewed journals. Of the five papers, two papers have been published and the remaining three papers have been submitted but are still in review. Chapter one deals with the introduction, which covers

the current state of the research problem and the objectives of study. The second chapter provides a background of optical remote sensing and its application to the prediction of forest structural attributes (published). The third chapter describes the study area. In this chapter the location, climate, geology, soil, topography, vegetation, and the main land use practices are discussed. Following this, chapter four investigates image-based atmospheric correction methods for ASTER and IKONOS imagery (submitted). The fifth chapter examines the potential of high spectral resolution ASTER satellite imagery for the estimation of *Eucalyptus* forest structural attributes (published). Chapter six analyses the textural information of IKONOS imagery for the estimation of *Eucalyptus* forest structural attributes using linear and non-linear statistical analysis (submitted). Following this, chapter seven deals with the detection of trees using both variable and fixed window size approaches to local maximum filtering for the estimation of stems per hectare, based on panchromatic IKONOS data (submitted). Finally, a general conclusion is presented in chapter eight.

Chapters 4-7 have been prepared to each form a stand-alone chapter of this thesis, contributing to the overall research objectives. As far as possible, the content of the journal papers has been maintained, meaning that each of these chapters is separately introduced with separate conclusions being made, which link with subsequent chapters. The approach which was used invariably resulted in some overlap in terms of method description and illustrations. However, these limitations are deemed to be insignificant when considering the critical peer-review process and the fact that the chapters are presented as stand-alone research papers that can be read and understood in their specific research context and on their own merit.

1.4 References

Barth, A., Lind, T., Pettersson, H. and Ståhl, G., 2006, A framework for evaluation data acquisition strategies for analyses of sustainable forestry at national level. *Scandinavian Journal of Forest Research*, 21: 94-105.

Beedlow, P.A., Tingey, D.T., Phillips, D.L., Hogsett, W.E. and Olszyk, D.M., 2004, Rising atmospheric CO₂ and carbon sequestration in forests. *Frontiers in Ecology and the Environment*, 2: 315-322.

Boyd, D.S. and Danson, F.M., 2005, Satellite remote sensing of forest resources: Three decades of research development. *Progress in Physical Geography*, 29: 1-26

Brown, S., 2002, Measuring carbon in forests: current status and future challenges. *Environmental Pollution. International Journal of Remote Sensing*, 116: 363–372.

Chamberlain, D., Essop, H., Hougaard, C., Malherbe, S. and Walker, R., 2005, Genesis Report: Part I. The contribution, costs and development opportunities of the forestry, timber pulp and paper industries in South Africa. Genesis Analytics (Pty) Ltd, Johannesburg, South Africa.

Chamshama, S.A.O. and Nwonwu, F.O.C., 2004, Forest plantations in sub-Saharan. A report prepared for the project: Lessons learnt on sustainable forest management in Africa. Royal Swedish Academy of Agriculture and Forestry, African Forest Research Network at the African Academy of Science, and Food and Agriculture Organization of the United Nations.

Chen, J.M., Govind, A., Sonnentag, O., Zhang, Y., Barr, A. and Amiro, B., 2006, Leaf area index measurements at fluxnet Canada forest sites. *Agricultural Forest Metrology*, 140: 257-268.

Department of water affairs and forestry 2005, State of the Forest Report: A pilot report to test the National Criteria and Indicators. March 2005.

Dong, J., Kaufmann, R.K., Myneni, R.B., Tucker, C.J., Kauppi, P., Liski, J., Buermann, W., Alexeyev, V. and Hughes, M.K., 2003, Remote sensing estimates of boreal and temperate forest woody biomass: carbon pools, Sources, and sinks. *Remote Sensing of Environment*, 84: 393 – 410.

Duvemo, K. and Lämäs, T., 2006, The influence of forest data quality on planning processes in forestry. *Scandinavian Journal of Forest Research*, 21: 327-339.

Esler, B.W., 2004, The basics of forest mensuration. MONDI SA, working document

Esler, B.W., 2005, Forest excellence field data. MONDI SA working document

Eugster, W., Burkard, R., Holwerda, F., Scatena, F.N. and Bruijnzeel, L.A., 2006, Characteristics of fog and fog water fluxes in a Puerto Rican elfin cloud forest. *Agricultural and Forest Meteorology*, 139: 288-306.

FAO, 2005, Global Forest Resources Assessment 2005: South Africa Country Report. Food and Agriculture Organization of the United Nations. Country Report 004. Rome, pp. 320

Frahm, J.P. and Gradstein, S.R., 1991, An altitudinal Zonation of tropical rain forests using bryophytes. *Journal of Biogeography*, 18: 669-676

Franco-lopez, H., Ek, A.R. and Bauer, M.E., 2001, Estimation and mapping of forest stand density, volume, and cover type using the k-nearest-neighbours method. *Remote Sensing of Environment*, 77: 251-274.

Franklin, S.E., 2001, Remote sensing for sustainable forest management. Publisher Taylor and Francis Ltd. Lewis publishers, U.S.A. pp. 407.

Frost, B., Mayers, J., and Roberts, S., 2003, Growing credibility: impact of certification on forests and people in South Africa. London, UK, International Institute for Environment and Development.

Goodale, C.L., Apps, M.J., Birdsey, R.A., Field, C.B., Heath, L.S., Houghton, R.A., Jenkins, J.C., Kohlmaier, G.H., Kurz, W., Liu, S., Nabuurs, G.L., Nilsson, S. and Shvidenko, A.Z. 2002, Forest carbon sinks in the northern hemisphere. *Ecological Applications*, 12: 891- 899.

Grace, J., Berninger, F. and Nagy, L. 2002, Impacts of climate change on tree line. *Annals of Botany*, 90: 537 – 544.

Heiskanen, J., 2006, Estimating aboveground tree biomass and leaf area index in a mountain birch forest using ASTER satellite data. *International Journal of Remote Sensing*, 27: 1135 – 1158.

Holmgren, P. and Persson, R., 2002, Evolution and Prospects of Global Forest Assessments. *Unasylva*, 53: 3-9.

Holmgren, P. and Thuresson, T., 1998, A review-Satellite remote sensing for forestry planning. *Scandinavian Journal of Forest Research*, 13: 90-110.

Holmström, H. and Fransson, J. E. S., 2003, Combining remotely sensed optical and radar data in KNN-estimation of forest variables. *Forest Science*, 49: 409-418.

Hyypä, H., Inkinen, M., Engdahl, M., Linko, S. and Zhu, Y.H., 2000, Accuracy comparison of various remote sensing data sources in the retrieval of forest stand attributes. *Forest Ecology and Management*, 128: 109-120.

Ingram, J.C., Dawson, T.P. and Whittaker, R.J., 2005, Mapping tropical forest structure in south-eastern Madagascar using remote sensing and artificial neural networks. *Remote Sensing of Environment*, 94: 491-507.

Jensen, R.R. and Binford, M.W., 2004, Measurement and comparison of Leaf Area Index estimators from satellite remote sensing techniques. *International Journal of Remote Sensing*, 25: 4251-4265.

Kayitakire, F., Hamle, C. and Defourny, P., 2006, Retrieving forest structure variables based on image texture analysis and IKONOS-2 imagery. *Remote Sensing of Environment*, 102: 390-401

Kidron, G.J., 2005, Angle and aspect dependent dew and fog precipitation in the Negev Desert, Israel. *Journal of Hydrology*, 301: 66-74.

Landsberg, J. and Coops, N.C. 1999, modelling forest productivity across large areas and long periods. *Natural Resource Modelling*, 12: 383-411.

Loveland, T.R., Reed, B.C., Brown, J.F., Ohlen, D.O., Zhu, Z., Yang, L. and Merchant, J.W., 2000, Development of global land cover characteristics database and IGBP DISCover from 1km AVHRR data. *International Journal of Remote Sensing*, 21: 1303-1330.

Lu, D., Mausel, P., Brondizio, E. and Moran, E. 2004, Relationships between forest stand parameters and Landsat TM spectral response in Brazilian Amazon Basin. *Forest Ecology and Management*, 198: 149-167.

Mäkelä, H. and Pekkarinen, A., 2004, Estimation of forest stand volume by Landsat TM imagery and stem-level field-inventory data. *Forest Ecology and Management*, 196: 245-255.

Mather, A.S., 2005, Assessing the world's forests. *Global Environmental Change*, 15: 267-280.

Nambiar, E.K.S., 1999, Pursuit of sustainable plantation forestry. *Southern African Forestry Journal*, 184: 45-61.

National Forest Act, 1998, Republic of South Africa: Government Gazette. Volume, 400 No 84, Cape Twon, 30 October 1998.

Peichl, M. and Arain, M.A., 2006, Above-and belowground ecosystem biomass and carbon pools in an age-sequence of temperate pine plantation forests. *Agricultural and Forest Metrology*, 140: 51-63

Poso, S. Wang, G. and Tuominen, S. 1999, Weighting alternative estimates when using multisource auxiliary data for forest inventory. *Silva Fennica*, 33: 41- 50.

Quaife, T., Lewis, P., De Kauwe, M., Williams, M., Law, B.E., Disney, M. and Bowyer, P., 2008, Assimilating canopy reflectance data into an ecosystem model with an Ensemble Kalman Filter. *Remote Sensing of Environment*, 112: 1347-1364.

Running, S.W., Queen, L. and Thornton, M., 2000, The earth observing system and forest management. *Journal of Forestry*, 98: 29-31.

Sivanpillai, R., Smith, C.T., Srinivasan, R., Messina, M.G. and Wu, X.B. 2006, Estimation of managed loblolly pine stand age and density with Landsat ETM+ data. *Forest Ecology and Management*, 223: 247-254.

Tewari, D.D. 2001, Is commercial forestry sustainable in South Africa? The changing institutional and policy needs. *Forest Policy and Economics*, 2: 333-353

Tomppo, E. 2005, The Finnish Multi-Source Inventory. In: OLSSON, H (Eds). *Proceedings of ForestSat 2005*, 31 May – 2 June, National Board of Forestry, Boras, pp. 27-34.

Tomppo, E., Nilsson, M., Rosengren, M., Aalto, P. and Kennedy, P., 2002, Simultaneous use of Landsat-TM and IRS-1c WiFS data in estimating large area tree stem volume and aboveground biomass. *Remote Sensing of Environment*, 82: 156– 171.

United Nations Conference on Environment and Development (UNCED), 1992, Rio de Janeiro, 3-14 June 1992, Brazil

Valerie, A. R., and Sherri, R. D., 2005, Got Science? Getting Science to people who care about Forests. *Proceedings: International Conference on Transfer of Forest Science Knowledge and Technology* Troutdale, OR, USA, may 10-13, 2005.

Wulder, M. A. 1998, Optical remote sensing techniques for the assessment of forest inventory and biophysical parameters. *Progress in Physical Geography*, 22: 449 – 476.

Wulder, M.A. and Franklin, S.E., 2007, *Understanding forest disturbance and spatial pattern*. Published by CRC Press, pp. 246.

CHAPTER 2

LITERATURE REVIEW

* This chapter is based on:

Roberts, W., Gebreslasie, M., R., Gebrmaiam, S., Ahmed, F. B., van Aardt, J. (2007) Forest Structural Assessment using Remote Sensing Technologies: An Overview of the current state of the art. *Southern Hemisphere Forestry Journal* 2007, 69(3): 183–203

2.1 Introduction

Remote sensing is defined by Lillesand et al. (2004) as the science of processing and interpreting images and related data obtained by sensing systems which, without being in physical contact with the object, are able to record electromagnetic energy reflected/emitted by the earth's surface. Thus, the object-related interaction between matter and electromagnetic radiation is represented. Aerial photography in the visible portion of the electromagnetic wavelength was the original form of remote sensing, but technological developments have enabled the acquisition of information at high spectral resolution. The capacity of remote sensing to identify and monitor land surfaces and environmental conditions has expanded greatly over the last few years and it appears that remotely sensed data will become an essential tool in natural resource management. The general aim of forest remote sensing is to infer information on the physiological and biochemical conditions of the forests from the measurements of the reflected electromagnetic radiation (Wulder, 1998; Franklin, 2001; Lillesand et al., 2004). The amount of radiation is measured by a variety of passive and active sensors, which are at a time onboard (air and/or space platforms). The focus of this thesis is on high spectral and spatial resolution optical satellite remote sensing i.e. ASTER and IKONOS satellite imagery.

2.2 Properties of Optical Remote Sensing

Optical remote sensing can be defined as using reflected sunlight energy from the visible to shortwave infrared (SWIR) spectral domains (400 - 2500 nm wavelengths). The optical sensors designed to study the land surface operate in spectral wavelength in which the atmospheric transmission is high (Lillesand et al., 2004). The atmosphere scatters and absorbs the radiation on its path from the sun to Earth's surface and from Earth's surface to the sensor. Reflectance (Figure 2.1), which is the interaction between the solar radiation and the Earth's surface, in this case vegetation canopy, is a compound of absorption and scattering processes occurring at the leaf level, combined with structural influences operating at the canopy level. The amount of reflected radiation varies as a function of five optical domains: spectral, spatial, temporal, angular, and polarization (Rees, 1990; Sabins, 1997; Donoghue, 2000; Lillesand et al., 2004). The polarization

domain is not covered in this chapter. These domains are interdependent and yet they are often considered individually during sensor development and image analysis.

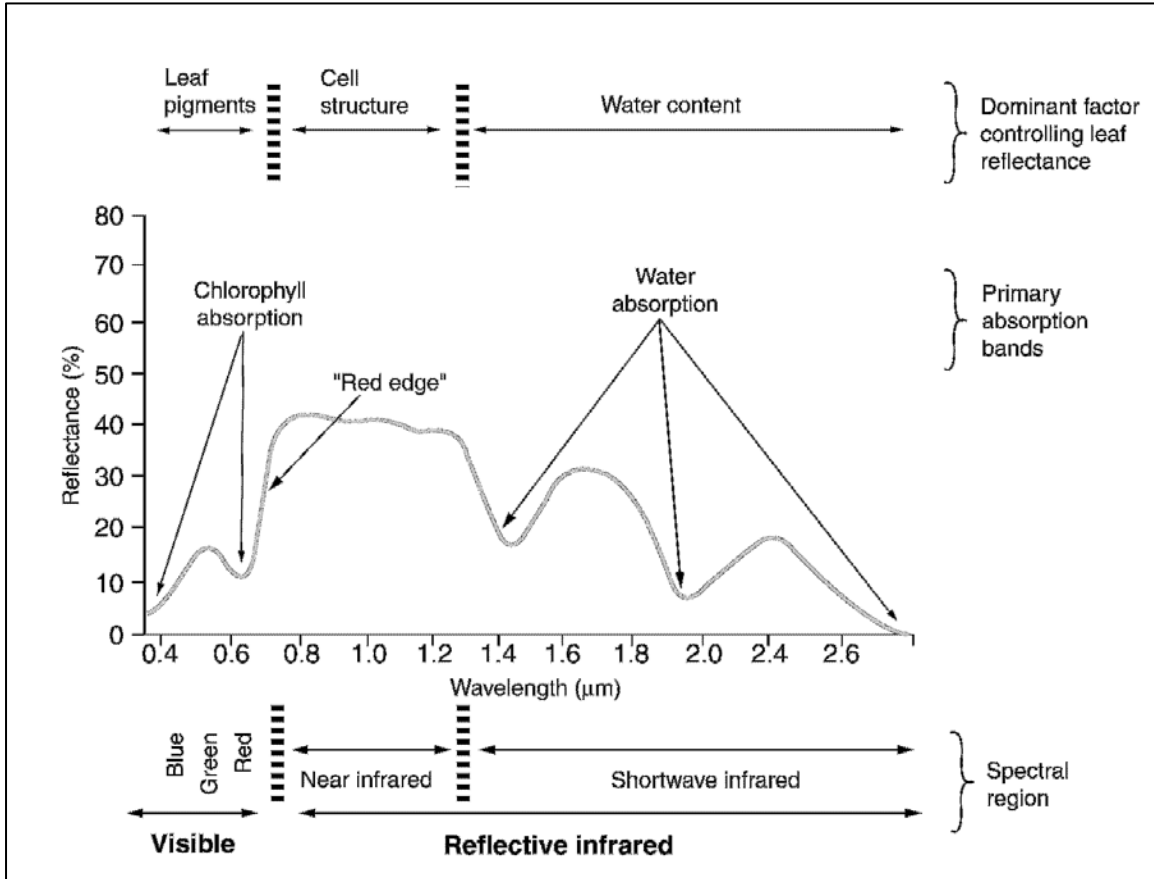


Figure 2.1 Spectral reflectance curve of green vegetation (Sabins, 1997)

Spectral variability of reflectance is probably the most applied source of information in the remote sensing of vegetation studies (Sabins, 1997; Lillesand et al., 2004). Vegetation typically shows a low reflectance in the visible range of the spectrum, mainly in the blue and red band. The main factors are absorption by chlorophylls and carotenoid photosynthetic pigments which absorb light in the visible spectrum (Woolley, 1971; Baret and Guyot, 1991; Danson and Curran, 1993; Lucas and Curran, 1999; Lillesand et al., 2004). Reflectance increases as we move up around 700nm (red edge) and high reflectance occur in the near infrared (NIR) range of the spectrometer (Lillesand et al., 2004). The cellular structure of the leaf chiefly determines the high levels of reflectance

in the near infrared spectrum, where absorption by pigments and water is generally low (Franklin and Wulder, 2002).

The reflectance varies also as a function of the images' spatial resolution. Spatial resolution refers to the level of spatial detail that is provided by the image (Strahler et al., 1986; Wulder, 1998). The content of the pixel is determined by the sensors instantaneous field of view on the ground and spatial response function (Lillesand et al., 2004). The pixel size denotes to the area on the ground covered by a single pixel in the image. Although it is common to categorize the image data according to the absolute pixel size, the spatial resolution is probably best understood relative to the size of objects that needs to be sensed. Strahler et al. (1986) developed a systematic typology for remote sensing models and introduced the concepts of low-resolution (L) and high-resolution (H). Important concepts are scene and image, and size of the scene objects and spatial resolution of the image. In the H-resolution case, the scene varies at a lower spatial frequency than image sampling and individual features can be resolved. On the other hand, in L resolution case, the scene objects are smaller than the spatial resolution of the image. Mixed pixels are a typical L-resolution problem, occurring when two or more scene objects of interest fall within a single pixel. The spatial resolution is also closely related to the selection of image processing methods (Strahler et al., 1986; Woodcock et al., 1988).

The reflectance of the land surface, particularly vegetations, can also vary considerably as a function of time due to the seasonality of vegetation cover (Song et al., 2001; Franklin 2001; Franklin and Wulder, 2002). The temporal resolution refers to the average revisit period at a constant site (Chen and Cihlar, 1996; Lillesand et al., 2004; Aplin, 2005). It depends on various factors, including the swath width, satellites orbital altitude, sensor view angle, sensor tilting capabilities and latitude.

The reflectance varies also as a function of the sensor viewing angles and sun illumination angles (Liesenberg et al., 2007). This angular variation of the reflectance is described by the bidirectional reflectance distribution function. The reflectance of forests

is distinctively determined by the optical properties of canopy components, structural characteristics, and topography (Asner et al., 1998).

2.3 Forest attributes extraction approaches using optical remote sensing

2.3.1 Medium spatial resolution and forest structural attributes

Contextual attributes refer to those variables that can be determined using medium resolution satellite sensors such as Landsat Thematic Mapper, SPOT HRV and the Advanced Space-borne Thermal Emission and Reflection Radiometer (ASTER). These variables are usually derived at the stand and forest scale, because the spatial resolution of the sensor is not fine enough to discriminate between tree canopies. Various forest structural and biophysical attributes have been assessed using medium resolution passive remote sensing and empirical approaches. Appendix 2.1 provides an overview of some of the significant publications in this area of research. Maselli et al. (2005) used the K-nearest neighbours approach and were able to estimate basal area with a reasonable amount of accuracy (RMSE = 4.02 m² ha⁻¹). Ingram et al. (2005) also modelled and mapped basal area and stand density but used correlation and artificial neural networks (ANN). Basal area was found to be correlated with spectral reflectance ($r = -0.77$, $p < 0.01$: MIR band) while weak relationships were identified between spectral response and stand density ($r = -0.21$, $p < 0.01$: Red band). On the other hand, stand density was strongly correlated with the Normalised Difference Vegetation Index ($r = 0.69$, $p < 0.01$). Further analysis using an ANN (jackknife method) revealed that the ANNs produced strong and significant relationships between *in situ* measures of basal area and predicted measures of the same variable ($r = 0.79$, $p < 0.01$). The discrepancy between spectral reflectance and vegetation indices is also highlighted in the mapping and modelling of leaf-area-index (LAI), an important structural parameter that is directly related to rates of energy-mass exchange, biomass partitioning, and productivity (Jensen and Binford, 2004).

Curran et al. (1992); Brown et al. (2000) originally suggested that LAI should be estimated and mapped using vegetation indices. Several studies have taken place since then with the notable publications mentioned in Appendix 2.1, wherein most of the

researchers report good relationships between LAI and spectral reflectance. Recently Heiskanen (2006) used ASTER data to estimate tree biomass and LAI. Both spectral reflectance data and vegetation indices returned similar results with differences between the two highlighted only when advanced statistical techniques and transformed indices were used. The lowest Root Mean Square Errors (RMSEs) reported were 3.45 t ha⁻¹ (41%) and 0.28 m² m⁻² (37%) for biomass and LAI, respectively (Heiskanen, 2006). This result highlights the advances made in terms of sensor design and performance. Nearly all published literature on modelling and mapping of LAI use either Landsat TM or ETM+. With the launch of ASTER, the research community enters a new age where both high spectral resolution reflectance and vegetation indices can be used. The approach now becomes increasingly important since it determines the outcome and gives researchers the freedom to explore various quantitative procedures. However, critical to forest inventory is the move from canopy structure to practical inventory-related variables, e.g. stems-per-hectare, mean height, and stem volume.

Stem volume is arguably the most important variable in plantation forestry in South Africa and the ability to model and map the spatial distribution of merchantable timber volume using remote sensing technologies is a central goal of much research. International research such as described in Appendix 2.1 focuses on the derivation of timber volume for planning purposes, while Steininger (2000) focussed on deriving timber volume estimates in support of quantifying carbon sequestration in regenerating forests in the Amazon basin. The approach remains fairly standard irrespective of the application; empirical relationships are derived between *in situ* timber volume estimates and spectral reflectance data (Rahman et al., 2005). These empirical relationships are then used to derive spatially explicit maps of timber volume, which in turn are used for planning purposes. The accuracy of these methods is tested using reference areas of known volume. Both Franco-Lopez et al. (2001); Mäkelä and Pekkarinen (2004) reported similar results using the k-nearest neighbours approach (Appendix 2.1), while Steininger (2000) reported that relationships between *in situ* forest parameters and remotely sensed estimations of forest structure tend to saturate in old growth forests. Lu (2005) supports the findings of Steininger (2000) in that regenerating forests return stronger relationships

than mature forests. Similar to volume, biomass plays an important role in understanding the function of forests in the carbon cycle. Zheng et al. (2004) show that models vary between species and that the combined use of different species in empirical modelling does not necessarily improve estimation. It can be concluded from studies presented in Appendix 2.1 that it is possible to model and map biomass using medium resolution remotely sensed data and *in situ* biomass measures, while Foody et al. (2003) illustrated that it is not possible to transfer empirically derived models between sites when using these types of methods.

2.3.2 High spatial resolution and forest structural attributes

The increased availability of high spatial resolution imagery, together with improvements in scene processing and interpretation techniques, allows for the extraction of additional information based on image texture (Coops et al., 1998). Image texture is an important product of high resolution image analysis as it describes the variation of image tones that are related to the spatial distribution of tree features in the forests (Cohen et al., 1990; Franklin, 2001). The texture of a scene is primarily related to the size of the objects in the scene and the spatial resolution of the remote sensing instrument (Van der Sanden and Hoekman, 2005). Two most utilised methods exist for the derivation of spatial information from remotely sensed data; semi-variogram modelling and grey-level co-occurrence matrices (GLCM). Semi-variogram modelling, as described by Woodcock et al. (1988) has been used for various forest-related researches including damage caused by pollution (Levesque and King, 1999). The authors identified several relationships between *in situ* measurements of forest structure and various attributes of a semi-variogram model, for example the range and sill of the variogram were strongly related to a visual stress index, while the ranges of all variogram models were also strongly related to crown size and canopy closure. Levesque and King (1999) concluded that different image resolutions were suited to different tasks, while Treitz (2001) examined spatial resolution but included an analysis of the spatial structure of canopies in the visible and NIR reflectance bands. Optimal image resolution for crown delineation was determined by Hyppänen (1996) using semi-variograms and spatial autocorrelation. The range of the semi-variogram was used to measure the autocorrelation of pixels while local variance

curves were used to determine the spatial resolution that maximises the variance between adjacent pixels. Variogram modelling has for instance been used by Treitz and Howarth (2000) to investigate spatial scale and ecosystem classifications.

Grey-level co-occurrence matrices (GLCM) have been used to enhance multispectral classification of high resolution satellite imagery. GLCM use filters combined with first and second order measures of variance to determine the grey level differences within a predefined region. They inform on the general variation or structure of the image which in turn reflects the variation of forest canopies (Haralick et al., 1973). Franklin et al. (2000) incorporated textural measures derived from GLCM (homogeneity and entropy) into a classification of forest species composition using airborne multispectral images. Results indicated that the inclusion of the GLCM layer improved classification by between 5 and 12 % depending on whether hardwood or softwood stands were analysed. Franklin et al. (2001) once again used GLCM in testing first (variance) and second (homogeneity) order textural measures to determine the optimal application for forest age separability using an IKONOS panchromatic image. Findings indicated that second-order texture values derived using larger filter windows returned better results than first order measures. Further analysis by Kayitakire et al. (2006) showed that it was possible to use textural indices derived from a GLCM of an IKONOS-2 image to derive and estimate forest structural variables such as age, crown circumference, tree height, stand density and basal area. Empirical relationships were derived between *in situ* measures of forest structure and GLCM features. Coefficients of determination ranged from 0.35 (basal area) to 0.82 (tree height). The authors reported that prediction errors of four out of five variables were within accepted sampling inventory errors (RMSE of less than 20%).

High spatial resolution remotely sensed images, both airborne and space-borne, have been also used to measure tree level structural characteristics. Most applications of high spatial resolution imagery chiefly focus on automated identification of tree location and crown delineation (Larsen and Rudemo, 1998; Culvenor, 2002; Pouliot et al., 2002; Wulder et al., 2000; Wulder and White, 2004; Leckie et al., 2005; Pouliot and King, 2005). Furthermore, high spatial resolution imagery has also been used for direct estimation of canopy cover (Levesque and King, 2003; Furusawa et al., 2004; Wang et

al., 2005; Xu et al., 2006), age (Franklin et al., 2001), and predicting various forest structural attributes (Greenberg et al., 2005; Kayitakire et al., 2006). High spatial resolution data with image pixels smaller than the dimensions of individual tree crowns can provide information on the physical structure of individual trees as well as health and degradation (Goodwin et al., 2005; Souza and Roberts, 2005). Appendix 2.2 provides an overview of various approaches used to quantify forest resources using high spatial resolution imagery. The table highlights three broad approaches used, namely image segmentation, textural analysis, and pixel- and object-based approaches.

Derivation of location-based variables from high resolution imagery typically involves some form of image segmentation. Pal and Pal (1993) give a detailed review of image segmentation procedures. Segmentation procedures attempt to segment and identify tree crowns in high-resolution multispectral imagery. These algorithms originally attempted to map the location of each individual tree. Gougeon (1995) used a fairly simple approach that exploited valleys in image brightness seen between tree crowns to segment and then count individual tree crowns within an image (Valley-following approach). The approach described by the author identified 81 % of the trees within the study area correctly. The valley-following approach has also been used by Leckie et al. (2005) returning accuracies ranging from 50 – 80 %. Pitkänen (2001) also attempted to identify individual trees but used an image smoothing supported by binarization approach, with accuracies ranging from 70 – 95 %. Culvenor (1998) extended the valley following approach and developed the Tree Identification and Delineation Algorithm (TIDA), an approach that attempts to not only identify individual trees but also delineate individual tree crowns using a top-down spatial clustering approach. The author did not report any quantitative results but noted that the algorithm was developed for applications in native *Eucalyptus* forests. Tree crown delineation algorithms have also been developed by Pinze (1998); Uuttera et al. (1998); Pouliot et al. (2002); Pouliot and King (2005). Local maxima filtering techniques have also been employed by Dralle and Rudemo (1997) with Wulder et al. (2000) extending the approach by using variable window sizes based on tree size and species. The authors found that errors of omission and commission were a function of crown radii. In addition to variable size windows, authors have also used

region growing techniques supported by fuzzy rule classification to identify and delineate individual trees as well as their crowns (Brandtberg, 2002; Erikson, 2003). The extension of these algorithms is those designed to locate and classify individual trees in mixed-species forests (Leckie et al., 2003; 2005). The specification of both tree location and species type stems from the need to develop accurate volume assessments of mixed species forests, facilitating effective and sustainable management. These methods of tree detection and tree crown delineation have been used in various forest conditions. An alternative approach to deriving information on the structural characteristics of forests involves the use of image textural attributes.

Finally, in recent years the use of contextual or object-oriented classification procedures such as those implemented in the eCognition (Definiens, 2005) software package have returned interesting results. Contextual classifiers utilize both the spectral and spatial characteristics of a pixel. In these methods the classification of an individual pixel is influenced by the characteristics of the surrounding pixels (Gong and Howarth, 1992). Sharma and Sarkar (1998) have demonstrated a contextual classification technique that is modifiable for either high or low-resolution imagery and Bunting and Lucas (2006) have used object orientated classification procedures to delineate and classify tree crowns in Australian mixed species forests. Wang et al. (2004) tested both pixel-based and object-based classification for mapping Mangrove forests with IKONOS imagery. Even though both procedures provided adequate results, the authors found that they were able to increase the accuracy of the species classification from 80.4 % to 91.4 % by combining the two in a scale parameter optimisation procedure.

2.4 References

Aplin, P., 2005, Remote sensing: Ecology. *Progress in Physical Geography*, 29: 104 – 113.

Asner, G.P., Braswell, B.H., Schimel, D.S., and Wessman, C.A., 1998, Ecological research needs from multiangle remote sensing. *Remote Sensing of Environment*, 63: 155-165.

Baret, F. and Guyot, G., 1991, Potentials and limits of vegetation indices for LAI and APAR assessment. *Remote Sensing of Environment*, 35: 161-173.

Brandtberg, T., 2002, Individual tree-based species classification in high spatial resolution aerial images of forests using fuzzy sets. *Fuzzy Sets and Systems*, 132: 371-387.

Brown, L., Chen, J.M., Leblanc, S.G. and Cihlar, J., 2000, A shortwave infrared modification to the simple ratio for LAI retrieval in boreal forests: an image and model analysis. *Remote Sensing of Environment*, 71: 16-25.

Bunting, P., and Lucas, R., 2006, The delineation of tree crowns in Australian mixed species forests using hyperspectral Compact Airborne Spectrographic Imager (CASI) data. *Remote Sensing of Environment*, 101: 230-248.

Chen, J.M. and Cihlar, J. 1996, Retrieving leaf area index of boreal conifer forests using Landsat TM images. *Remote Sensing of Environment*, 55: 153– 162.

Cohen, W.B., Spies, T.A. and Bradshaw, G.A., 1990, Semivariograms of Digital Imagery for Analysis of Conifer Canopy Structure. *Remote Sensing of Environment*, 34: 167-178.

Coops, N., Culvenor, D., Preston, R. and Catling, P., 1998, Procedures for predicting habitat and structural attributes in eucalypt forests using high spatial resolution remotely sensed imagery. *Australian Forestry*, 61: 244-252.

Culvenor, D.S., Coops, N., Preston, R. and Tolhurst, K. G., 1998, A spatial clustering approach to automated tree crown delineation. In *Proceedings of the International Forum on Automated Interpretation of High Spatial Resolution Digital Imagery for Forestry*, Victoria, BC: Natural Resources Canada, Forestry Canada, Pacific Forestry Centre, 10-12 February, 1998.

Culvenor, D.S., 2002, TIDA: an algorithm for the delineation of tree crowns in high spatial resolution remotely sensed imagery. *Computers and Geosciences*, 28: 33-44.

Curran, P.J., Dungan, J.L. and Gholz, H.L., 1992, Seasonal LAI in slash pine estimated with Landsat TM. *Remote Sensing of Environment*, 39: 3-13.

Danson, F.M. and Curran, P.J., 1993, Factors affecting the remotely sensed response of coniferous forest plantations. *Remote Sensing of Environment*, 43: 55-65.

Definiens, 2005, eCognition Version 5 Object Orientated Image Analysis User Guide. Munich, Germany: Definiens AG, 486 pp.

Donoghue, D.N.M., 2000, Remote sensing: sensors and application. *Progress in Physical Geography*. 24, 407-414.

Dralle, K. and Rudemo, M., 1997, Stem number estimation by kernel smoothing of aerial photographs. *Canadian Journal Forest Research*, 26: 1228-1236.

Erikson, M., 2003, Segmentation of individual tree crowns in colour aerial photographs using region growing supported by fuzzy rules. *Canadian Journal of Forest Research*, 33: 1557-1563.

Foody, G.M., Boyd, D.S. and Cutler, M.E.J., 2003, Predictive relationships of tropical forest biomass from Landsat TM data and their transferability between regions. *Remote Sensing of Environment*, 85: 463-474.

Franco-lopez, H., Ek, A.R. and Bauer, M.E., 2001, Estimation and mapping of forest stand density, volume, and cover type using the k-nearest-neighbours method. *Remote Sensing of Environment*, 77: 251-274.

Franklin, S.E, Wulder, M. and Gerylo, G., 2001, Texture analysis of IKONOS panchromatic data for Douglas-fir forest age class separability in British Columbia. *International Journal of Remote Sensing*, 22: 2627-2632.

Franklin, S.E., 2001, Remote sensing for sustainable forest management. Publisher Taylor and Francis Ltd. Lewis publishers, U.S.A. pp. 407.

Franklin, S.E. and Wulder, M.A., 2002, Remote sensing methods in medium spatial resolution satellite data land cover classification of large areas. *Progress in Physical geography*, 26: 173-205.

Franklin, S.E., Hall, R.J., Moskal, L.M., Maude, A.J. and Lavigne, M.B., 2000, Incorporating texture into classification of forest species composition from airborne multispectral images. *International Journal of Remote Sensing*, 21: 61-79.

Furusawa, T., Pahari, K., Umezaki, M. and Ohtsuka, R., 2004, Impacts of selective logging on New Georgia Island, Solomon Islands evaluated using very-high-resolution satellite (IKONOS) data. *Environmental Conservation*, 31: 349-355.

Gong, P. and Howarth, P., 1992, Frequency based contextual classification and gray-level vector reduction for land use identification. *Photogrammetric Engineering and Remote Sensing*, 58: 423-437.

Goodwin, N., Coops, N. C. and Stone, C., 2005, Assessing plantation canopy condition from airborne imagery using spectral mixture analysis and fractional abundances. *International Journal of Applied Earth Observation*, 7: 11-28.

Gougeon, F.A., 1995, A crown following approach to the automatic delineation of individual tree crowns in high spatial resolution aerial images. *Canadian Journal of Remote Sensing*, 21: 274-284.

Greenberg, J.A., Dobrowski, S.Z. and Ustin, S.L., 2005, Shadow allometry: estimating tree structural parameters using hyperspatial image analysis. *Remote Sensing of Environment*, 97: 15-25.

Haralick, R.M., Shanmugam, K. and Dinstein, I., 1973, Textural features for image classification. *IEEE Transactions on Systems, Man and Cybernetics*, 3: 610-621.

Heiskanen, J., 2006, Estimating aboveground tree biomass and leaf area index in a mountain birch forest using ASTER satellite data. *International Journal of Remote Sensing*, 27: 1135 – 1158.

Hyppänen, H., 1996, Spatial autocorrelation and optimal spatial resolution of optical remote sensing data in boreal forest environment. *International Journal of Remote Sensing*, 17: 3441-3452.

Ingram, J.C., Dawson, T.P. and Whittaker, R.J., 2005, Mapping tropical forest structure in south-eastern Madagascar using remote sensing and artificial neural networks. *Remote Sensing of Environment*, 94: 491-507.

Jensen, R.R. and Binford, M.W., 2004, Measurement and comparison of Leaf Area Index estimators from satellite remote sensing techniques. *International Journal of Remote Sensing*, 25: 4251-4265.

Kayitakire, F., Hamle, C. and Defourny, P., 2006, Retrieving forest structure variables based on image texture analysis and IKONOS-2 imagery. *Remote Sensing of Environment*, 102: 390-401.

Larsen, M. and Rudemo, M., 1998, Optimising templates for finding trees in aerial photographs. *Pattern Recognition Letters*, 19: 1153-1162.

Leckie, D.G., Gougeon, F.A., Tinis, S. Nelson, T., Burnett, C.N., and Paradine, D., 2005, Automated tree recognition in old growth conifer stands with high resolution digital imagery. *Remote Sensing of Environment*, 94: 311-326.

Leckie, D.G., Gougeon, F.A., Walsworth, N., and Paradine, D., 2003, Stand delineation and composition estimation using semi-automated individual tree crown analysis. *Remote Sensing of Environment*. 85, 355-369.

Levesque, J. and King, D.J., 1999, Airborne digital camera image semivariance for evaluation of forest structural damage at an acid mine site. *Remote Sensing of Environment*, 68: 112-124.

Levesque, J., and King, D.J., 2003, Spatial analysis of radiometric fractions from high resolution multispectral imagery for modelling individual tree crown and Forest canopy structure and health. *Remote Sensing of Environment*, 84: 589-602.

Liesenberg, V., Galvão, L.S., and Ponzoni, F.J., 2007, Variation in reflectance with seasonality and viewing geometry: Implications for classification of Brazilian savanna physiognomies with MISR/Terra data. *Remote Sensing of Environment*, 107: 276-286.

Lillesand, T., Keifer, R.W. and Chipman, J.W., 2004, *Remote Sensing and Image Interpretation*. John Wiley & Sons, New York. pp. 785.

Lu, D., 2005, Aboveground biomass estimation using Landsat TM data in the Brazilian Amazon. *International Journal of Remote Sensing*, 26: 2509-2525.

Lucas, N.S. and Curran, P.J., 1999, Forest ecosystem simulation modelling: the role of remote sensing. *Progress in Physical Geography*, 23: 391-423.

Mäkelä, H. and Pekkarinen, A., 2004, Estimation of forest stand volume by Landsat TM imagery and stem-level field-inventory data. *Forest Ecology and Management*, 196: 245-255.

Maselli, F., Chirici, G., Bottai, L., Corona, P. and Marchetti, M., 2005, Estimation of Mediterranean forest attributes by the application of k-NN procedures to multitemporal Landsat ETM+ images. *International Journal of Remote Sensing*, 26: 3781-3796.

Pal, N.R. and Pal, S.K., 1993, A Review of Image Segmentation Techniques. *Pattern Recognition*, 26: 1277 – 1294.

Pinze, A. 1998, Tree isolation and species classification. In *Proceedings of the International Forum on Automated Interpretation of High Spatial Resolution Digital Imagery for Forestry*, 10 – 12 February 1998, Victoria, BC: Pacific Forestry Centre, Canada Forest service, Natural Resources Canada, 127-139.

Pitkänen J., 2001, Individual tree detection in digital aerial images by combining locally adaptive binarization and local maxima methods. *Canada Journal of Forest Research*, 31: 832-844.

Pouliot, D.A., King, D. J., Bell, F. W. and Pitt, D. G., 2002, Automated tree crown detection and delineation in high-resolution digital camera imagery of coniferous forest regeneration. *Remote Sensing of Environment*, 82: 322-334.

Pouliot, D.A. and King, D., 2005, Approaches for optimal automated individual tree crown detection in regenerating coniferous forests. *Canadian Journal of Remote Sensing*, 31: 255 – 267.

Rahman, M.M., Csaplovics, E. and Koch, B. 2005, An efficient regression strategy for extracting forest biomass information from satellite sensor data. *International Journal of Remote Sensing*, 26: 1511-1519.

Rees, W.G. 1990, *Physical principles of remote sensing*. Cambridge University Press, pp. 372.

Sabins, F.F., 1997, *Remote Sensing Principles and Interpretation*. 3rd Ed. W.H. Freeman, New York, pp. 494

Sharma, K. and Sarkar, A., 1998, A modified contextual classification technique for remote sensing data. *Photogrammetric Engineering and Remote Sensing*, 64: 273-280.

Song, C. Woodcock C. E. Seto, K. Pax, L. and Macomber, S., 2001, Classification and change detection using Landsat TM Data: When and How to correct Atmospheric Effects? *Remote Sensing of Environment*, 77: 241 – 250.

Souza, C.M. and Roberts, D., 2005, Mapping forest degradation in the Amazon region with Ikonos images. *International Journal of Remote Sensing*, 26: 425-429.

Steininger, M.K., 2000, Satellite estimation of tropical secondary forest above-ground biomass: Data from Brazil and Bolivia. *International Journal of Remote Sensing*, 21: 1139-1157.

Strahler, A., Woodcock, C. and Smith, J., 1986, On the nature of models in remote sensing. *Remote Sensing of Environment*, 20: 121 - 39.

Treitz, P., 2001, Variogram analysis of high spatial resolution remote sensing data: An examination of boreal forest ecosystems. *International Journal of Remote Sensing*, 22: 3895-3900.

Treitz, P. and Howarth, P., 2000, High Spatial Resolution Remote Sensing Data for Forest Ecosystem Classification: An Examination of Spatial Scale. *Remote Sensing of Environment*, 72: 268-289.

Utterer, J., Haara, A., Tokola, T. and Maltamo, M., 1998, Determination of the spatial distribution of trees from digital aerial photographs. *Forest Ecology and Management*, 110: 275-282.

Van Der Sanden, J.J. and Hoekman, D.H., 2005, Review of relationships between grey-tone co-occurrence, semivariance, and autocorrelation based image texture analysis approaches. *Canadian Journal of Remote Sensing*, 31: 207-213.

Wang, L., Sousa, W.P. and Gong, P., 2004, Integration of object-based and pixel-based classification for mapping mangroves with Ikonos imagery. *International Journal of Remote Sensing*, 25: 5655-5668.

Wang, Q., Adiku, S., Tenhune, J. and Granier, A., 2005, On the relationships of NDVI with leaf area index in a deciduous forest site. *Remote Sensing of Environment*, 94: 244-255.

Woodcock, C., Strahler, A. and Jupp, D. 1988. The use of variograms in remote sensing. I. Scene models and simulated images. *Remote Sensing of Environment*, 25: 323-348.

Woolley, J.T., 1971, Reflectance and transmittance of light by leaves. *Plant Physiology*, 47: 656-662.

Wulder, M. A. 1998, Optical remote sensing techniques for the assessment of forest inventory and biophysical parameters. *Progress in Physical Geography*, 22: 449 – 476.

Wulder, M., Niemann, K. O. and Goodenough, D., 2000, Local maximum filtering for the extraction of tree locations and basal area from high spatial resolution imagery. *Remote Sensing of Environment*, 73: 103-114.

Wulder, M.A. and White, J.C., 2004, Comparison of airborne and satellite high spatial resolution data for the identification of individual trees with local maxima filtering. *International Journal of Remote Sensing*, 25: 2225-2232.

Xu, Y. Prather, J. W., Hampton, H.M., Aumack, E.N., Dickson, B.G. and SISK, T.D., 2006, Advanced exploratory data analysis for mapping regional canopy cover. *Photogrammetric Engineering and Remote Sensing*, 72: 31-38.

Zheng, D. Rademacher, J., Chen, J., Crow, T., Bresse, M., Moine, J. L. and Ryu, S. 2004, Estimating aboveground biomass using Landsat ETM+ data across a managed landscape in northern Wisconsin, USA. *Remote Sensing of Environment*, 93: 402-411.

CHAPTER 3

STUDY AREA

3.1 Introduction

This study has been conducted in the Kwazulu-Natal province of South Africa. The province is situated on the eastern-half of the country. The study sites are situated approximately 50 km south of Pietermaritzburg around the town of Richmond. The area is located in what is known locally as the southern Natal Midlands. The sites chosen for this research are all managed by the Midlands District of MONDI SA – Forest Company. Geographically, the site lies between 29° 43' 4" and 29° 56' 49" South and 30° 1' 43" and 30° 17' 26" East. Figure 3.1 provides a map of the study site, the location of the sampled forest stands.

3.2 Climate

The study area falls within the summer rainfall region of South Africa experiencing cold, dry winters and warm, wet summers. Figure 3.2 provides some information regarding the climate of the study area (Temperature in °C is on the left y-axis while rainfall is on the right y-axis). Mean annual rainfall ranges from 746 mm to 1100 mm (Schulze, 1997). Rainfall is associated with either frontal weather systems originating from the south or thunderstorms generated from convection activity. Temperatures range from the high 20's to below 10 °C. The extreme temperature changes are a function of altitude and proximity to the warm Indian Ocean, with higher lying areas experiencing much colder temperatures than low lying areas. This has a direct impact on the site selection for various plantation species and will be discussed in section 3.5 below.

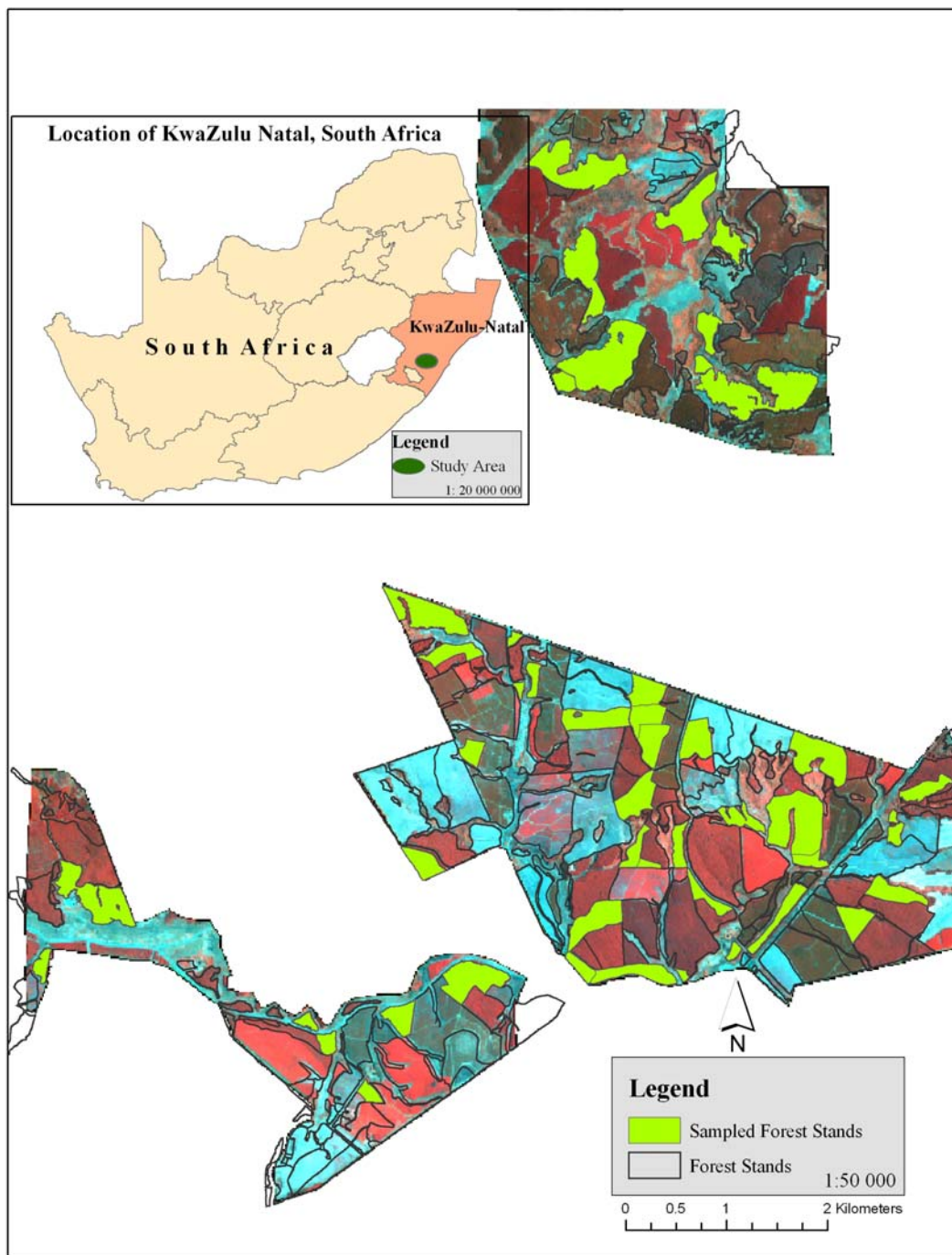


Figure 3.1 Map showing the location of the study area

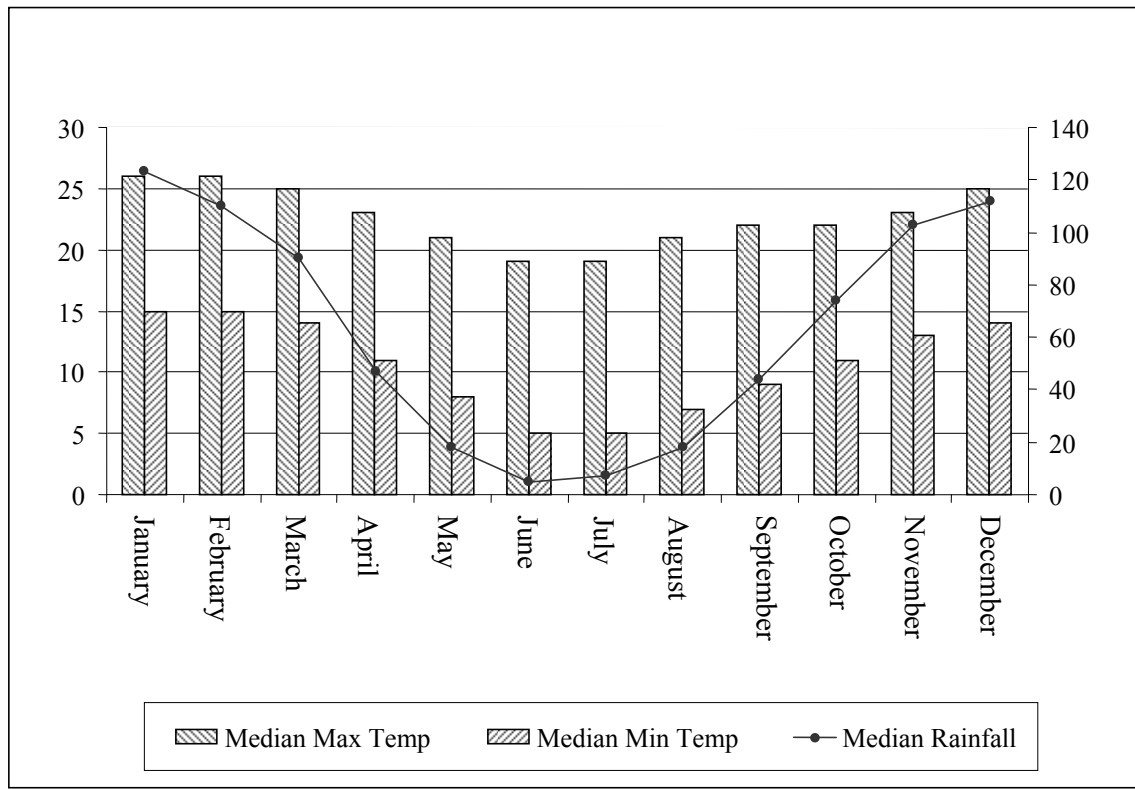


Figure 3.2 Climate of the Richmond area and surrounds (Schulze, 1997).

3.3 Geology and soils

The soils of the study area characterized by fine, sandy clay and humic topsoils underlain by yellow or red apedal subsoils. Dominant soil forms are Inanda and Mogwa, with Hutton being the subdominant soil form (Pallett, 1993). Clay content varies between 34 % and 45 % in topsoil horizons and attains values of up to 60 % in deeper subsoils (Kunz and Pallett, 2000). Dolerite dykes and sills occur commonly in the landscape with associated “red” soils of the Hutton and Inanda forms (Kunz and Pallett, 2000). Narrow riparian areas have hydeomorphic soils of the Tukulu and Katspruit forms. The Mispah soil form is also present in this area, as are shallow soils on shales (Kunz and Pallett, 2000).

3.4 Topography

The topography of the Richmond area is flat with undulating hills and is classified by Schulze (1997) as being low mountains. Altitude ranges from 362 meters to over 1500 meters with an average altitude of around 874 meters. Once past the Umkomaas River valley, the topography becomes progressively flatter as one moves west towards the Eastern Cape.

3.5 Land Use

The primary land use in the Richmond area is agriculture. The primary agricultural activities include plantation forestry, sugar cane and to a lesser extent dairy farming. Local subsistence farming also takes place in and around rural villages. The plantation forests are stocked with exotic hardwood and softwood species that are grown primarily for pulp and paper production, with smaller industries in the area making use of timber for furniture and construction purposes. Softwood species are of the genus *Pinus* with *P. patula*, *P. taeda* and *P. elliottii* and hardwood species are either *eucalyptus* (Gum) or *acacia* (wattle). The *eucalyptus* species (the subject of this research) can be broken into two categories, defined by their wood density. Soft gums (sub-tropical) are generally grown in the warmer areas and have a lower wood density than the hard gums (cold-tolerant). Soft gums include the *E. saligna* and *E. grandis* species while hard gums include the *E. dunnii*, *E. nitens* and *E. smithii* variants. Recently the industry has been experimenting with clonal hybrids such as *E. grandis* x *E. nitens*.

3.6 References

Schulze, R. E. 1997, South African Atlas of Agrohydrology and Climatology. Water Research Commission, Pretoria, Report TT82/96, pp. 31.

Pallett, R.N. 1993, Forest land types of the Natal Region. SAPPI Forests (pty) Ltd.

Kunz, R.P., Pallett, R.N. 2000, A stratification system based on climate and lithology for locating commercial forestry permanent sample plots. Institute for commercial forestry research Bulletin series 01/2000. Pietermaritzburg.

CHAPTER 4

Image-based reflectance conversion of ASTER and IKONOS imagery as precursor to structural assessment of plantation forests in KwaZulu-Natal, South Africa

* This chapter is based on:

Gebreslasie, M., Ahmed, F. B., and van Aardt, J. (2008) Image-based atmospheric correction of ASTER and IKONOS imagery for plantation forests in KwaZulu-Natal, South Africa *Southern Forests: A Journal of Forest Science* (Submitted)

Abstract. Reflectance-converted imagery is a requirement for establishing temporally robust remote sensing algorithms, given the reduction of time-specific atmospheric effects. Thus, in this study image-based atmospheric correction methods for ASTER and IKONOS imagery for retrieving surface reflectance of plantation forests in KwaZulu-Natal, South Africa were evaluated. This effort formed part of a larger initiative that focused on retrieval of forest structural attributes from resultant reflectance imagery. Atmospheric correction methods in this study included the apparent reflectance model (AR), dark object subtraction model (DOS), and the cosine approximation model (COST). Spectral signatures derived from different image-based models for ASTER and IKONOS was inspected visually as first departure. This was followed by comparison of the total accuracy and Kappa index computed from supervised classification of images that were derived from different image-based atmospheric correction of ASTER and IKONOS imagery. The classification accuracy of DOS images derived from ASTER and IKONOS imagery exhibited percentages of 93.3 % and 94.7 %, respectively. Classification accuracies for images from AR and COST, on the other hand, resulted in lower accuracy values of 87.9 % and 83.6 % for ASTER and 90.5 % and 92.8 % for IKONOS, respectively. We concluded that the image-based DOS model was better suited to atmospheric correction for ASTER and IKONOS imagery in this study area and for the purpose of forest structural assessment. This has important implications for the operational use of similar imagery types for forest inventory approaches.

Keywords: Image-based atmospheric correction, surface reflectance, ASTER, IKONOS, plantation forests

4.1 Introduction

Remote sensing satellite sensors typically record the intensity of electromagnetic radiation (EMR) as digital number (DN) values (Jensen, 1996). The DN values of each

image are specific to the type of sensor and the atmospheric condition during image acquisition (Richter, 1996). In principle any sensor that observes the earth's surface in the visible or near-infrared regions of the electromagnetic spectrum will record a signal that consists of two kinds of brightness (Lillesand et al., 2004). The first brightness is due to reflectance from the earth's surface, which is usually of interest for remote sensing scientists. The second is brightness related to the signal interacting with atmospheric particles and is ultimately seen as image noise that should be removed. Atmospheric correction is an essential component of the image processing chain, especially as far as multi-temporal studies are concerned (Lillesand et al., 2004). Many studies are aimed at establishing proof-of-concept, and as such implement radiance imagery and stop short of conversion to reflectance. For example, in satellite remote sensing research conducted in South Africa, Ghebremicael et al. (2003) and Norris-Rogers (2005) applied either radiance-based analysis or reflectance at top of atmosphere. This can be circumvented by applying a number of existing atmospheric correction methods to remove or reduce atmospheric effects and extract surface reflectance.

Methods that convert radiance imagery to reflectance generally are grouped into radiative transfer models and relative atmospheric correction or reflectance conversion models. Radiative transfer models include MODTRAN (Berk et al., 1998), FLAASH (Matthew et al., 2002), and 6S (Vermote et al., 1997). Various researchers have claimed that radiative transfer models provide higher levels of accuracy when compared to relative atmospheric correction models (Wu et al., 2005; Kotchenova et al., 2006; Richter et al., 2006). However, Tachiiri (2005) and Kotchenova et al., (2006) ascertained that the operational aspect of radiative transfer models requires a large selection of parameters, which are often difficult to measure. Such approaches typically require *in-situ* measurements of Rayleigh scattering, aerosol attenuation, water vapor absorption, and ozone absorption at the time of satellite over flight (Vermote et al., 1997; Berk et al., 1998). These measurements are often difficult to obtain in practice and the procedures involved are too expensive to be used operationally. The caveat is that unacceptable levels of accuracy would result if the default parameters of these methods are applied (Wu et al., 2005).

Relative atmospheric correction methods avoid the measurement of atmospheric components at the time of satellite over-flight. Examples of these methods include the apparent reflectance model (Caselles and Garcia, 1989), DOS (Kaufman and Sendra, 1988), and COST (Chavez, 1996). Furthermore, the input information required to run the relative atmospheric correction methods are derived from the image itself (Karpouzli and Malthus, 2003). One primary assumption to take note of, however, is that these methods assume a linear relationship between the radiances at top of atmosphere and at ground level for the variety of earth features present in the image for a specific image band (Chavez, 1996; Perry et al., 2000). Relative atmospheric correction methods are useful when limited ground level image information is available. These methods are aimed at simplification of atmospheric correction, further minimizing the cost of image processing.

Operational forestry inventory could greatly benefit from atmospheric correction that is based on the acquired digital image itself, without the need for atmospheric measurements during satellite over-flight. This would reduce cost of operations, while also ensuring that algorithms are transferable through time, given the use of reflectance, as opposed to radiance. However, a limited body of literature exists that might assist in the selection of an effective method for particular applications in different climatic zones of the world (Song et al., 2001; Lu et al., 2002). This part of the study therefore has as objective the evaluation of relative atmospheric correction methods for retrieving canopy surface reflectance using ASTER and IKONOS imagery for study sites located in the warm-temperate KwaZulu-Natal province of South Africa, which is home to large scale industrial forestry operations. This study presented results from a visual evaluation of atmospheric correction outcomes as well as verifying which approach is best suited to general forestry operations, with “forest classification” used as a proxy for such operations.

4.2 Materials and Methods

4.2.1 Study Site

The study area used to assess the effectiveness of atmospheric correction methods is located in a warm temperate zone in the southern KwaZulu-Natal province of South Africa, also known as the KwaZulu-Natal Midlands. The sites chosen for this research are all managed by MONDI-SA Forest Company. Geographically, the site lies between 29° 43' 4" and 29° 56' 49" South and 30° 1' 43" and 30° 17' 26" East, as shown in Figure 4.1. It contains many water bodies, including the Umkomaas river valley, where lakes formed as a result of gravel extraction and are now used for recreation, and includes 10 large and medium reservoirs that provide water to the livestock and poultry farms in the area.

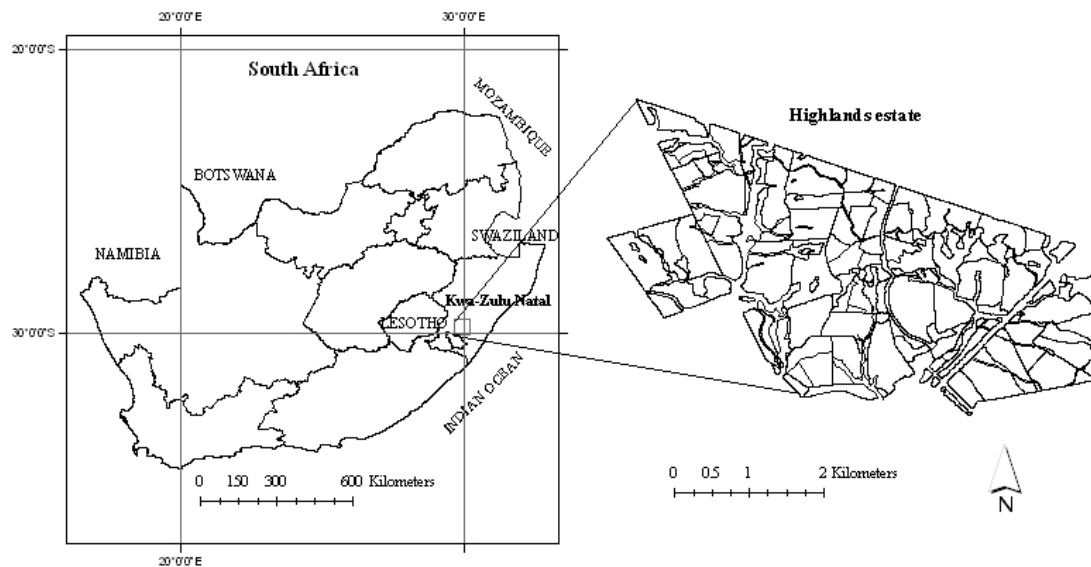


Figure 4.1 Map showing the location of the study site

The study area falls within the summer rainfall region of South Africa and experiences cold dry winters and warm wet summers. The mean annual rainfall ranges from 746 mm to 1100 mm (Schulze, 1997). Rainfall is associated with either frontal weather systems originating from the south or thunderstorms generated from convection activity.

Temperatures range from upper 20 °C to below 10 °C. The extreme temperature change is a function of altitude and proximity to the warm Indian Ocean with higher lying areas experiencing much colder temperatures than low lying areas. Generally, the area is characterized by dense natural and commercial forests. Large areas are stocked with exotic hardwood and softwood species that are grown primarily for pulp and paper production. Sugar cane production and dairy farming, to a lesser extent, are also practised in the area. Local subsistence farming is prevalent in and around rural villages.

4.2.2 Remote sensing data

ASTER and IKONOS imagery, which cover the entire study area, were captured during October, 2006. The ASTER data were delivered in HDF format and processed to radiance level. The spatial resolution of the ASTER image is 15 m in the visible-near-infrared (VNIR) region and 30 m in the shortwave-infrared (SWIR) region (Abrams, 2000). The IKONOS images were acquired at an off-nadir angle (25°) with pixel size of 4 m in the VNIR region. The data were provided in Geo-tiff format with metadata and rational polynomial coefficient equations (RPC). The RPC file contains rational function polynomial coefficients that are generated by the data provider based on the position of the satellite at the time of image capture. Both data sets were geometrically corrected using ancillary metadata, e.g., RPC inputs, as well as differentially corrected GPS ground control points and a digital terrain model and the over all total root mean square error (RMSE) of less than half a pixel was obtained.

4.2.3 Atmospheric Correction Methods

The conversion of remotely sensed DN or radiance values to at satellite radiance (L_{rad}) is the first step in the relative atmospheric correction procedure. Various methods of DN to L_{rad} conversion exist; however, equations 1 and 2 were used to convert digital numbers of ASTER and IKONOS, respectively, to satellite radiance. Coefficients for the derivation of L_{rad} , such as the *calCoef* factor, and bandwidths for ASTER and IKONOS imagery are listed in Table 4.1.

$$L_{rad} = (DN-1) * \text{Unit conversion coefficient} \quad (1)$$

$$L_{rad} = \frac{10^4 * DN}{calCoef * Bandwidth} \quad (2)$$

where:

L_{rad} = satellite radiance ($mWcm^{-2} ster^{-1} \mu m^{-1}$)

DN = Digital Number

$calCoef$ = calibration coefficient

Table 4.1 ASTER and IKONOS band dependent parameters

Bands	ASTER			IKONOS		
	calCoef [mW/cm ² /sr]	ESUN	Bandwidth (μm)	calCoef [mW/cm ² /sr]	ESUN	Bandwidth (μm)
1	None	None	None	72.8	1939	0.071
2	67.6	1847	0.089	72.7	1847	0.089
3	70.8	1553	0.066	94.9	1536	0.066
4	42.3	1118	0.13	84.3	1147	0.13

The next step was to correct effects due to both solar angle and the atmospheric conditions, with the output being surface reflectance (L_{λ}). Mean solar irradiance ($ESUN$) for ASTER and IKONOS are listed in Table 4.1. These coefficients were obtained from the user guide for each sensor, which can also be computed based on the image acquisition date and time, and the longitude and latitude of the study area. After computing the at-satellite radiance for the imagery, relative reflectance conversion models were applied.

4.2.3.1 Apparent reflectance model

The apparent reflectance model (Equation 3) was used in the first instance. This method corrects the effects caused by variations in solar radiance and sun zenith angle, while ignoring the effects caused by atmospheric scattering and absorption. Users should thus take note that this is not a true atmospheric correction, but merely a conversion to apparent reflectance without taking atmospheric conditions into account.

$$L\lambda = \frac{(\Pi * L_{rad} * d^2)}{(ESUN * \cos \theta_z)} \quad (3)$$

where :

$L\lambda$ = Satellite reflectance

Π = 3.14152

L_{rad} = Satellite radiance ($\text{mWcm}^{-2} \text{ster}^{-1} \mu\text{m}^{-1}$)

d^2 = the square of the Earth-Sun distance in Astronomical units

$ESUN$ = mean solar irradiance in ($\text{mWcm}^{-2} \mu\text{m}^{-1}$)

θ_z = sun zenith angle in radiance

The earth-sun distance (d) can be obtained from the Astronomical Almanac according to the image acquisition date that is Julian day (refer to Table 4.2). The square of the Earth-Sun distance in astronomical units (d^2) is calculated using equation 4,

$$d^2 = (1 - 0.01674 \cos (0.9856 (\text{Julian day} - 4)))^2 \quad (4)$$

Table 4.2 Julian day for IKONOS and ASTER

Characteristic	IKONOS	ASTER
Date/time(GMT)	2006-10-23/08:17	2006-10-10/ 10:55
Julian day	2454032	2454050
d^2	1.033108	1.00882

4.2.3.2 Dark object subtraction model

The DOS model is also strictly an image-based procedure, corrects for the effects caused by sun zenith angle, solar radiance, and atmospheric scattering, but cannot correct for atmospheric absorption (Wu et al., 2005). Equation 5 below was applied to ASTER and IKONOS imagery:

$$L\lambda = \frac{[\Pi * d^2 * (L_{rad} - L_{rad\ haze})]}{(ESUN * \cos \theta_z)} \quad (5)$$

where: $L_{rad\ haze}$ is Atmospheric scattered path radiance for band

The haze value was derived from the image DN values using the histogram of a dark object method for the purposes of this study. An iterative process was used to generate more acceptable values in image locations with limited or no black or high absorption features. This was achieved by iteratively using a lower starting haze value until no over corrections occurred. That is, if an initialization haze value resulted in the predicted values for other bands being higher than some of the actual image DNs, a lower starting haze value was iteratively selected. Chavez (1988) contended that a realistic haze value for most warm temperate zones should range between 1% and 2%.

4.2.3.3 Cosine of atmospheric transmittance model

The COST model (Equation 6) is also an image based procedure, which incorporates all the corrections of the above two models and also takes into account the atmospheric transmittance components.

$$R\lambda = \frac{[\Pi * d^2 * (L_{rad} - L_{rad\ haze})]}{(TAU_v * ESUN * \cos \theta_z * TAU_z)} \quad (6)$$

where:

TAU_v = Atmospheric transmittance along the path from the ground surface to the sensor

TAU_z = Atmospheric transmittance along the path from the sun to the ground surface

TAU_v and TAU_z typically can be estimated from optical thickness. Chavez (1996) proposed two approaches to estimate the atmospheric transmittance. One method uses the cosine of the solar zenith angle for TAU_z , which is called the COST model. Another method uses default TAU_z values, which are the average for each spectral band, derived from the radiative transfer code. TAU_v was set equal to 1, because the viewing (zenith) angles for both satellites used in this study were minimal.

4.3 Accuracy Assessment of Atmospheric Corrections

The most appropriate way to evaluate atmospheric correction approaches for any given study area, is to compare *in situ* measurements of surface reflectance at the time of image acquisition with estimates for these parameters resulting from the various approaches to atmospheric correction (Moran et al., 1997). Unfortunately, such *in situ* measurements are not generally available, which was the case in this study. This caveat can be mitigated through comparison of spectral signatures from the same land cover, which were extracted from both images after AR, DOS, and COST atmospheric correction methods were applied. Such a qualitative comparison can be used to assess which atmospheric correction method resulted in the most reasonable outcome based on the spectral distribution at different wavelengths for that land cover. This approach is based on the assumption that the reflectance for the same land cover for each correction model should be similar for disparate, but spectrally comparable imaging sensors, given that atmospheric and radiometric effects are removed and environmental conditions remain similar.

An additional, quantitative attempt was made to evaluate the usefulness of these methods based on the accuracies of image supervised classifications using a maximum likelihood classification rule. The most crucial aspect in traditional supervised classification is the selection of training pixels. The selection of training samples largely depends upon the knowledge of the study area and data, well as the classes to be extracted (ERDAS, 2006). In this study a database from a forest company, which lists the land cover, plantation species (*Acacia*, *Eucalyptus*, and *Pinus*), and age, was used to support the selection of the training samples and to validate the classification results. We included specifically *wattle* (*Acacia mearnsii*), *Eucalyptus* (*E. grandis* and *E. Grandis x nitens*), and *pine* (*P. patula*) in the training sample selection. Supervised classification was conducted using the identified training pixels for the atmospherically corrected data, i.e., AR, DOS, and COST processed imagery. Finally, accuracy assessment of classification results was performed based on an error matrix. The overall classification accuracies and Kappa coefficients were used to compare the classification accuracy assessments among atmospheric correction approaches.

4.4 Results and Discussion

4.4.1 Visual Assessment

Figure 4.2 shows a comparison of forest reflectance signatures from ASTER and IKONOS imagery after atmospheric correction using the AR, DOS, and COST correction methods and the maps of ASTER and IKONOS after atmospheric correction are also illustrated in appendix 4.1 and 4.2. The reflectances of each band, such as green, red and NIR, is represented by the average values from matured stands of wattle, *Eucalyptus*, and *Pine* forest stands, as well as from roads and open areas within the study site.

The AR model for reflectance conversion resulted in the highest surface reflectance in the visible and near infrared bands (Figure 4.2 a-f), when compared to the DOS and COST approaches in the case of the ASTER and IKONOS imagery. This was attributed to the fact that the apparent reflectance model only corrects for the effects caused by the sun angle, sun-earth distance, and the solar radiance. This model ignores the effects of atmospheric scattering. However, reflectance in the visible bands is heavily impacted by atmospheric scattering, which results in image additive effects (Lillesand et al., 2004). While the DOS and COST model correct for the sun angle, sun-earth distance, solar radiance, and atmospheric scattering, the COST model additionally corrects for the atmospheric transmittance along the path (Chavez, 1996). The COST model exhibited similar reflectance values to the DOS model in the visible bands (Figure 2 a, b, d, and e). This was attributed to the geometrical source-target-sensor properties when the satellite images were captured ($\theta < 35^\circ$); atmospheric transmittance is less affected by atmospheric conditions at smaller observation/zenith angles (Wu et al., 2005). The results from Wu et al. (2005) showed that the COST model suffers from over- and under-correction when the sensor angle is respectively higher or lower than 35° .

The NIR reflectance of ASTER and IKONOS imagery (Figure 4.2 c and f), derived from the COST model, was distinctively lower than that from the DOS model used in this study. This was attributed to the fact that atmospheric scattering is limited at longer wavelengths (Lillesand et al., 2004) and as a result the COST model over-corrected in this spectral region (Wu et al., 2005). Wu et al. (2005) corroborated this finding by

concluding that the COST model underestimated (over-corrected) surface reflectance in especially the near-infrared spectral region. This lead to our conclusion that the DOS model provided the most reasonable results in the case of this study site and source-target-sensor geometry.

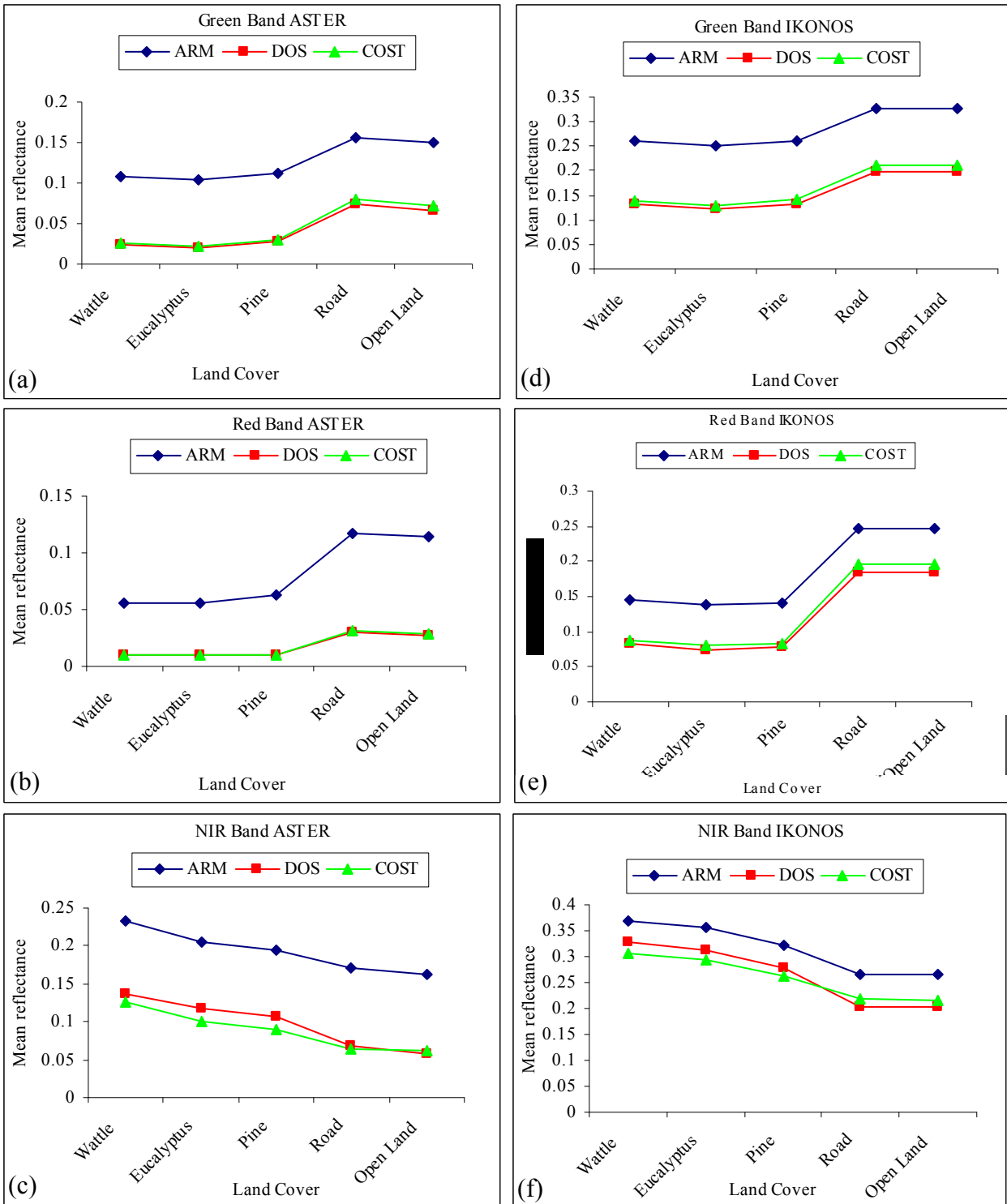


Figure 4.2 Surface reflectance signatures of derived using the ARM, DOS, and COST reflectance conversion models for ASTER and IKONOS imagery

4.4.2 Classification

Supervised classification was also employed to assess the performance of the AR, DOS, and COST reflectance conversion or atmospheric correction methods. The overall supervised classification accuracies are presented in Table 4.3. Comparison of the overall accuracies and Kappa indices of the three reflectance images, computed from ASTER and IKONOS radiance imagery, showed that the accuracy of the DOS image was marginally higher than for the other two models. The AR model performed surprisingly well, given that this model generally overestimates surface reflectance, since atmospheric scattering and absorption are neglected in its calculation. The apparent reflectance model approach does not correct for the effects of the atmosphere, it only converts the radiance data into normalised, unit-less reflectance. This is a very popular method since it is easy to implement and is less likely to produce an erroneous result.

This study concluded that the improvement in classification accuracy of DOS over COST resulted from the viewing angle (θ) being considered in the COST model. Wu et al. (2005) have shown that areas that are located away from the direct viewing angle (nadir) tend to be strongly over-corrected or under-corrected. Instead of reducing the effect of atmospheric effects on surface reflectance, the COST model potentially could increase image degradation in areas at off-nadir viewing.

It should be noted that a variety of sensor and scene characteristics have been assumed negligible in terms of impact on this study. These characteristics include differences related to sensor spatial and spectral specifications, scene geometry, and scene component qualities. This latter aspect refers specifically to the nature of the selected land cover classes and their differentiability in spectral space. We assumed that these classes are spectrally separable to a reasonable degree and that this separability would pronounce itself in the case of both sensors. More research is required to establish whether or not any one reflectance conversion approach might prove superior in the case of different land cover classes or varying multispectral sensor characteristics.

Table 4.3 Comparative data of supervised image classification accuracies for all three reflectance conversion approaches

Classified images	ASTER Image			IKONOS Image		
	AR model	DOS model	COST model	AR model	DOS model	COST model
Total accuracy (%)	87.9	93.3	89.6	90.5	94.8	92.8
Kappa index	0.78	0.85	0.72	0.89	0.94	0.90

4.4.3 Conclusions

This paper discussed the basic concepts and theory of relative atmospheric correction methods, followed by qualitative and quantitative evaluation of the performance of three popular reflectance conversion methods. Spectral signature interpretation and supervised classification were applied to compare the performance of reflectance conversion methods for ASTER and IKONOS imagery in a warm temperate plantation forestry environment. Both assessment methods indicated that the dark object subtraction (DOS) atmospheric correction method for ASTER and IKONOS imagery, given image and sensor parameters and the specific study site, performed better than the apparent reflectance (AR) and Cosine of atmospheric transmittance (COST) models.

Many remote sensing researchers (e.g., Lu et al., 2002; Wu et al., 2005) recommend as simple as possible atmospheric correction method for remote sensing forestry applications. Although we concluded that the DOS model (ASTER and IKONOS imagery) was best suited to the study site in question, the influence of specific sensor characteristics and spectral scene properties were not investigated. We also argue that the two true atmospheric correction methods, namely DOS and COST, are preferable to the AR reflectance conversion approach, since the latter does not take atmospheric conditions into account. This could prove limiting in the case of multi-temporal studies or applications. It is furthermore recommended that future work focus on validation of the results presented here, using *in situ* measurements of surface reflectance at the time of image acquisition. However, it is encouraging to note that relatively simple, non-radiative transfer models potentially could be used to convert imagery to reflectance for the purposes of multi-temporal plantation forestry operations in temperate warm climates.

4.4.4 Acknowledgements

This study was conducted as part of a remote sensing cooperative program between MONDI Business Paper SA, the Council for Scientific and Industrial Research (CSIR), and the University of KwaZulu-Natal to investigate the potential of satellite remote sensing imagery for prediction of plantation forest structural attributes. The authors would like to thank Wesley Roberts, Solomon Gebremariam, Thamsanqua Mzinyane, and Wesley Naidoo for their assistance during field work. Financial support for this study was provided by the CSIR and MONDI BP.

4.4.5 References

Abrams, M., 2000, The Advanced Spaceborne Thermal Emission and Reflection Radiometer (ASTER): Data products for the high spatial resolution imager on NASA's Terra platform. *International Journal of Remote Sensing*, 21: 847– 859.

Berk, A., Bernstein, L.S., Anderson, G.P., Acharya, P.K., Robertson, D.C. and Chetwynd, J.H., 1998, MODTRAN cloud and multiple scattering upgrades with application to AVIRIS. *Remote Sensing of Environment*, 65: 367 – 375.

Caselles, V. and Garcia, M.L., 1989, An alternative approach to estimate atmospheric correction in multitemporal studies. *International Journal of Remote Sensing*, 10: 1127 – 1134.

Chavez, Jr., P.S., 1988, An improved dark-object subtraction technique for atmospheric scattering correction of multispectral data. *Remote Sensing of Environment*, 24: 459 – 479.

Chavez, Jr., P.S., 1996, Image-based atmospheric corrections revisited and improved. *Photogrammetric Engineering Remote Sensing*, 62: 1025 – 1036.

ERDAS 2006, LeicaGeosystems Geospatial Imaging, LLC

Ghebremicael, S.T., Smith, C.W. and Ahmed, F., 2004, Estimating the leaf area index (LAI) of Black Wattle from Landsat ETM+ satellite imagery. *Southern African Forestry Journal*, 201: 3-12.

Jensen, J.R., 1996, *Introductory Digital Image Processing: A Remote Sensing Perspective*, Prentice-Hall, Englewood Cliffs, NJ.

Karpouzli, E. and Malthus, T., 2003, The empirical line method for the atmospheric correction of IKONOS imagery. *International Journal of Remote Sensing*, 24: 1143 – 1150.

Kaufman, Y.J. and Sendra, J., 1988, Algorithm for automatic atmospheric corrections to visible and near-IR satellite imagery. *International Journal of Remote Sensing*, 9: 1357 – 1381.

Kotchenova, S.Y., Vermote, E.F., Matarrese, R. and Klemm, F.J., 2006, Validation of a vector version of the 6S radiative transfer code for atmospheric correction of satellite data. Part I: Path radiance. *Applied Optics*, 45: 102 - 115

Lillesand, T.M., Kiefer, R. W. and Chipman, J. W., 2004, *Remote sensing and image interpretation*. New York: John Wiley and Sons, pp. 785

Lu, D., Mausel, P., Brondizio, E. and Moran, E., 2002, Assessment of atmospheric correction methods for Landsat TM data applicability to Amazon basin LBA research. *International Journal of Remote Sensing*, 23: 2651- 2671.

Matthew, M.W., Adler-golden, S.M., Berk, A., Felde, G., Anderson, G.P., Gorodetzky, D., Paswaters, S. and Shippert, M., 2002, Atmospheric Correction of Spectral Imagery: evaluation of the FLAASH algorithm with AVIRIS Data. *Applied Imagery Pattern Recognition Workshop, Proceedings*. 31st.

Moran, M.S., Inoue, Y. and Barns, E.M., 1997, Opportunities and limitations for image-based remote sensing in precision crop management. *Remote Sensing of Environment*, 61: 319– 346.

Norris-rogers, M., 2006, An investigation into using textural analysis and change detection techniques on medium and high spatial resolution imagery for monitoring plantation forestry operation, unpublished PhD thesis February 2006.

Perry, E.M., Warner, T. and Footers, P., 2002, Comparison of atmospheric modeling versus empirical line fitting for mosaicking HYDICE imagery. *International Journal of Remote Sensing*, 21: 799 – 803.

Richter, R., 1996, A spatial adaptive fast atmospheric correction algorithm. *International Journal of Remote Sensing*, 17: 1201 – 1214.

Richter, R., Schläpfer, D. and Müller, A., 2006, An automatic atmospheric correction algorithm for visible/NIR imagery. *International Journal of Remote Sensing*, 27: 2007 – 2085

Schulze, R.E., 1997, South African Atlas of Agrohydrology and Climatology. Water Research Commission, Pretoria, Report TT82/96, pp. 270.

Song, C., Woodcock, C.E. and Seto, K. C., 2001, Classification and Change detection using Landsat TM data: When and how to correct atmospheric effects? *Remote Sensing of Environment*, 75: 230 – 244.

Tachiiri, K., 2005, Calculating NDVI for NOAA/AVHRR data after atmospheric correction for extensive images using 6S code: A case study in the Mardabit District, Kenya. *ISPRS Journal of Photogrammetry and Remote Sensing*, 59: 103 – 114.

Vermote, E.F., Tanré, D., Deuzé, J.L., Herman, M. and Morcrette, J.J., 1997, Second simulation of the satellite signal in the solar spectrum: An overview. *IEEE Transactions on Geoscience and Remote Sensing*, 35: 675 – 686

Wu, J., Wang, D. and Bauer, M.E., 2005, Image-based atmospheric correction of QuickBird imagery of Minnesota cropland. *Remote Sensing of Environment*, 99: 315 – 325

CHAPTER 5

Estimating plot-level forest structural attributes using high spectral resolution ASTER satellite data in even-aged *Eucalyptus* plantation forests, in KwaZulu-Natal, South Africa

* This chapter is based on:

Gebreslasie, M., Ahmed, F. B., and van Aardt, J. (2008) Estimating plot-level forest structural attributes using high spectral resolution ASTER satellite data in even-aged *Eucalyptus* plantations, in KwaZulu-Natal, South Africa. *Southern Forests: A Journal of Forest Science* 71, 3: 227-236.

Abstract. This study assessed the suitability of both visible and shortwave infrared reflectance bands and various vegetation indices derived from ASTER imagery for estimating forest structural attributes of *Eucalyptus* species in the midlands southern KwaZulu-Natal, South Africa. The empirical relationships between forest structural attributes, i.e. stems per hectare (SPHA), diameter at breast height (DBH), mean tree height (MTH), basal area and volume, and ASTER data were derived using correlation and Canonical Correlation Analysis (CCA). The results indicated weak relationships between the studied forest structural attributes and ASTER data. In the younger plantation stands (4-6 years) the adjusted R^2 values from CCA regression for SPHA, DBH, MTH, basal area and volume were 0.54, 0.64, 0.34, 0.25 and 0.30, respectively. The adjusted R^2 values in the mature stands (7-9 years) were distinctly weaker with values of 0.51, 0.56, 0.25, 0.20, and 0.27 for SPHA, DBH, MTH, basal area, and volume, respectively. Although results could be construed as implying that ASTER satellite data are not amenable to mono-culture plantation structural attribute estimation, it was still encouraging that up to 64% of structural parameter variation could be explained by spectral data alone.

Keywords: ASTER dataset, spectral vegetation indices, plantation structural attributes

5.1 Introduction

Forest structural attributes, such as volume, basal-area, SPHA, and tree height are important data needed for effective forest management. Currently, in South Africa, field surveys are used to gather information regarding the structural attributes of plantation forests. Even though this method provides highly accurate measurements of forest structural attributes, it is costly and time consuming (Trotter et al., 1997; Ahmed 2006). Many researchers, e.g., Wulder (1998), Hyyppä et al. (2000), Lu et al. (2004), and McRoberts and Tomppo (2007), have recommended that remotely sensed data be investigated as an alternative means of acquiring information about forest resources. A large number of remote sensing studies has shown that prediction of forest structural attributes using optical remote sensing has been based on empirical relationships established between the field measured data and remote sensing data, such as wavelength

bands and vegetation indices. A variety of vegetation indices have been developed using broad-band remotely sensed data based on the spectral features of green vegetation.

The most common indices are the Simple Ratio (SR) (Birth and McVey 1968), Difference Vegetation Index (DVI) (Tucker 1979), and Normalized Difference Vegetation Index (NDVI) (Rouse et al., 1973). These indices enhance the spectral contribution of vegetation, while minimising that of the background. However, the empirical relationship between forest structural attributes and vegetation indices could be affected by canopy closure, under-storey vegetation, and soil background reflectance (Spanner et al., 1990). Thus, other indices, e.g., NDVIc (Nemani et al., 1993), Modified Soil-Adjusted Vegetation Index (MSAVI; Qi et al., 1994), Reduced Simple Ratio (RSR; Brown et al., 2000), Perpendicular Vegetation Index (PVI; Richardson and Wiegand, 1977), and Transformed Soil-Adjusted Vegetation Index (TSAVI; Baret and Guyot, 1991) were developed to reduce the effects of background reflectance. Brown et al. (2000) recommended that the integration of the shortwave infrared bands in vegetation indices could unify different cover types and reduce the background effects. In addition, remote sensing data transformation methods like Principal Components Analysis appear to provide acceptable estimation results (Lu et al., 2004).

Remote sensing studies, conducted in forested areas, have indicated that relationships between forest structural attributes and remote sensing data differ depending on the geographic settings of the study sites and level of management. Lu et al. (2004) analysed forest structural attributes and Landsat TM data in Brazilian Amazon basin. Single band TM-5 and linear transformed indices such as 1st principal component (PC1), brightness of the tasselled cap transform, and albedo were strongly correlated with forest structural attributes. Freitas et al. (2005), on the other hand, found a significant relationship between moisture vegetation index using band 5 and band 7 of Landsat TM-5 with forest structure attributes using linear regression methods in Atlantic rainforests. In addition, Hall *et al.* (2006) explored the empirical relationships between forest structural attributes and Landsat ETM+ data in west-central Alberta, Canada. The study concluded that bands 3, 4, 5, and 7 returned the strongest relationships with forest structural attributes prediction. In a managed forest plantation in northern Wisconsin, USA, Zheng et al.

(2004) found that DBH estimates for hardwood forest were strongly related to stand age and near-infrared reflectance, while for softwood forests the estimates were strongly related to the NDVI_c. Another study in mountain birch forests northernmost Finland conducted by Heiskanen (2006) indicated that NDVI, MSAVI and Simple Ratio (SR) of ASTER data showed a significant relationship with biomass and LAI. Sivanpillai et al. (2006), in turn, used multivariate regression techniques to generate relationships between Landsat ETM+ reflectance values and commercially managed loblolly pine stand characteristics in east Texas, USA. They suggested that combinations of NDVI, a simple ratio of ETM4/ETM3, and the tasselled cap wetness index were better predictors of stand age and stand density for young stands, whereas principal components yielded valuable information about the relationship between stand structure and reflectance values recorded by the ETM+ sensor for mature stands. These studies in a way indicated that satellite data in general are potentially valuable for characterizing forest structural attributes in a variety of environments, differently.

The statistical analysis used for understanding the relationships among spectral remote sensing responses and forest structural attributes should accommodate the possibility that these relationships may require complex solutions. Lu et al. (2004) and Sivanpillai et al. (2006) suggested that multiple-variable models offered substantial improvement over single variable approaches. Canonical Correlation Analysis (CCA) is a multivariate statistical analysis that provides a method to combine several independent variables into a single index (Cohen et al., 2003; Heiskanen, 2005). CCA enables the visual comparison of single indices with the multiple regression analysis, but it also enables the use of the Reduced Major Axis (RMA) method in the estimation (Cohen et al., 2003). The results of a CCA are comparable to studies that employ multiple regression analysis (Cohen et al., 2003).

The objective of this part of the study therefore was to analyse the potential of ASTER data sets (spectral wavelengths bands and spectral vegetation indices) for the estimation of plantation forest structural attributes using linear and non-linear canonical correlation statistical regression methods in *Eucalyptus* commercial plantations in the midlands southern KwaZulu-Natal, South Africa.

5.2 Materials and Methods

5.2.1 Study Area

The study area is located in the southern KwaZulu-Natal province of South Africa, also known as the KwaZulu-Natal Midlands. The sites chosen for this research are all managed by MONDI-SA Forest Company. Geographically, the site lies between 29° 43' 4" and 29° 56' 49" South and 30° 1' 43" and 30° 17' 26" East, as shown in Figure 5.1. The terrain in the study area ranges from gently undulating to highly dissected, strongly rolling, and hilly topography. Elevations range between 800 and 1400 m above-mean-sea-level. The geology consists of sandstone and clay formations, which have resulted in sandy clay to sandy clay loam soils. Plantation forestry is a major land use in the study area due to the suitable climate and soils. Rainfall ranges from 820 to 1300 mm, but averages 1000 mm per annum mostly falling between October and April. Temperatures vary between 24 °C to 26 °C in summer, but drop to between 5°C and 14 °C in winter.

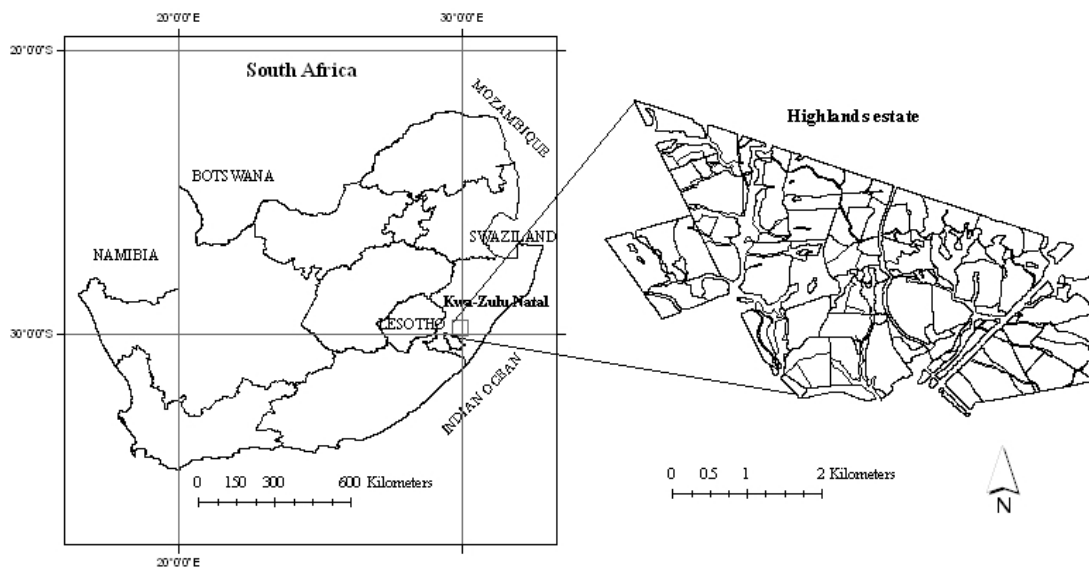


Figure 5.1 Map showing the location of the study site

5.2.2 Field measurements

A Geographical Information System (GIS) database of the forest company was consulted in order to select stands of interest. This data set is considered accurate by the forest practitioners (scale of 1:10000) and is routinely updated. The data indicates the current status of the plantations, including spatial characteristics and detailed management information. Attributes used in the selection procedure were the spatial location and extent of each compartment or stand, species type, planting and felling dates (age), stand site index, and coppice status.

The centre of each circular, 15 m radius plot was located using a compass and distance tape, relative to an accurate differential GPS location external to the stand in order to avoid within-stand GPS multi-path effects. Plot area was adjusted for slope in non-horizontal topography using a slope reading taken from a Vertex III hypsometer. Plots subsequently were mapped and spatially referenced in a GIS using these data (i.e. GPS readings, bearings, and distance).

The field data collection was conducted in October 2006. Plantation structural attributes measured during the field surveys were DBH and total height. These variables were in turn used to derive plot-level basal area and volume. Since height measurements were only taken for selected trees, plot-level relationships between height and DBH of corresponding trees were established using regression equations. The heights of non-measured trees were modelled using the equation with the highest R^2 value. In total 84 plots, representing two age groups were (4-6 and 7-9 years) surveyed in this study; the descriptive statistics for each group are presented in Table 5.1.

Table 5.1 Descriptive statistics of tree-level plantation structural attributes

4-6 years						7-9 years				
	SPHA	DBH (cm)	Tree height (m)	BA (cm ²)	Volume (m ³)	SPHA	DBH (cm)	Tree height (m)	BA (cm ²)	Volume (m ³)
N	44	44	44	44	44	40	40	40	40	40
Minimum		12.2	13.9	124	0.073		14.6	18.1	180.2	0.14
Maximum		19.8	23	326.5	0.314		29.4	36.1	708.4	1.17
Mean		15.6	18	212	0.169		18.7	24.1	307.1	0.352
S.D		2.1	2.453	58.5	0.064		3.1	0.6	110.5	0.212

BA = basal area, DBH = Diameter at breast height, SPHA stem per hectare, cm = centimetre, m = metre

Basal area and tree volume are dependent variables that incorporate DBH and tree height as independent or predictor variables. Equations 1 and 2 were used to derive basal area and volume per plot, respectively. Table 5.2 provides the coefficients used for volume estimations. These equations are standard formulae used by commercial forest companies in South Africa.

$$\text{Basalarea} = \frac{\pi}{4} \sum_{i=1}^n \text{DBH}^2 \dots\dots\dots 1$$

$$\text{Volume} = 10^{\left[\beta_1 \log_{10}(\text{DBH}) + \beta_3 \log(\text{tree height}) \right]} \dots\dots\dots 2$$

Table 5.2 Coefficients used for volume estimation

Species	β1	β3	Reference
<i>Eucalyptus grandis</i>	2.1513	1.0007	Coetzee, 1992
<i>Eucalyptus nitens</i>	2.0752	1.4279	Coetzee, 1992

5.2.3 Remote sensing data and processing

An ASTER scene acquired on October 2006 and processed to level 1A product (Abrams, 2000) was used in this study. ASTER is a medium spatial resolution multispectral imager

onboard NASA's Terra spacecraft, launched in December 1999 (Yamaguchi et al., 1998). ASTER has three subsystems operating in different spectral regions, namely the visible and near infrared (VNIR), and shortwave infrared (SWIR) regions as shown in table 5.3. The spatial resolutions are 15, 30, and 90 m for VNIR, SWIR, and TIR, respectively. The thermal data were not used in this study, given the focus on plantation attribute assessment using relatively standard VNIR to SWIR wavelengths. The imagery was ortho-rectified and converted to Universal Transverse Mercator (UTM) projection and WGS 84 datum (zone 36). A 10 m spatial resolution digital terrain model and 45 ground control points, which were collected during field campaign, were used for this purpose. A nearest neighbour re-sampling technique was used and an overall total root mean square error (RMSE) of less than half a pixel was obtained.

Table 5.3 Characteristics of the ASTER VNIR and SWIR subsystems

System	Band number	Spectral range (μm)	Spatial resolution
VNIR	1	0.52 - 0.60	15
	2	0.63 - 0.69	
	3	0.76 - 0.86	
SWIR	4	1.600 - 1.700	30
	5	2.145 - 2.185	
	6	2.185 - 2.225	
	7	2.235 - 2.285	
	8	2.295 - 2.365	
	9	2.360 - 2.430	

An atmospheric correction method, namely improved dark object subtraction (Chavez, 1988), was applied to convert the imagery from radiance to reflectance. The offset and gain, satellite viewing angle, and sun elevation were obtained from the ASTER header file. The band-centre wavelength for each band was obtained from the ASTER User Handbook (Abrams, 2000). A range of spectral vegetation indices that theoretically are capable of reducing background effect subsequently were calculated as shown in table 5.4 in order to evaluate their potential for predicting plantation structural attributes. These indices were NDVI, MSAVI, PVI, TSAVI, and Reduced Simple Ratio (RSR). Principal

components were also evaluated in order to determine if these components, aligned to the axes of variation within the image, improved estimation of plantation structural attributes. Although principal components are time-dependent imagery derivatives, they serve to elucidate which spectral region combinations are best suited to address the objective of this study. Principal components therefore should be applied with caution, since the axes of variation for time t_1 , might be different from the axes found during time t_2 .

Table 5.4 Spectral vegetation indices examined in this study

Spectral Index	Equations	Reference
NDVI	$\frac{\text{NIR} - \text{Red}}{\text{NIR} + \text{Red}}$	Rouse et al. (1973)
MSAVI	$\text{NIR} + 0.5 - \sqrt{(\text{NIR} + 0.5)^2 - 2(\text{NIR} - \text{Red})}$	Qi et al. (1994)
PVI	$\frac{\text{NIR} - a * \text{Red} + b}{\sqrt{a^2 + 1}}$	Richardson and Wiegand (1977)
TSAVI	$a * \frac{\text{NIR} - a * \text{Red} - b}{\text{Red} + a(\text{NIR} - b) + 0.08(1 + a^2)}$	Baret and Guyot (1991)
RSR	$\frac{\text{NIR}}{\text{Red}} \left(1 - \frac{\text{SWIR} - \text{SWIR}_{\min}}{\text{SWIR}_{\max} - \text{SWIR}_{\min}} \right)$	Brown et al. (2000)

where: SWIR_{\min} and SWIR_{\max} in the RSR are the minimum and maximum reflectances observed in the field plots, a and b in the PVI and TSAVI formulae represent the soil gradient and intercept, respectively.

5.2.4 Spectral data extraction

A plot-level average reflectance value was derived from the corresponding image for each plot subsequent to calculation of vegetation indices. These data were then used as part of the empirical model development. The average reflectance for each field plot was extracted from ASTER spectral reflectance and computed vegetation indices in order to reduce errors of image registration and location of the sample plots (Heiskanen, 2006). ASTER band 2 was assigned to the “Red”, band 3 to the “NIR”, and band 4 to the “SWIR” variable in the index equations. The slope and intercept of the soil line required

for the derivation of the PVI and TSAVI were determined from a scatter-plot as shown in figure 5.2 of the red and NIR ASTER reflectance values. Finally, the extracted spectral information and plantation attributes were imported into Statistical Analysis Software (SAS) for statistical analysis (SAS Inc. 1999). The final dataset consisted of 14 ASTER spectral information (independent variables) in addition to 5 plot-level plantation attributes (dependent variables) for 84-sample plots (observations).

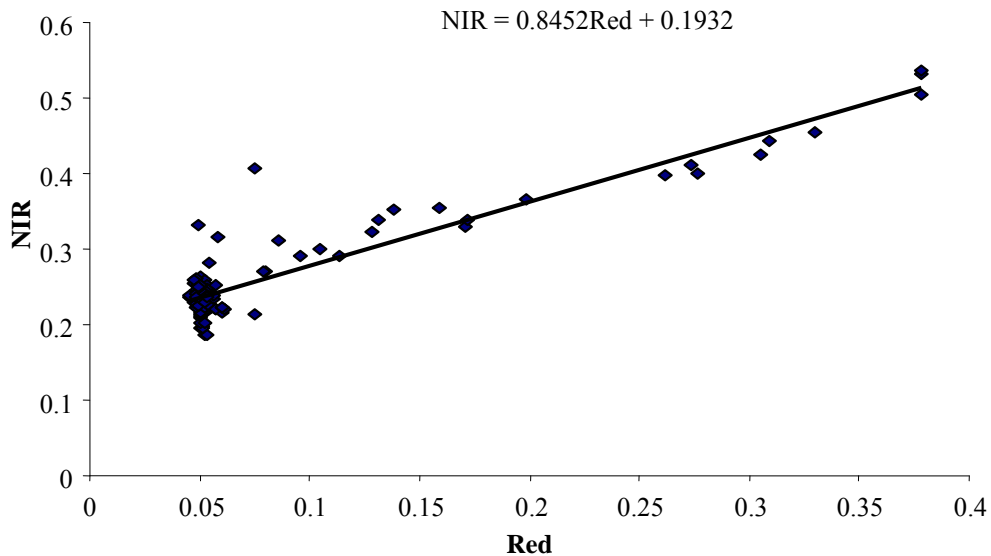


Figure 5.2 Scatter-plot of the ASTER Red band and NIR band reflectance and estimated soil line

5.2.5 Statistical analysis

Preliminary analyses of the plantation structural attributes and ASTER spectral reflectance were conducted within the SAS statistical package using descriptive statistics and correlation analyses. The total observations were sorted into age groups of 4-6 years (44 sample plots/observations) and 7-9 years (40 sample plots/observations). Accordingly, descriptive statistics were extracted for each plantation attribute to verify that no extreme outliers existed in the database and that a sufficient range for each of the plantation attributes was surveyed. Pearson's product moment correlation coefficients were calculated for the entire dataset (regardless of age) in order to identify how variables were related to each other. Spectral response curves were also plotted in order to build an understanding of how remote sensing spectral response was affected by plantation (tree) age. Finally, correlation analyses were conducted separately for the identified age groups,

young plantations and mature plantations, to determine which ASTER spectral information were significantly related to each plantation attribute.

Multiple linear regression methods that incorporate a variety of independent variables were required to test the significance of ASTER spectral information for estimating plantation structural attributes. CCA is a well-known technique in multivariate statistical analysis that measures the linear relationship between multiple data sets (Cohen et al., 2003). In this case plantation structural attributes and ASTER spectral information were investigated. CCA maximizes the correlation between sets of variables and provides a set of coefficients for the independent variables that aligns them with the variation in the dependent variables (Cohen et al., 2003). When those coefficients are applied to the independent variables, the result is a set of CCA scores corresponding to a single integrated index.

In this study the CCA coefficients were computed for dependent variables, i.e., SPHA, DBH, MTH, basal area, and volume, while independent variables, namely ASTER spectral bands, spectral vegetation indices, and log-transformed ASTER spectral bands were converted to the corresponding CCA scores. CCA was computed for the two age groups separately. Non-linear relationships between the plantation attributes and ASTER spectral information also were investigated in this study. The natural log transformation of the ASTER spectral bands and the pertinence of exponential and natural log transformations of the plantation attributes (dependent variables) models were examined. Model selection was based on the correlation coefficient of determination for each of the dependent plantation attributes.

5.2.6 Model evaluation

We used cross-validation, a procedure in which each sample value is iteratively removed from the data set while the model is fitted on the remainder of the data points, to check the consistency of the models. For CCA models, cross-validation results were assessed with scatter-plots of the observed versus predicted values, mainly to evaluate model linearity.

5.3 Results and Discussion

Appendix 5.1 summarizes the plot-level correlation coefficients between the plantation structural attributes and ASTER reflectance bands, vegetation indices, and log-transformed ASTER bands using all datasets, regardless of age. Relatively low correlation coefficients were evident for all plantation structural attributes; in most cases the correlation (r) was less than 0.39. Despite the poor correlation, a general evident trend was that vegetation indices performed better than ASTER reflectance bands in terms of absolute correlations when related to plantation structural attributes (refer to Appendix 5.1).

Figure 5.3 (a-d) shows the ASTER spectral response curves observed between ages 4-9 years. Spectral reflectance generally decreased with increasing stand age. A distinct decrease in spectral reflectance is observed at age 7 (Figure 5.3 a-d). A more subtle decrease in NIR spectral reflectance is observed between stand ages of 4-6 years old, while the NIR spectral reflectance decreased sharply at the age of 7 (Figure 5.3-c). The visible bands of ASTER (green and red bands) and NDVI changed in a similar fashion, with ASTER band-2 (red band) showing a gentle and constant decrease between the ages of 4-9 years old (Figure 3-b). However, ASTER NIR provided the best distinction between stand ages, thus it is interesting to note that 4-6 years old plantation stands exhibited higher reflectance values when compared to stands that were 7-9 years old.

From field observations we deduced that younger stands in a plantation forest scenario often are denser with fewer canopy gaps, thereby creating a smoother and more homogenous canopy layer with reduced shadows and subsequent increased infrared reflectance. On the other hand, mature plantation stands, unlike young stands, typically have lower densities and more gaps in the canopy because of thinning practices and mortality, which result in increased canopy shadows. Infrared radiation therefore penetrates deeper into the plantation canopy and internal scattering and absorption reduce total outgoing radiance (Danson and Curran, 1993; Sivanpillai et al., 2006). Analysis in this study therefore was conducted separately for young plantation stands (4-6 years) and mature stands (7-9 years).

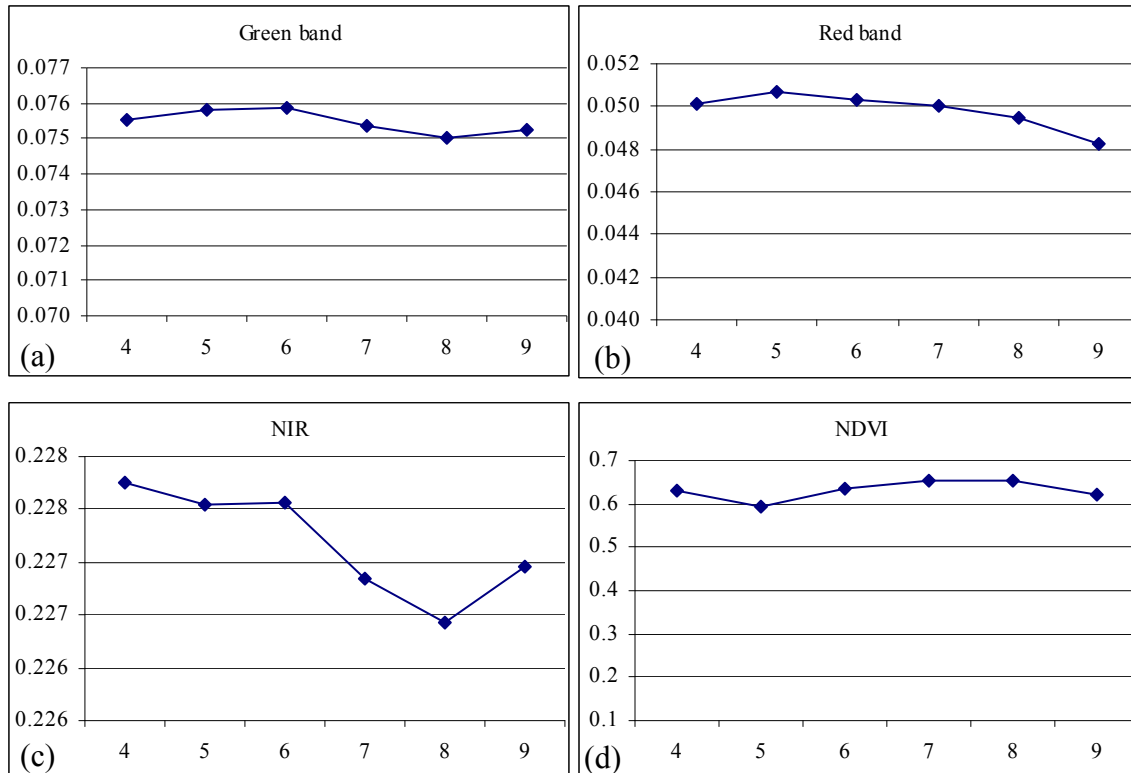


Figure 5.3 ASTER VNIR spectral response curves observed between ages 4-9 years

Appendix 5.2 summarizes the correlation coefficients between the structural attributes and ASTER spectral information (ASTER reflectance bands, vegetation indices, and log-transformed ASTER bands) at plot-level for the young and mature plantation stands, respectively. In spite of the low overall r values, the red band, NIR band, and NDVI performed distinctly better than other variables in this study (Appendix 5.2). Red band of the Landsat TM, SPOT XS, and ASTER sensors were reported as the best predictor of forest attributes in a number of studies. Heiskanen (2005), for example, found that the red band was the best predictor of volume and Leaf Area Index (LAI) in mountain birch forests in northern Sweden, while Eklundh and Olsson (2003) and Xu et al. (2003) also reported high correlations between the red spectral region and forest attributes in more productive deciduous stands and broadleaved stands in savanna regions. Furthermore, the red band has proven to be well correlated to forest attributes in coniferous stands (Häme et al., 1997). However, Fassnacht et al. (1997) logged poor performance by the red spectral region in a study conducted in hardwoods, where the ASTER NIR band (Band 3) was noted as the best predictor of forest structural attributes. Direct relationships between

the NIR spectral region and forest structural attributes have been reported for deciduous stands (Eklundh and Olsson 2003; Lu et al., 2004).

It is also interesting to note that highest correlations are observed between mature plantation forest attributes and NDVI. NDVI has been shown to be particularly useful in more open forest stands (Badwar et al., 1986; Nemani et al., 1993; Zheng et al., 2004). SWIR bands exhibited a very weak correlation coefficient for young and mature age groups of plantation stands, which was mainly attributed to their spatial resolution (30 m) as related to the local scale of the variables to be inventoried.

The analysis, which was conducted on separate age classes of forest stand (4-6 years and 7-9 years), resulted in an improvement in the relationships between plantation attributes and ASTER spectral information (Appendix 5.2). Thus, the prediction models in the next section were developed for these age classes.

5.3.1 Canonical correlation analysis

The correlation values between plantation attributes (SPHA, DBH, MTH, basal area, and volume) and the CCA scores from ASTER spectral bands, vegetation indices, and log-transformed spectral bands for young and mature plantation stands are shown in Appendix 5.2. In most cases the CCA scores computed from ASTER vegetation indices and log-transformed data resulted in the highest correlation with plantation structural attributes.

The CCA scores exhibited an improved correlation with plot-level plantation attributes over the single ASTER reflectance bands and ASTER vegetation indices. CCA scores, which showed the highest correlation with the structural attributes were selected, the relationships are statistically significant (significant at $p < 0.05$) but moderate relationship. The CCA scores were insensitive to the variability in the commercially managed plantations. Further modelling of these selected CCA scores are discussed in the next section.

5.3.2 Models for young plantation stands

The linear regression models of the plantation attributes and the coefficients of determination (R^2), RMSE, and RMSE values are reported in Table 5.5. CCA scores of vegetation indices exhibited the highest predictive ability for SPHA, DBH, MTH, and volume at plot-level. The coefficient of determination (R^2) values were 0.57, 0.64, 0.34, 0.25 and 0.30, respectively, while the RMSE values were 171 SPHA, 1.23 cm, 1.98 m, 3.91 cm^2 and 67.8 m^3/ha , respectively, for the young stands (Table 5.5). A direct relationship was observed between the CCA scores of vegetation indices and plot-level assessments of plantation structural attributes, i.e., SPHA, DBH, MTH, and volume. CCA scores of ASTER spectral bands returned the highest predictor of basal area at plot-level ($R^2 = 0.25$; RMSE = 3.91 m^2/ha) for young stands (Table 5.5). An inverse relationship was observed between the CCA score of ASTER reflectance bands and plot-level basal area (Table 5.5). Prediction error estimation using the leave-one-out cross-validation method yielded relative errors for young plantation stands of 16%, 17.9%, 20.7%, 17.9%, and 26.9% for SPHA, DBH, MTH, basal area, and volume, respectively (Table 5.5).

Table 5.5 Regression models, coefficients of determination (R^2), RMSE, and RSME % values for young plantation stands (n = 44)

	Model	R^2	RMSE	RMSE %
SPHA	1283 x CCA-VIs + 1060.8	0.57	171	16
DBH (cm)	11.01 x CCA-VIs + 15.613	0.64	1.23	17.91
MTH (m)	9.47 x CCA-VIs + 18.044	0.34	1.98	20.7
BA (cm^2)	-15.47 x CCA-bands + 21.334	0.25	3.91	17.89
Volume (m^3)	205.1 x CCA-VIs + 168.55	0.30	67.8	26.9

5.3.3 Models for mature plantation stands

Modelling based on CCA scores, computed from ASTER vegetation indices, proved superior for SPHA assessment at plot-level with adjusted $R^2 = 0.51$; RMSE = 242 SPHA; (Table 5.6) when compared to CCA scores of ASTER bands and log-transformed ASTER bands in the case of older plantation stands. The model exhibited a positive relationship between the CCA scores of vegetation indices and SPHA. A linear

regression of CCA scores of log-transformed ASTER spectral bands resulted in the best predictions for DBH, MTH, and volume at the plot-level with the adjusted $R^2 = 0.56$, 0.25, and 0.27, respectively (Table 5.6) when compared to CCA scores of ASTER bands and ASTER vegetation indices. The models for DBH and MTH exhibited a negative relationship between CCA scores for vegetation indices and the dependent variables DBH and MTH. The model based on CCA scores of ASTER reflectance bands was a better predictor of basal area at plot-level ($R^2 = 0.20$; RMSE = 5.07 m²/ha; Table 5.6) when compared to CCA scores of ASTER vegetation indices and log-transformed ASTER reflectance bands. The model exhibited positive relationships between CCA scores of ASTER reflectance bands and basal area.

Table 5.6 Regression models, coefficients of determination, RMSE and RMSE% for mature plantation attributes (n = 40)

	Model	R^2	RMSE	RMSE %
SPHA	843 x CCA-VIs + 1105.7	0.51	242	21
DBH (cm)	-10.42 x CCA-log-T-bands + 15.613	0.56	2.7	28.0
MTH (m)	-14.21 x CCA-log-T-bands + 24.185	0.25	3.01	21.9
BA (cm ²)	26.01 x CCA-bands + 32.068	0.20	5.07	15.4
Volume (m ³)	181 x CCA-log-T-bands + 620	0.27	56.2	32.9

Prediction error estimation using the leave-one-out cross-validation method yielded relative errors for mature plantation stands of 21%, 28%, 21.9%, 15.4%, and 32.9% for SPHA, DBH, MTH, basal area, and volume, respectively (Table 5.6). Relative prediction errors for all five plantation structural attributes did not comply with required accuracy for operational purposes, as the %RMSE were higher than the tolerated sampling survey error of 15%.

These relatively weak regression models for the estimation of plantation attributes at plot-level were attributed to the pattern of plantation stand development. In most cases higher crown closure and stems per hectare were observed in young plantation stands when compared to mature stands. As the plantation stands advanced towards later development stages, mortality rates increase as a result of competition for light, water, and soil nutrients. Thinning practices in commercial forests also influence crown closure and

resultant canopy gaps in older stands. Therefore, decreasing stems per hectare and increasing size and visibility of shadows are commonly observed in older plantation stands. These patterns of stand development and management, which cause increased absorption of in the NIR spectral region, were identified as key factors that resulted in generally weaker regression models for the prediction of plantation forest attributes in older stands. Another factor that potentially could have contributed to the weak regression models within the two studied age groups was similar crown closures within young and/or mature age groups of plantation stands. This in effect causes reduced within-age-group-spectral variable ranges and hence leads to potentially weaker models. Therefore, plantation forests of similar ages often exhibit comparable levels of crown closure and could potentially have similar spectral reflectances, even given varying sub-canopy plantation structural attributes. Homogenous canopy-level properties within age groups of plantation forests was identified as one of the key factors that prevented development of stronger regression models from medium spatial resolution remote sensing data.

5.4 Conclusions

In this study, relationships between reflectance data recorded by the ASTER sensor and structural attributes of *Eucalyptus* plantation forests were analysed through correlation and regression techniques. It was shown that reflectance-based data, e.g., reflectance, vegetation indices, and Canonical Correlation Analysis (CCA), extracted from various ASTER bands, resulted in acceptable, but not stellar modelling of plantation forest structural attributes in homogenous *Eucalyptus* stands. We therefore concluded that ASTER spectral data on their own are not sufficient for the prediction of plantation structural attributes in commercially managed *Eucalyptus* plantation stands, especially given operationally unacceptable RMSE values ($> 15\%$). However, one should consider that (i) the models generated in this study are limited to this geographic area and commercially managed *Eucalyptus* plantation stands, (ii) the addition of auxiliary variables such as *in situ* stand attributes could improve modelling abilities, and (iii) R^2 values greater than 0.60 in the case of selected structural variables indicates potential for the application of these types of remote sensing data to plantation forest structural

assessment. This latter observation is especially critical in the sense that limited canopy-level variation, at the level where most spectral-vegetation interaction takes place, could mask sub-canopy structural variation in homogenous stands. Hence the achieved R^2 results could also be deemed promising where essentially two-dimensional remote sensing image data are used for structural assessment in such forest environments.

These types of spectral datasets could also be useful for obtaining information about stand characteristics following events like pest infestation or natural disasters (Eva and Lambin, 1998) and for fire and moisture stress detection (Rock et al., 1986; Musick and Pelletier, 1988).

Recent studies have demonstrated that certain plantation stand attributes could be derived with greater accuracies from high spatial resolution satellite remote sensing data. For example, Coops and Culvenor (1999), Hyypä et al. (2000), Kiyatikire et al. (2006), and Chubey et al. (2006) demonstrated that IKONOS and Quickbird satellite data could be used estimate such stand characteristics. Although information derived from IKONOS data could perhaps better be used in plantation forest environments to gain insights about stand characteristics, the application of medium resolution data, such as those used in this study, has potential for scaling purposes.

5.5 Acknowledgements

This study was conducted as part of a remote sensing cooperative program between MONDI BP, the Council for Scientific and Industrial Research (CSIR), and the University of KwaZulu Natal to investigate the potential of satellite remote sensing imagery for prediction of plantation forest structural attributes. The authors would like thank Wesley Roberts, Solomon Gebremariam, Thamsanqa Mzinyane, and Wesley Naidoo for their assistance during field work. Financial support for this study was provided by the CSIR and MONDI BP.

5.7 References

Abrams, M. 2000, The Advanced Spaceborne Thermal Emission and Reflection Radiometer (ASTER): Data products for the high spatial resolution imager on NASA's Terra platform. *International Journal of Remote Sensing*, 21: 847– 859.

Ahmed, F., 2006, Remote Sensing and current forestry information needs in South Africa. *Proceedings of the International Precision Forestry Symposium*, Stellenbosch.

Badhwar, G.D., Macdonald, R.B., Hall, F.G., and Carnes, J.G. 1986, Spectral characterization of biophysical characteristics in a boreal forest: Relationship between Thematic Mapper band reflectance and leaf area index for aspen. *IEEE Transactions on Geoscience and Remote Sensing*, 24: 322– 326.

Baret, F. and Guyot, G. 1991, Potentials and limits of vegetation indices for LAI and APAR assessment. *Remote Sensing of Environment*, 35: 161 – 173.

Birth, G.S., and Mcvey, G.R. 1968, Measuring the colour of growing turf with a reflectance spectrophotometer. *Agronomy Journal*, 60: 640 – 643.

Brown, L., Chen, J.M., Leblanc, S.G. and Cihlar, J., 2000, A shortwave infrared modification to the simple ratio for LAI retrieval in boreal forests: An image and model analysis. *Remote sensing of Environment*, 71: 16-25.

Chavez, Jr., P.S., 1988, An improved dark-object subtraction technique for atmospheric scattering correction of multispectral data. *Remote Sensing of Environment*, 24: 459 – 479.

Chubey, M.S., Franklin, S.E. and Wulder, M.A., 2006, Object based analysis of IKONOS-2 imagery for extraction of forest inventory parameters. *Photogrammetric Engineering and Remote Sensing*, 72: 383-394.

Coetzee, J. 1992, I: An improved method of estimating tree volume utilization of *Eucalyptus grandis*. II: A revised tree volume table for short rotation *Eucalyptus grandis* timber crops. ICFR Bulletin 9/92.

Cohen, W.B., Maersperger, T.K., Gower, S.T. and Turner, D.P., 2003, An improved strategy for regression of biophysical variables and Landsat ETM+ data. *Remote Sensing of Environment*, 84: 561–571.

Coops, N. and Culvenor, D., 1999, Utilizing local variance of simulated high spatial resolution imagery to predict spatial pattern of forest stands. *Remote Sensing of Environment*, 71: 248 – 260.

Danson, F.M. and Curran, P.J., 1993, Factors affecting the remote sensed response of coniferous forest plantations. *Remote sensing of Environment*, 43: 55- 65

Eklundh, L. and Olsson, L., 2003, Vegetation index trends for the African Sahel 1982–1999, *Geophysical Research Letters*, 30: 1430–1433.

Eva, H. and Lambin, E.F. 1998, Burnt area mapping in central Africa using ASTER data. *International Journal of Remote Sensing*, 19: 3473 – 3497.

Fassnacht, K.S., Gower, S.T., Mackenzie, M.D., Nordheim, E.V. and Lillesand, T. M., 1997, Estimating the leaf area index of North Central Wisconsin forests using the Landsat Thematic Mapper. *Remote Sensing of Environment*, 61: 229–245.

Freitas, S.R., Mello, M.C.S. and Cruz, C.B.M. 2005, Relationships between forest structure and vegetation indices in Atlantic Rainforest. *Forest Ecology and Management*, 218: 353-362.

Hall, R.J., Skakun, R.S., Arsenault, E.J. and Case, B.S., 2006, Modelling forest stand structure attributes using Landsat ETM+ data: application to mapping of aboveground biomass and stand volume. *Forest Ecology and Management*, 225: 378-390.

Häme, T., Salli, A., Andersson, K. and Lohi, A., 1997, A new methodology for estimation of biomass of conifer-dominated boreal forest using NOAA AVHRR data. *International Journal of Remote Sensing*, 18: 3211– 3243.

Heiskanen, J., 2006, Estimating aboveground tree biomass and leaf area index in a mountain birch forest using ASTER satellite data. *International Journal of Remote Sensing*, 27: 1135 – 1158.

Hyypä, H., Inkinen, M., Engdahl, M., Linko, S. and Zhu, Y.H., 2000, Accuracy comparison of various remote sensing data sources in the retrieval of forest stand attributes. *Forest Ecology and Management*, 128: 109-120.

Kayitakire, F., Hamle, C. and Defourny, P., 2006, Retrieving forest structure variables based on image texture analysis and IKONOS-2 imagery. *Remote Sensing of Environment*, 102: 390-401

Lu, D., Mausel, P., Brondizio, E. and Moran, E., 2004, Relationships between forest stand parameters and Landsat TM spectral response in Brazilian Amazon Basin. *Forest Ecology and Management*, 198: 149-167.

Mcroberts, R.E. and Tomppo, E.O., 2007, Remote sensing support for national forest inventories. *Remote Sensing of Environment*, 110: 412-419.

Musick, H.B. and Pelletier, R.E., 1988, Response to soil moisture of spectral indexes derived from bidirectional reflectance in Thematic Mapper wavebands. *Remote Sensing of Environment*, 25: 167–184.

Nemani, R., Pierce, L., Running, S.W. and Band, L. 1993, Forest ecosystem processes at the watershed scale: Sensitivity to remotely sensed leaf area index estimates. *International Journal of Remote Sensing*, 14: 2519–2534.

Qi, J., Chehbouni, A., Huete, A.R., Kerr, Y.H. and Sorooshian, S., 1994, A modified soil adjusted vegetation index. *Remote Sensing of Environment*, 48: 119-126.

Richardson, A.J. and Wiegand, C.L., 1977, Distinguishing vegetation from soil background information. *Photogrammetric Engineering and Remote Sensing*, 43: 1541-1552.

Rock, B.N., Vogelmann, J.E., Williams, D.L., Vogelmann, A.F. and Hoshisaki, T., 1986, Remote detection of forest damage *BioScience*, 36: 439–445.

Rouse, J., Haas, R., Schell, J., Deering, D. and Harlan, J., 1973, Monitoring the vernal advancements and retrogradation (greenwave effect) of nature vegetation. NASA/GSFC Final Report, NASA, Greenbelt, MD.

SAS User Guide 1999, SAS Institute Inc., SAS/STAT User's Guide, Version 8, Cary,NC: SAS Institute Inc., 1999.

Sivanpillai, R., Smith, C.T., Srinivasan, R., Messina, M.G. and Wu, X.B., 2006, Estimation of managed loblolly pine stand age and density with Landsat ETM+ data. *Forest Ecology and Management*, 223: 247-254.

Spanner, M.A., Pierce, L.L., Peterson, D.L. and Running, S.W. 1990, Remote sensing of temperate coniferous forest leaf area index: The influence of canopy closure, understory vegetation, and background reflectance. *International Journal of Remote Sensing*, 11: 95–111

Trotter, C.M., Dymond, J.R. and Goulding, C.J., 1997, Estimation of timber volume in a coniferous plantation forest using Landsat TM. *International Journal of Remote Sensing*, 18: 2209-2223.

Tucker, C.J. 1979, Red and photographic infrared linear combinations for monitoring vegetation. *Remote Sensing of Environment*, 8: 127– 150.

Wulder, M.A., 1998, Optical remote sensing techniques for the assessment of forest inventory and biophysical parameters. *Progress in Physical Geography*, 22: 449 – 476.

Xu, B., Gong, P. and Pu, R., 2003, Crown closure estimation of oak savannah in a dry season with Landsat TM imagery: comparison of various indices through correlation analysis. *International Journal of Remote Sensing*, 24: 1811–1822.

Yamaguchi, Y., Kahle, A., Tsu, H., Kawakami, T. and Pniel, M., 1998. Overview of Advanced Spaceborne Thermal Emission and Reflection Radiometer (ASTER). *IEEE Transactions on Geoscience and Remote Sensing*, 36: 1062–1071.

Zheng, D. Rademacher, J., Chen, J., Crow, T., Bresse, M., Moine, J. L. and Ryu, S., 2004, Estimating aboveground biomass using Landsat ETM+ data across a managed landscape in northern Wisconsin, USA. *Remote Sensing of Environment*, 93: 402-411.

CHAPTER 6

Extracting structural attributes from high spatial resolution IKONOS imagery using image texture analysis and artificial neural networks in even-aged *Eucalyptus* plantation forests in KwaZulu-Natal, South Africa,

* This chapter is based on:

Gebreslasie, M., Ahmed, F.B., and van Aardt, J. *in review* Estimating forest structural attributes from high spatial resolution IKONOS imagery using image texture analysis and artificial neural networks in even-aged *Eucalyptus* plantation forests in KwaZulu-Natal, South Africa. *International Journal of Remote Sensing*.

Abstract. In this study the suitability of optical IKONOS satellite data (multispectral and panchromatic) for the estimation of forest structural attributes, i.e. stems per hectare (SPHA), diameter at breast height (DBH), mean tree height (MTH), basal area, and volume in plantation forest environments was assessed. The relationships of these forest structural attributes to image texture that were derived from statistically-based texture analysis were analyzed. The coefficients of determination of multi-linear regression models developed for the estimation of SPHA, DBH, MTH, basal area, and volume using texture features derived from multispectral data were 0.63, 0.68, 0.81, 0.86, and 0.86, respectively. When the statistical texture features derived from panchromatic data were applied the coefficients of determination for the respective forest structural attributes increased by 25%, 31%, 6%, 0.2%, and 0.2%, respectively. Artificial neural network (ANN) models also developed to predict the same forest structural attributes. The ANN produced strong and significant relationships between estimated and actual measures of SPHA, DBH, MTH, basal area, and volume ($r = 0.83, 0.83, 0.93, 0.94, \text{ and } 0.94$, respectively) based on multispectral imagery and ($r = 0.98, 0.95, 0.95, 0.93, \text{ and } 0.98$, respectively) based on panchromatic imagery. The relative estimation errors of the five studied forest structural attributes were comparable to the usual sampling inventory errors when statistical texture indicators, derived from panchromatic data and the ANN statistical method, were applied. Errors were 7.8%, 5.1%, 5.8%, 8.7%, and 8.7% for SPHA, DBH, MTH, basal area and volume, respectively. A sensitivity analysis of ANN and stepwise regression algorithms showed that the most important texture features were the entropy, variance, and contrast for panchromatic data. Results such as these bode well for the application of high spatial resolution imagery to forest structural assessment.

Keywords: Forest structural attributes Texture, IKONOS, and ANN

6.1 Introduction

Forest structural attributes are currently collected manually through field surveys and established inventory approaches in South Africa. Even though these methods provide highly accurate measurements of forest structural attributes, South African forest companies have concluded that existing approaches are costly and time consuming.

Consequently, a remote sensing research cooperative between the forestry industry and the Council for Scientific Industrial Research's Forestry and Forest Product centre (CSIR-FFP) was established to investigate the potential of satellite remote sensing data for the estimation of forest structural attributes at reasonable accuracies. The premise for this cooperative stems from the general acknowledgement that remote sensing can play an important role in forestry as a tool for acquiring information about the location, extent, composition, and structure of forest resources as part of industrial forest inventories (Muinonen et al., 2001; Lu et al., 2004; Boyd and Danson, 2005; Chubey et al., 2006; McRoberts and Tomppo, 2007). Remote sensing studies have also been recommended as cost-effective sources of gathering information (Hyypä et al., 2000; Boyd and Danson, 2005; Kayitakire et al., 2006).

Much research has been conducted to measure forest structural attributes since the advent of environmental satellite remote sensing in approximately 1972. Examples of such studies are numerous: Coops and Culvenor (1999) used SPOT imagery to delineate compartments boundaries, Sivanpillai et al. (2006) applied Landsat ETM+ to estimate stand age and density, Lu et al. (2004) and Rahman et al. (2005) used Landsat TM and ETM+ to estimate forest biomass. Similarly, Heiskanen (2006) used ASTER to estimate biomass and leaf area index (LAI), Ingram et al. (2005) used Landsat to estimate volume, basal area, and diameter at breast height (DBH), and Hall et al. (2006) used Landsat ETM+ to map aboveground biomass and volume, to name but a few. Gebreslasie et al. (2008) applied ASTER imagery for the prediction of volume, basal area, DBH, and mean tree height for the same species and geographical area applicable to the current study. Results in terms of coefficients of determination were as high as 0.64 for DBH and as low as 0.20 for volume, which indicated a need for the evaluation of multispectral and panchromatic imagery of higher spatial resolution as applied to the same species/area.

The listed studies have shown varying degrees of success in predicting forest structural attributes; however, none of them have achieved a satisfactory result as far as operational uses in a plantation forest management scenario is concerned. A review paper by Holmgren and Thuresson (1998) concluded that results from low spatial resolution multispectral sensors can best be considered to be insignificant for forest management

planning. Hyyppä et al. (2000) showed that the accuracy of models for the prediction of forest inventory parameters was greatly influenced partly by spatial resolution of the remote sensing data employed and partly by the size of the forest compartments being studied. Subsequently, low spatial resolution satellite sensors were found to be insufficient for measuring spatial variation at homogenous and relatively small forest stands. As stated below the advances in high spatial resolution satellite imagery, such as those found in imagery from the IKONOS and QuickBird sensors, therefore present important new opportunities for the estimation of forest structural attributes.

However, the current techniques to process and analyze satellite image data, e.g., the use of vegetation indices or single band approaches, may not be amenable for extraction of more detailed structural information provided by high spatial resolution image data (Goetz et al., 2003). A special emphasis therefore has been placed on feature extraction and structural image analysis methods in the case of such imagery. Gougeon et al. (1999), Wulder et al. (1998), Culvenor (2002), Kayitakire et al. (2006) have acknowledged that textural and/or spatial information often plays a major role in the interpretation of high spatial resolution remotely sensed images of forests.

Textural analysis is one of the approaches used to extract spatial information from high spatial resolution imagery and is founded on the precept that images are composed of spectral/tonal and textural information (Lillesand et al., 2004). The texture of an image contains important information about the spatial and structural information of objects (Franklin et al., 2001; Coburn and Roberts, 2004; Kayitakire et al., 2006). A number of techniques have been developed for image texture analysis. Coburn and Roberts (2004) identified four main approaches, namely statistical, geometrical, model-based, and signal processing. This study examines the potential of statistical texture analysis for the estimation of forest structural attributes. Detailed explanations of the other three techniques of textural analysis can be found in Ojala and Pietikynen (1996), Materka and Strzelecki (1998), Mihran and Jain (1998), Tuceryan and Jain (1998).

Statistical texture analysis, which is the most frequently cited method for image texture analysis, takes into consideration the distribution and variation of spectral/tonal

variability in a given local area (Haralick, 1979; St-Louis et al., 2006). Depending on the number of pixels that define the local area, statistical methods can be classified into first order statistical texture analysis or Gray Level Occurrence Matrix (GLOM) and second order statistical texture or Gray Level Co-occurrence Matrix (GLCM) approaches (Haralick et al., 1979; Mihran and Jain, 1998). The basic difference is that GLOM estimates properties of individual pixel values in a given moving window size, thereby largely ignoring the spatial interaction between image pixels. In contrast, GLCM estimate properties of more than two pixel values occurring at specific locations relative to each other.

Statistical texture information has often been used in feature detection or feature classification (Franklin et al., 2000; Rao et al., 2002; Norris-Rogers, 2006). Franklin et al. (2001) used the variance and homogeneity statistical texture features, derived from IKONOS panchromatic images, for stand age estimation. Their results showed that second order homogeneity texture values were the most effective in estimation of stand age, returned R^2 of 78 %. Kayitakire et al. (2006) have also used variance, contrast, and correlation statistical texture features, extracted from IKONOS panchromatic data, for the prediction of stand age, top height, diameter at breast height, stand density, and basal area. The coefficients of determination of the models were 0.81, 0.76, 0.82, 0.82, and 0.35, respectively. The authors also showed that the most important parameters were the texture feature, window size, and displacement, whereas the direction (θ) parameter had a minimal effect on the coefficients of determination. These studies sourced the spatial characteristics of a forest, which were used to estimate forest structural attributes, from single band high spatial resolution imagery, while also relying on limited statistical texture features. This is in contrast to a recent study by Johansen et al. (2007), who showed that textural information of an image greatly depends on the type of image analyzed with regard to spectral domain, the spatial resolution, and the characteristics of sensed objects (dimension, shape, and spatial distribution). This outlines the importance of expansion of such approaches to multispectral, high spatial resolution imagery.

However, although studies by Franklin et al. (2001) and Kayitakire et al. (2006) used linear regression statistical analysis to estimate forest structural attributes from statistical

texture features, such an approach typically assume a linear relationship between variables of interest. The statistical analysis used for understanding the relationships among remote sensing information and forest structural attributes should accommodate for the possibility that these relationships may be non-linear and complex. An Artificial Neural Network offers a powerful method for analysing complex relationships among variables, without making assumptions about data distributions and variable linearity (Pao, 2008). ANNs are capable of handling non-normality, non-linearity, and collinearity in a system (Haykin, 1994). Thus the major attraction of ANNs is that they offer a powerful means for analyzing complex datasets without making pre-emptive assumptions about data characteristics, as opposed to many conventional statistical approaches (Boyd et al., 2002).

The objectives of this part of the study therefore were to (i) investigate the significance of statistical texture features computed from multispectral and panchromatic IKONOS imagery for the estimation of forest structural attributes, namely SPHA, DBH, MTH, BA, and volume, (ii) compare the significance of window/kernel size on such an analysis, and (iii) investigate and compare the existing linear and non-linear relationships between statistical texture features and field-measured forest structural attributes, with the aim of identifying the best estimator for the forest variable of interest.

6.2 Materials

6.2.1 Study site

The study area is located in the southern KwaZulu-Natal province of South Africa, also known as the KwaZulu-Natal Midlands. The sites chosen for this research are all managed by MONDI-SA Forest Company. Geographically, the site lies between 29° 43' 4" and 29° 56' 49" South and 30° 1' 43" and 30° 17' 26" East, as shown in Figure 5.1. The terrain in the study area ranges from gently undulating to highly dissected, strongly rolling, and hilly topography. Elevations range between 800 and 1400 m above-mean-sea-level. The geology consists of sandstone and clay formations, which have resulted in sandy clay to sandy clay loam soils. Plantation forestry is a major land use in the study area due to the suitable climate and soils. Rainfall ranges from 820 to 1300 mm, but

averages 1000 mm per annum mostly falling between October and April. Temperatures vary between 24 °C to 26 °C in summer, but drop to between 5°C and 14 °C in winter.

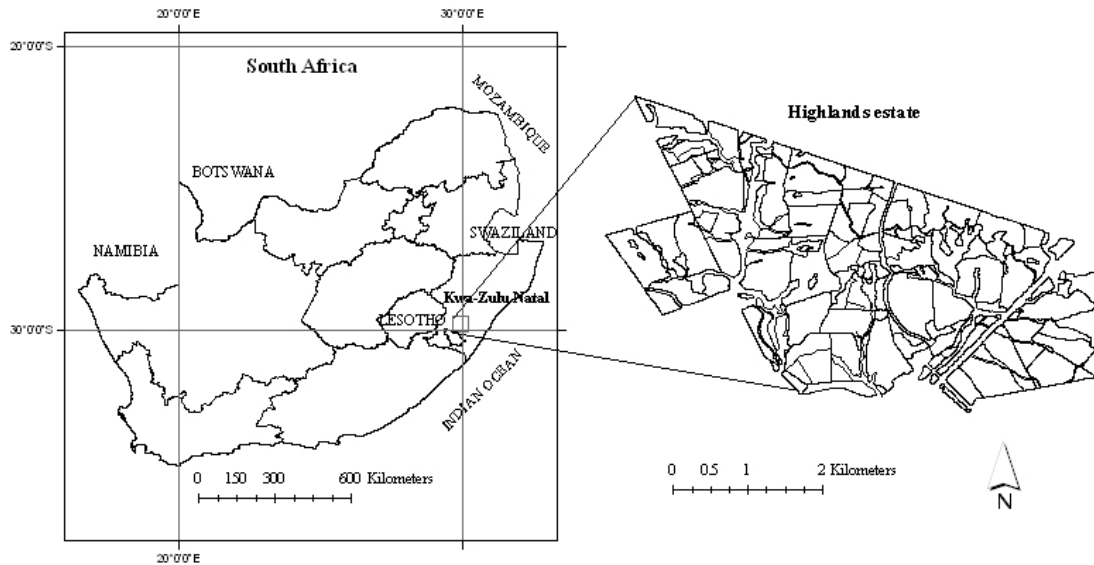


Figure 6.1 Map showing the location of the study site

6.2.1 Field data

A Geographical Information System (GIS), compiled and provided by MONDI-SA, was consulted in order to select stands of interest. This data set is considered accurate by the forest practitioners (spatial resolution of 1:10000) and is routinely updated. The data indicate the current status of the plantations, including spatial characteristics and detailed management information. Attributes used in the selection procedure were the spatial location and extent of each compartment or stand, species type, age, planting and felling dates, and coppice status. Only *Eucalyptus* species were considered from this dataset. These species were chosen given the need identified by the forestry sector to focus on their management towards increased productivity, which was in turn driven by the growing demands for various end products.

A circular 15 m radius plot was delimited in each selected stand. The centre of each circular plot was located using a compass and distance tape, relative to an accurate differentially-corrected GPS location external to the stand in order to avoid within stand

GPS multi-path effects. Plot area was adjusted for slope in non-horizontal topography using a slope reading taken from a Vertex III hypsometer. Plots subsequently were mapped and spatially referenced in a GIS using these data (i.e., GPS readings, bearings, and distance).

The field data collection was conducted in October 2006. Forest structural attributes measured during the field surveys were DBH and total height. These variables were in turn used to derive basal area and volume. Since height measurements were taken for selected trees, the relationships between height and DBH of corresponding trees could be established using regression equations. The height of non-measured trees was modelled using the equation with the highest R^2 value. A total of 122 plots, located in 37 stands, were surveyed in this study.

Basal area and tree volume are dependent variables that incorporate DBH and tree height as independent or predictor variables. Equations 1 and 2 were used to derive tree basal area and volume, respectively. Table 6.1 provides the coefficients used for volume estimations. These equations are standard formulae used by South Africa forestry companies.

$$\text{Basal area} = \frac{\pi}{4} \sum_{i=1}^n \text{DBH}^2 \quad (1)$$

$$\text{Volume} = 10^{[\beta_1 \log_{10}(\text{DBH}) + \beta_3 \log(\text{tree height})]} \quad (2)$$

Table 6.1 Coefficients used for volume estimation

Species	β_1	β_3	Reference
<i>Eucalyptus grandis</i>	2.1513	1.0007	Coetzee, 1992
<i>Eucalyptus nitens</i>	2.0752	1.4279	Coetzee, 1992

6.2.2 Remote sensing data

IKONOS multispectral and panchromatic images that were acquired on October 2006 were used in this study. Detailed information about the acquisition configuration is reported in Table 6.2.

Table 6.2 IKONOS image characteristics

Characteristic	Specifications
Date/time(GMT)	2006-10-23/08:17
Sun angle elevation	52.875°
Sun Angle azimuth	41.4681°
Sensor angle elevation	66.99317°
Sensor angle azimuth	359.97°
Spectral bands wavelengths	
Band 1 (blue)	0.45 - 0.52 μm
Band 2 (green)	0.52 - 0.6 μm
Band 3 (red)	0.63 - 0.69 μm
Band 4 (NIR)	0.76 - 0.9 μm
Panchromatic	0.45 - 0.9 μm

The imagery was geo- and ortho-rectified and converted to Universal Transverse Mercator (UTM) projection and WGS 84 (zone 36) datum. A 10 m spatial resolution digital terrain model (DTM) and 48 ground control points, which were collected during the field campaign, were used for this purpose. A nearest neighbour re-sampling technique was used and an overall total root mean square error (RMSE) of less than half a pixel was obtained.

6.3 Methods

6.3.1 Texture feature extraction

GLOM and GLCM features were studied in terms of their ability to estimate target forest structural attributes. The ability of quantifying image texture using statistical texture analysis (Haralick et al., 1979; Hay et al., 1996) creates an opportunity to estimate forest structural attributes (Franklin et al., 2001; Kayitakire et al., 2006).

The size of the matrix computed from the statistical texture features depends on the data range of pixel grey values; images of large numbers of data bits may result in large matrices during statistical operation and require a substantial amount of memory and

computer processing unit (CPU) cycles to handle the computation (Tsai and Chou, 2006). Only a pick of these features, which are relevant for remote sensing image analysis, were therefore selected in order to reduce the computational complexity. Six GLOMs, namely data range, mean, variance, entropy and angular second moment (ASM) as shown in Appendix 6.1, were calculated for the four spectral bands and the panchromatic band of the IKONOS image using 3x3, 5x5, and 7x7 moving window sizes. These window sizes were chosen to cover a range of sizes corresponding roughly to the space between the homogenous patches of trees in the plantation forest. Six GLCMs, namely mean, variance, entropy, correlation, contrast and ASM (refer to Appendix 6.1) were also calculated using the three above-mentioned window sizes. The description of the selected statistical texture models is given in Appendix 6.1. These selected statistical textures were used to extract image texture features from IKONOS multispectral and panchromatic imagery on a per-band basis.

The GLCM of an image is an estimate of the second order joint probability, $P_{\delta}(i, j)$, of the intensity value of two pixels (i and j) and a displacement (δ) along a given angle (θ), i.e. the probability that i and j have the same intensity (Haralick et al., 1979). Haralick et al. (1979) furthermore suggested using GLCMs calculated from four angles (θ), namely $\theta = 0^{\circ}, 45^{\circ}, 90^{\circ},$ and 135° and displacement vectors (δ) with $\delta = 1$ or 2 pixels. However, finding GLCMs for all angles (θ) would require a large amount of calculations. Literature also shows that the angle (θ) parameter has a minimal effect on the coefficients of determination (Kayitakire et al., 2006). In this study, the selected GLCMs were calculated using $\delta = 1$ and $\delta = 2$ as displacement vector, with $\theta = 90^{\circ}$. Because of the homogenous nature of the plantation forests in question and the minimal effect of angle on the coefficients of determination, a single angle was deemed adequate for this study. The designed methodology accordingly resulted in a total of 226 statistical texture features, calculated using GLOMs, GLCMs ($\delta = 1$), and GLCMs ($\delta = 2$) from multispectral IKONOS imagery. Calculations for panchromatic IKONOS imagery resulted in a total of 54 statistical texture features.

6.3.2 Statistical analyses

Preliminary analysis, including a normality test, was conducted in SPSS (SPSS V.15 2006) using a Kolmogorov-Smirnov z-test. This effectively tested whether the observations could reasonably have come from the specified normal distribution. Generally, the datasets in this study conformed to statistically normal distributions, while allowing for potential outliers in the histogram distribution. Thus, the applicability of the statistical texture features and the effect of the three moving window sizes for the estimation of forest structural attributes were studied using Pearson's correlation coefficients. A stepwise selection algorithm was also employed to select a subset of independent variables that explain most of the variability in the dependent variable. The stepwise algorithm was designed to start with the null model, with a probability for entry of 0.05. Specifying a null model (forward selection) as a starting point is more conservative than the usual method of starting with the full model. Using this method avoids issues related to model over-fitting that could occur giving the high correlations between the covariates present in the full model (Diamantopoulou, 2005). These selected variables were used to develop a model using multiple linear regression and non-linear (ANN) statistical methods.

6.3.3 Multiple linear regressions

A multiple linear regression statistical method (Equation 3) was used to develop models for the estimation of forest structural attributes, i.e., DBH, MTH, SPHA, BA, and volume. Multiple linear regression models were fitted using the selected statistical texture features as independent variables, computed separately from multispectral and panchromatic IKONOS images. Performance of the regression models was evaluated based on the coefficient of determination, RMSE, and fit of the field-measured versus predicted forest structural attributes.

$$Y = \beta_0 + \beta_1 X_1 + \beta_2 X_2 + \dots + \beta_i X_i \quad (3)$$

6.3.4 Artificial neural network

Multi Layer Perceptron (MLP) neural networks were used in this study, to predict the selected forest structure attributes (Jensen et al., 1999; Carvalho et al., 2004; Chitroub, 2005; Ingram et al., 2005). MLP neural networks are often classified as back propagation training, where back propagation consists of fitting the weights of the model by a criterion function, usually squared error or maximum likelihood, using a gradient optimization method (Fauselt, 1994; Haykin, 1994; Patterson, 1996). The error in back propagation MLP neural networks, i.e., the difference between the predicted and observed outcomes, is propagated back from the output to the connection weights in order to modify the weights so as to minimize the error of prediction (Fauselt, 1994; Haykin, 1994; Patterson, 1996). The geometry of a MLP neural network, which determines the number of connection weights and how these are arranged, depends on the number of hidden layers and number of nodes in these hidden layers. It has been recommended that a network with one hidden layer can appropriately be used in most general problems (Jensen et al., 1999; Ingram et al., 2005). Three interconnected layers of neurons, namely an input layer, hidden layer, and output layer, consequently were employed in this study to develop the final ANN model.

Division of the available data sample into two subsets, one each for model development and model validation, is a common practice in ANN statistical analysis methods (Haykin, 1994). We used a subset of 70% of the sampled dataset for ANN model development and the remaining 30% was kept for testing the ANN model. Cross-validation was also used to assess the robustness of the developed model for the estimation of forest structure attributes. Therefore, the best model was selected based on the coefficient of determination and absolute error of the three models encompassed by the development model, test model, and validation model.

The input variables, selected using the stepwise selection algorithm, were kept constant for both the multiple linear regression and ANN approaches in this study. Therefore, the individual ANN model developed in this study has multiple input variables (independent) and one output variable (field enumerated forest structural attribute). Figure 6.2 below

summarizes the basic expressions that describe the structure of the ANN developed for this study.

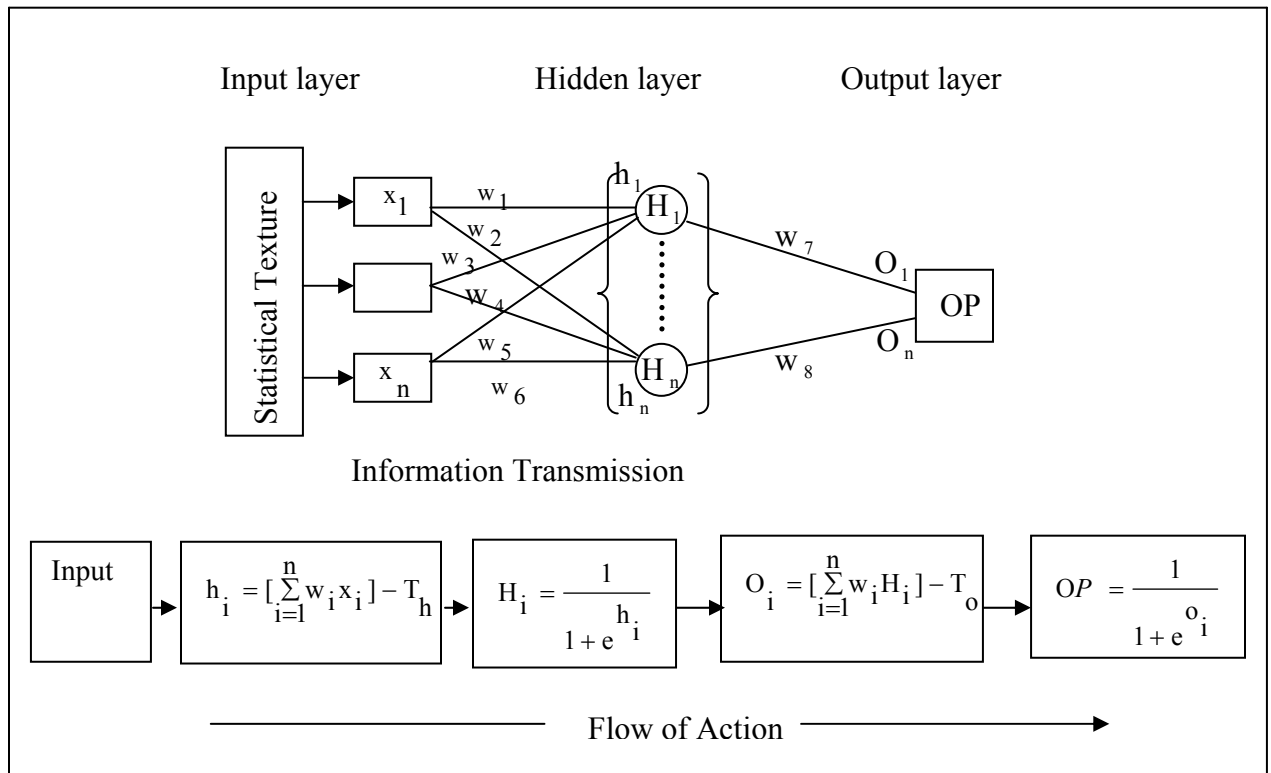


Figure 6.2 A schematic representation of the ANN.

where X_i represents the input parameters (statistical texture features), w_i is the weight value, h_i is the hidden value after subtraction of the threshold (bias), T_h constitutes the hidden nodes' threshold (bias), H_i is the hidden value after sigmoid transformation, O_i is the preliminary output value after subtraction of the threshold (bias), T_o constitute the outputs' threshold (bias), OP is the final output after sigmoid transformation.

The input parameters of ANN models should be standardized between 0 and 1 (Jensen *et al.*, 1999), hence a linear transformation equation (Equation 4) was developed for this purpose.

$$\text{Standardized value} = (R - \text{min}) / (\text{max} - \text{min}) \quad (4)$$

where R is the real input value, min is the minimum value in the training data input, and max is the maximum value in the training data input.

In this study, the optimum number of neurons in the hidden layer of each model was determined by varying their number, starting with a minimum of 1 and then increasing the network size by iteratively adding 1 neuron. STATISTICA 7 neural network toolbox (Statsoft, 2004) was used for training and testing of ANN models. Finally, the maximum number of training epochs (training cyclone) to train was set at 5000. The correlation coefficient and the mean absolute error of the training dataset and test dataset were used to evaluate the performance of the developed ANN models.

6.3.5 Performance assessment

The reliability of the models for the estimation of forest structural attributes was assessed using the coefficient of determination (R^2), coefficient of correlation (r), root-mean-square error (RMSE; Equation 5), and absolute root-mean-square error percentage (ARMSE %; Equation 6). Generally, a high R^2 , low RMSE value, and an ARMSE% < 10%, are indicative of a good model fit. Although the performance of the developed ANN models was assessed using the correlation between the observed and predicted values for both model development and model test datasets, cross-validation was also used in this study.

$$RMSE = \sqrt{\frac{\sum_{x=1}^n (X_{pred} - X_{obs})^2}{N}} \quad (5)$$

$$ARMSE\% = \frac{RMSE}{\mu_{obs}} \quad (6)$$

where X_{pred} is the model-predicted value, X_{obs} is the observed value, and μ_{obs} is the mean of the field-observed values.

6.4 Results

6.4.1 General

Figure 6.3 shows the correlation coefficients that were obtained for each of the forest structural attributes and average result of all texture features, computed separately for each multispectral IKONOS band. This figure is aimed at assessing the reliability of each band for estimation of forest structural attributes. Band 3 returned the highest correlation coefficients in all cases, while Band 4 resulted in the second highest correlation coefficients and Bands 1 and 2 returned the lowest value in all cases as shown in figure 6.3.

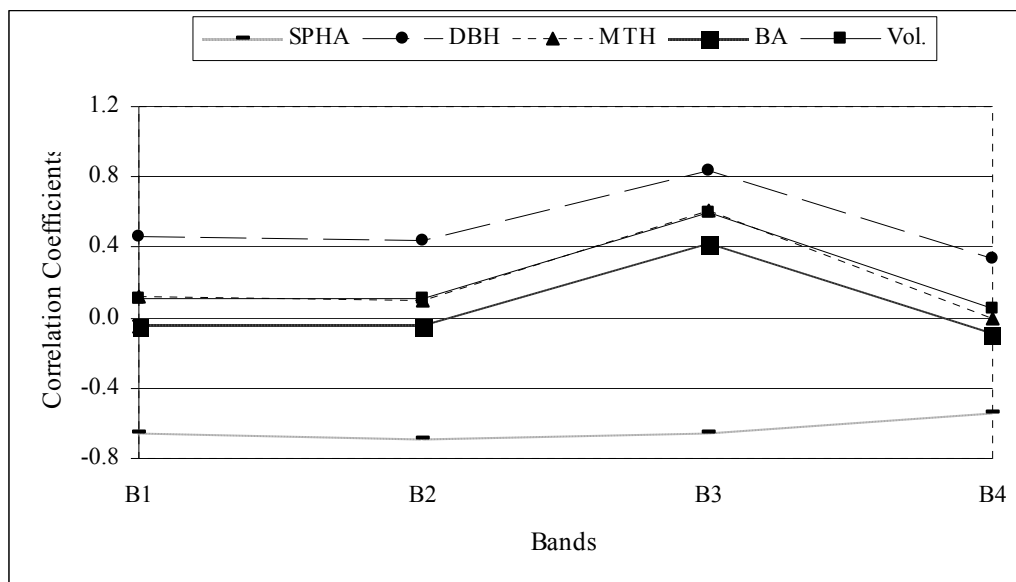


Figure 6.3 Illustration of the IKONOS bands effect for the estimation of forest structural attributes

The moving window size used to extract statistical texture features is a key parameter in image texture analysis, usually selected by semivariogram analysis (Zawadzki et al., 2005). However, in this study an effort was made to understand how the correlation coefficient varied with varying window size. Where several values are tested in an effort to identify the value that minimizes a given error function. Figure 6.4 shows the correlation coefficient that was obtained for each forest structural attribute and statistical texture feature, computed using window sizes of 3x3, 5x5, and 7x7 pixels. The results

showed that statistical texture features computed using a 3x3 window size returned the highest correlation coefficient for the estimation of all selected forest structural attributes. Generally, the correlation coefficients declined substantially with increasing window size and tended to level off at a window size 5x5 pixels for both multispectral and panchromatic datasets. This outcome was however expected, given the homogenous and regularly-patterned tree objects in the imagery.

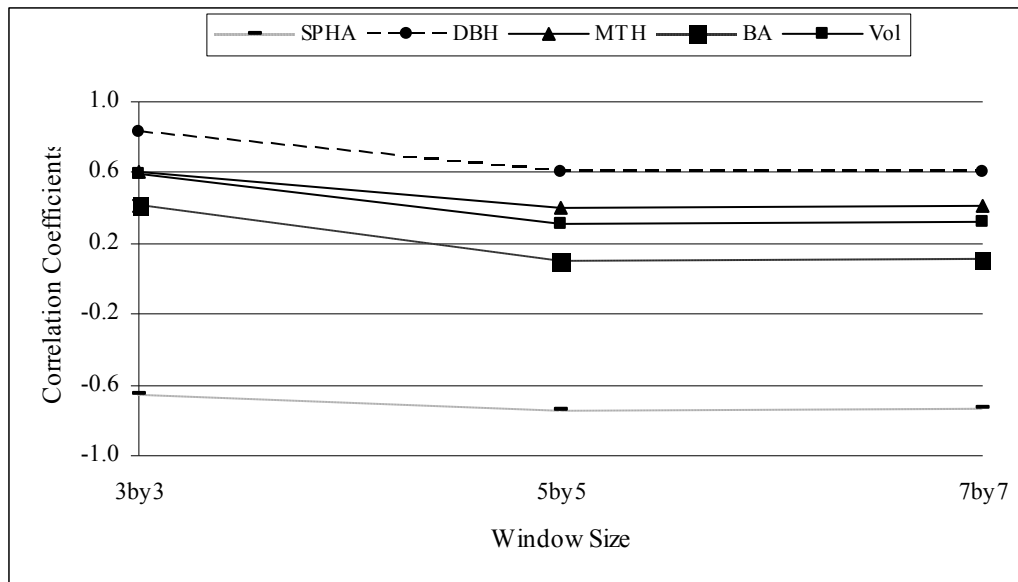


Figure 6.4 Illustration of the window size effect for the estimation of forest structural attributes

Figure 6.5(a) shows the coefficient of determination that was obtained for each forest structural attribute and GLOM, GLCM ($\delta 1$), and GLCM ($\delta 2$) features computed from multispectral IKONOS bands 2, 3, and 4 using a 3x3 window size. GLCM ($\delta 1$) features computed from multispectral IKONOS bands 2, 3, and 4 using a 3x3 window size consistently were the best estimators. Figure 6.5(b) also shows the coefficient of determination that was obtained for each forest structural attribute and GLOM, GLCM ($\delta 1$), and GLCM ($\delta 2$) features computed from panchromatic IKONOS image using a 3x3 window size. Figure 6.5 (a&b) depicts that generally the strength of models developed from GLCM declined with an increase in pixel displacement. The coefficient of determination returned from GLCM $\delta 2$ (pixel displacement of 2) is slightly lower than the coefficient of determination returned from GLCM $\delta 1$ (pixel displacement of 1).

These results support the published results of Kayitakire et al. (2006) for a similar comparison.

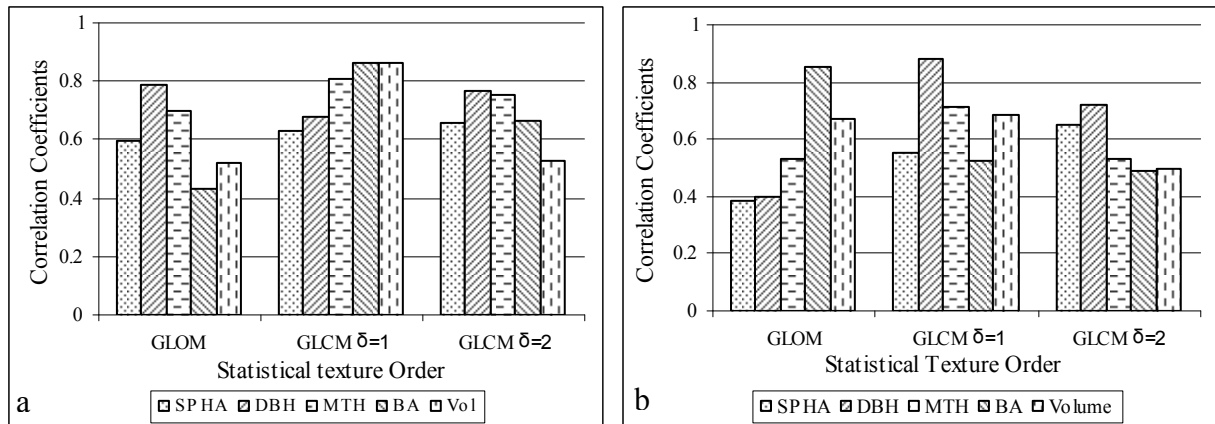


Figure 6.5 Illustration of the statistical texture order and pixel displacement parameter effect on the estimation of forest structural attributes

6.4.2 Multiple linear regression models

A multiple linear combination of GLCM $\delta = 1$ texture features computed from multispectral IKONOS image were identified based on their strength for the estimation of forest structural attributes. Table 6.4 summarizes the coefficients of determination for forest structural attributes and predictor variables derived from the GLCM $\delta = 1$ feature for multispectral IKONOS. SPHA was best explained by the combination of ASM, correlation computed from Band 3, and ASM computed from Band 4 (adjusted $R^2 = 0.63$). ASM and correlation computed from Band 4 and Band 3, respectively, were inversely related with SPHA, whereas ASM computed from Band 3 was directly related with SPHA as shown in Table 6.4. A linear combination of Band 3 mean and Band 4 entropy was the best predictor of DBH (adjusted $R^2 = 0.68$). An inverse relationship was observed between Band 3 mean and DBH, whereas a direct relationship was observed between Band 4 entropy and DBH. A linear combination of entropy and ASM, both computed from Band 2, as well as the mean and entropy, both computed from Band 3, resulted in the best predictive capability for MTH (adjusted $R^2 = 0.81$). Basal area (BA) was best explained by the combination of ASM computed from Bands 3 and 4, and correlation and entropy computed from Band 3 (adjusted $R^2 = 0.81$). ASM, entropy and correlation computed from bands 3 were directly related with BA, whereas ASM

computed from Band 4 was inversely related with BA (Table 6.4). Finally, volume was found to be related to correlation and entropy computed from Band 3 (adjusted R² = 0.86). Entropy and correlation computed from band 3 were directly related with volume as shown in Table 6.4.

Table 6.4 Best regression model for each forest structural variable, based on multi-spectral IKONOS imagery and GLCM $\delta=1$ (n=37)

	Model	Adj R ²	RMSE	ARMSE %
SPHA	4829.466 + 3136.982 (B3-ASM) - 5172.186 (B4-ASM) - 194.35 (B3-Correlation)	0.63	155 spha**	13.4
DBH	28.207 - 1.191 (B3-Mean) + 17.278 (B4 - Entropy)	0.68	1.6 cm**	8.6
MTH	219.224 - 1.651 (B3-Mean) + 9.509 (B3-Entropy) - 131.015 (B2-Entropy) -187.217 (B2-ASM)	0.81	1.8 m*	7.7
BA	88.179 -99.756 (B4-ASM) + 4.545 (B3-Correlation) + 19.822 (B3-Entropy) + 25.276 (B3-ASM)	0.85	2.4 cm*	8.3
Vol.	-289.694 + 140.690 (B3-Correlation) + 427.378 (B3-Entropy)	0.86	43.9cm ³ *	16.0

** Significant at 0.05

* Significant at 0.01

ASM = Angular second moment energy

A separate analysis was conducted for panchromatic IKONOS imagery, which is characterised by a high spatial resolution and a single band data. A multiple linear combination of GLOM and GLCM $\delta=1$ features resulted in the best predictors of forest structural attributes (refer to Figure 6.5b). Table 6.5 summarizes the coefficients of determination for forest structural attributes and selected statistical texture analysis features (GLOM and GLCM $\delta=1$) computed for the panchromatic IKONOS image. SPHA was best explained by the combination of entropy and variance of GLOM, as well as contrast and variance of GLCM $\delta=1$ (adjusted R² = 0.78). Entropy and contrast were inversely related with SPHA, whereas variance of GLOM and GLCM $\delta=1$ was directly related with SPHA (Table 6.5). A linear combination of entropy and variance of GLOM and GLCM $\delta=1$, respectively, proved to be the best estimator of DBH (adjusted R² = 0.89). An inverse relationship was observed between variance and DBH, whereas a direct relationship was observed between entropy and DBH (Table 6.5). A linear combination of entropy, computed from GLOM, and contrast and entropy, computed from

GLCM $\delta=1$, was the best estimator of MTH (adjusted $R^2 = 0.85$). Basal area (BA) were best explained by the combination of variance computed from GLOM and GLCM $\delta=1$ (adjusted $R^2 = 0.86$). A direct relationship was observed between BA and variance of GLOM, whereas inverse relationship was observed between variance of GLCM $\delta=1$ and BA (Table 6.5). Finally, volume was found to be related to variance and entropy, both computed from GLOM and GLCM $\delta=1$ (adjusted $R^2 = 0.88$). Variance and entropy of GLOM as well as entropy of GLCM $\delta=1$ were directly related with volume, whereas variance of GLCM $\delta=1$ was inversely related with volume (Table 6.5).

Table 6.5 Best regression model for each forest structural variable, based on panchromatic IKONOS imagery and GLCM $\delta=1$ (n=37)

	Model	Adj R ²	RMSE	ARMSE %
SPHA	- 5737.757 - 1134.248 (GLOM-Entropy) + 1.744 (GLOM-Variance) + 1.017 (GLCM-Variance) - 15.292 (GLCM-Contrast)	0.78	118 spha*	10.1
DBH	21.379 + 18.809 (GLOM-Entropy) - 0.0125 (GLCM-Variance)	0.89	0.9 cm*	4.5
MTH	- 611.98 + 236.512 (GLOM-Entropy) + 73.127 (GLCM- Entropy) - 0.01017 (GLCM-Variance) - 0.146 (GLCM- Contrast)	0.85	1.7 m**	6.7
BA	- 150.2 + 0.05966 (GLOM Variance) – 0.00355 (GLCM Variance)	0.86	2.4 cm**	8.5
Vol.	- 14258.638 + 0.437 (GLOM-Variance) + 4850.217 (GLOM-Entropy) + 1543.938 (GLCM-Entropy) - 0.193 (GLCM-Variance)	0.88	41cm ³ **	15.4

** Significant at 0.05

* Significant at 0.01

As can be seen in Tables 6.4 and 6.5, model coefficients were statistically significant at 0.05 for functions that estimate SPHA and DBH in the cases of multispectral IKONOS variables. Model coefficients were statistically significant at 0.01 for the same variables, i.e., SPHA and DBH, in the case of panchromatic IKONOS imagery as shown in Table 6.5. Furthermore, the model coefficients for estimation of MTH, BA, and volume were statistically significant at 0.01 in the cases of multispectral IKONOS variables. Results for the same variables, but based on panchromatic IKONOS imagery, showed that coefficients were significant at the 0.05 level. Some caution in the interpretation of the SPHA and volume estimation models are necessary as their absolute root mean square

percentage error (ARMSE %) was greater than 10%, or slightly higher than the acceptable error level in South African commercial plantation forestry.

Figures 6.6 a-e and f-j show the scatter-plots of field-measured and predicted forest structural attributes for the multispectral IKONOS variables and panchromatic IKONOS variables, respectively. The figures also show the correlation coefficients between the field-measured and predicted forest structural attributes.

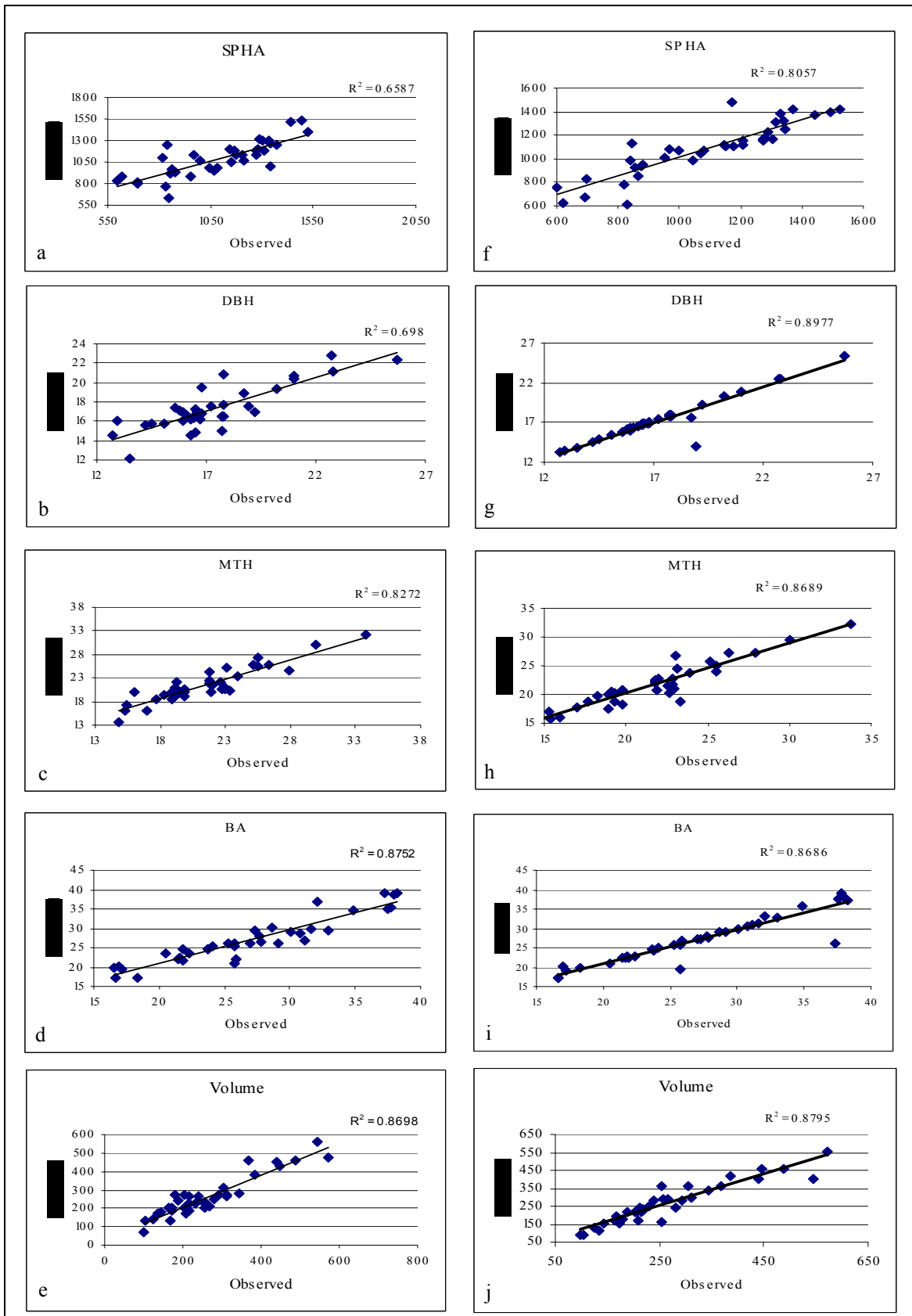


Figure 6.6 Comparison of field measured and predicted forest structural attributes (n=37). Subset figures a-e and f-j show cases for multispectral and panchromatic IKONOS data, respectively

Figure 6.7 shows the comparison between multiple linear regression models developed using statistical features calculated from multispectral and panchromatic IKONOS imagery. The models developed for the estimation of SPHA, DBH, MTH, BA, and volume using statistical texture features computed from panchromatic IKONOS imagery returned the highest correlation coefficients, even though results for BA and volume were almost similar.

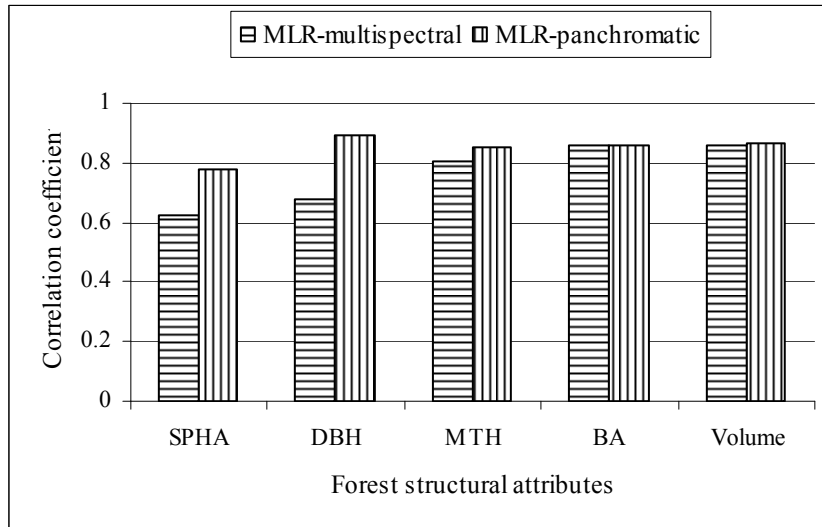


Figure 6.7 Comparison of models developed from multispectral and panchromatic IKONOS imagery

6.4.3 Artificial neural network models

Evaluation of experimental results of the developed ANN models with varying number of nodes in the hidden layer was conducted as a first step. We observed a significant difference in the use of varying number of nodes in the hidden layer architectures. The optimal number of nodes in the hidden layer with the best possible training parameter values is presented in Table 6.6 for the prediction of SPHA, DBH, mean tree height, basal area, and volume. Two and four nodes in the hidden layer were found to be most appropriate for the estimation of SPHA and DBH, while mean tree height, basal area, and volume each required three nodes in the hidden layer for the training and testing process using datasets computed from multispectral IKONOS imagery. Conversely, ANN models with four for SPHA, three for DBH and MTH, and two for BA and volume nodes in the

hidden layer were found to be appropriate for the training and testing process using datasets computed from panchromatic IKONOS imagery. An example showing the procedure used to select the optimal number of nodes in the hidden layer is illustrated in Figure 6.8.

Table 6.6 The ANN-MLP profile for prediction of the various structural parameters using multi-spectral and panchromatic imagery

	Multispectral			Panchromatic		
	Profile	Input	Hidden- node	Profile	Input	Hidden- node
SPHA	MLP 3:3-2-1:1	3	2	MLP 4:4-4-1:1	4	4
DBH	MLP 2:2-4-1:1	2	4	MLP 2:2-3-1:1	2	3
MTH	MLP 4:4-3-1:1	4	3	MLP 4:4-3-1:1	4	3
BA	MLP 4:4-3-1:1	4	3	MLP 2:2-2-1:1	2	2
Volume	MLP 2:2-3-1:1	2	3	MLP 4:4-2-1:1	4	2

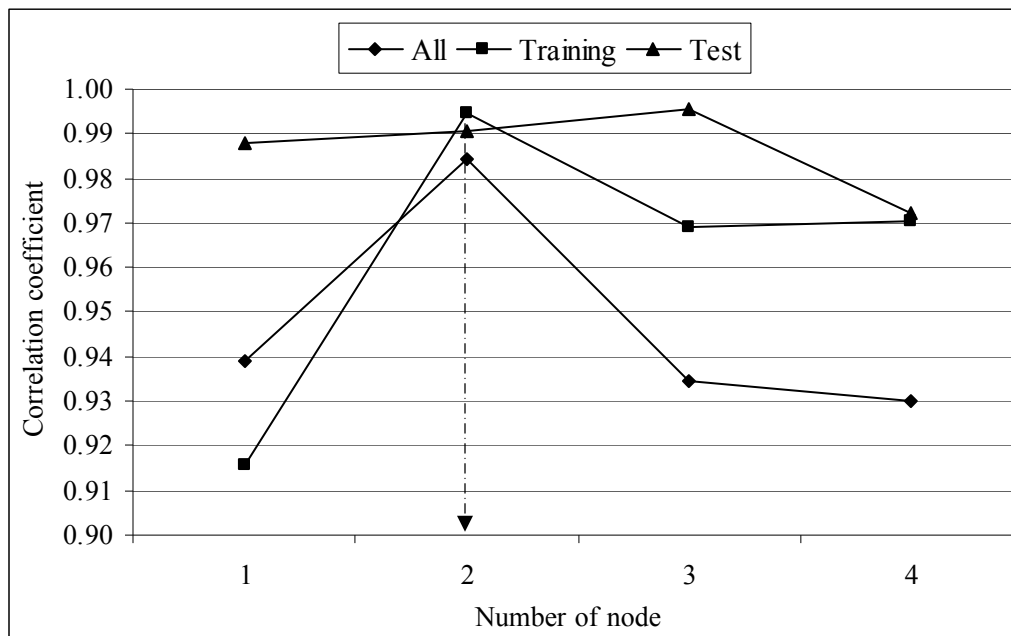


Figure 6.8 Selection of optimal number of nodes in the hidden layer

The optimum numbers of nodes, which returned the highest correlation coefficient for training, testing, and overall datasets, were selected for each model. In general, the procedure employed for the selection of the optimal number of nodes confirms the robustness of the models developed for the prediction of forest structural attributes in this study. Connection weights and thresholds for ANN-MLP models, computed using multispectral IKONOS and panchromatic IKONOS imagery, are presented in Tables 6.7 and 6.8, respectively.

Table 6.7 Connection weights and thresholds of ANN-MLP models for forest structural attributes using multi-spectral IKONOS imagery

Model	Hidden Nodes	Weight				Threshold (bias)	
		Input			Output neuron	Hidden	Output
SPHA		B3-Correlation	B3-SM	B4-SM	HT		
	1	-1.09	1.72	-0.38	0.64	0.05	-0.23
	2	0.43	0.049	-0.76	0.74	-0.76	
DBH		B3-Mean	B4-Entropy		HT		
	1	0.07	0.06		-0.04	-0.82	-0.60
	2	0.19	-0.29		-0.26	-0.04	
	3	0.08	0.05		0.03	-1.28	
MTH		B2-Entropy	B2-SM	B3-Entropy	B3-Mean	HT	
	1	2.20	1.93	-0.99	-0.85	-3.43	1.60
	2	0.01	0.02	-1.17	-1.98	-0.76	0.54
	3	-0.88	0.12	-0.22	-0.56	1.80	-1.63
BA		B3-Correlation	B3-Entropy	B3-SM	B4-SM	HT	
	1	-0.49	-0.40	-0.11	0.33	-3.63	0.98
Volume		B3-Correlation	B3-Entropy			HT	
	1	-0.54	0.58			-0.45	0.93
	2	-1.11	0.79			1.03	-0.57
	3	2.06	0.07			0.83	1.16

Table 6.8 Connection weights and thresholds of ANN-MLP models for forest structural attributes using panchromatic IKONOS imagery

Model	Hidden Nodes	Weight				Output neuron	Threshold (bais)	
		Input					Hidden	Output
SPHA		GLOM-Entropy	GLOM-Variance	GLCM-Variance	GLCM-contrast	HT		
	1	-0.81	-0.50	1.51	-0.19	1.43	0.37	-0.17
	2	0.20	-0.84	0.25	0.08	1.14	-1.01	
	3	-0.46	-1.72	0.76	-0.02	-1.21	-0.40	
	4	0.46	0.73	0.99	0.86	-0.16	0.44	
DBH		GLOM-Entropy	GLCM-Variance			HT		
	1	0.01	-0.02			-0.01	-0.93	-0.71
	2	-0.52	1.11			-0.99	-0.20	
	3	-0.01	0.02			0.01	-0.63	
MTH		GLOM-Entropy	GLCM-Entropy	GLCM-Variance	GLCM-contrast	HT		
	1	0.43	-1.17	-0.80	-0.98	-0.47	-0.37	-0.16
	2	-0.30	-0.93	-0.28	0.69	-0.58	0.36	
	3	0.16	-0.29	-1.12	-0.17	0.99	-0.29	
BA		GLOM-Variance	GLCM-Variance			HT		
	1	-0.25	-0.50			-0.67	-0.74	-0.65
	2	1.09	-1.07			0.77	-0.30	
Volume		GLOM-Entropy	GLOM-Variance	GLCM-Entropy	GLCM-Variance	HT		
	1	-0.90	-0.46	0.83	1.37	-1.12	0.42	0.14
	2	-0.86	-0.66	2.18	1.38	1.35	0.39	

Table 6.9 shows the correlation coefficient and the root mean square error (RMSE), with the values of RMSE also being expressed as % of the mean of the observation values, between each measured forest structural attribute and the associated estimated forest structural attribute for training, test, and pooled datasets. Table 6.9 illustrates that the ANN models, which are developed using statistical texture features computed from multispectral IKONOS data, produced acceptable models for the estimation of forest structural attributes. The relationship between observed and predicted values based on the pooled dataset was $r = 0.83, 0.83, 0.93, 0.94,$ and 0.94 , while their respective RMSE values were 140 spha, 1.51 cm, 1.60 m, 2.23 cm^2 , and 42.82 cm^3 for SPHA, DBH, mean tree height, basal area, and volume, respectively. The corresponding values for the test dataset were 0.83, 0.85, 0.94, 0.94, and 0.95 (correlation coefficients), with RMSE values

of 195 spha, 1.46 cm, 1.92 m, 1.59 cm², and 44.74 cm³, respectively. The similarity between the coefficients of the pooled and testing datasets is indicative of the strength of the developed models.

Table 6.9 further serves to illustrate that the ANN models, which are developed using statistical features computed from panchromatic IKONOS imagery, arguably produced the best models for the estimation of forest structural attributes. The relationships between observed and predicted values using the pooled dataset were $r = 0.99, 0.95, 0.95, 0.93,$ and 0.98 , while their RMSE values were 86 spha, 0.88 cm, 1.25 m, 2.34 cm², and 22.79 cm³ for SPHA, DBH, MTH, BA, and volume, respectively. Application of the test dataset resulted in correlation coefficients of 0.95, 0.99, 0.93, 0.93, and 0.99; the corresponding RMSE values were 90 spha, 0.86 cm, 1.43 m, 2.54 cm², and 30.13 cm³, respectively. These results also bode well in terms of relative strength of the models developed.

Table 6.9 ANN model performance for forest structural attribute estimation using multi-spectral and panchromatic IKONOS imagery

Model	Data	Multispectral IKONOS			Panchromatic IKONOS			N
		Corr.Coef.	RMSE	ARMSE%	Corr.Coef.	RMSE	ARMSE%	
SPHA	Training	0.83	123	11.1	0.90	96	8.18	19
	Testing	0.83	195	17.4	0.95	90	9.14	9
	Cross validation	0.82	105	10.3	0.94	47	4.93	9
	Pooled	0.83	140	12.9	0.99	86	7.89	37
DBH	Training	0.86	1.3	7.4	0.93	1.04	6.25	19
	Testing	0.85	1.4	8.4	0.99	0.86	4.98	9
	Cross validation	0.84	1.9	11.4	0.99	0.37	2.14	9
	Pooled	0.83	1.5	8.7	0.95	0.88	5.07	37
MTH	Training	0.93	1.4	6.8	0.95	1.10	5.11	19
	Testing	0.94	1.9	9.0	0.93	1.43	6.37	9
	Cross validation	0.95	1.5	6.8	0.95	1.37	6.10	9
	Pooled	0.93	1.6	7.4	0.95	1.26	5.81	37
BA	Training	0.94	2.3	8.8	0.91	2.64	9.48	19
	Testing	0.94	1.6	5.9	0.93	2.54	9.78	9
	Cross validation	0.94	2.5	9.3	0.99	1.16	4.46	9
	Pooled	0.94	2.2	8.3	0.93	2.34	8.71	37
Volume	Training	0.92	39.9	15.5	0.99	10.97	4.32	19
	Testing	0.95	44.7	16.7	0.99	30.13	9.63	9
	Cross validation	0.96	46.7	21.2	0.95	31.20	9.97	9
	Pooled	0.94	42.8	16.3	0.98	22.80	8.68	37

Figure 6.9 shows the comparison between models developed using statistical texture features calculated from multispectral and panchromatic IKONOS imagery. The models developed for the estimation of SPHA, DBH, MTH and volume using statistical texture features computed from panchromatic IKONOS returned relatively higher correlation coefficients when compared to the corresponding models computed from multispectral IKONOS imagery. Models for the estimation of BA, using variables computed from either multispectral or panchromatic IKONOS imagery, resulted in similar correlation coefficients.

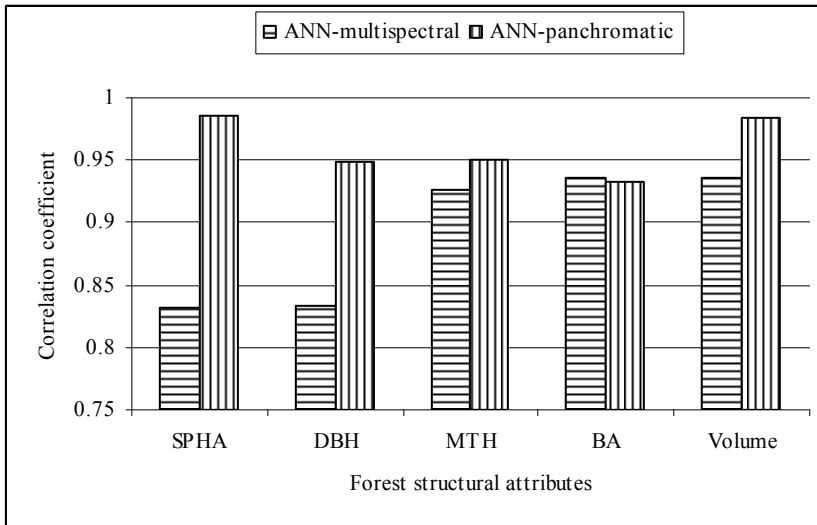


Figure 6.9 Comparison of models developed using statistical texture features computed from multispectral and panchromatic IKONOS imagery

6.4.4 Comparison of the MLR and ANN

Figure 6.10 (a) shows the performance comparison between MLR and ANN models developed using statistical texture features computed from multispectral IKONOS data. Figure 6.10 (a) illustrates that higher ARMSE% values were observed in the case of the MLR models for the estimation of SPHA and MTH; increases of 1.97% and 2.19% in ARMSE% were observed for SPHA and MTH, respectively, when comparing MLR to ANN models. Conversely, slightly higher (0.87%) ARMSE% values were observed for the ANN models in the cases of DBH and volume estimations. The ARMSE% of MLR and ANN models for the estimation of BA was the same, while they are below 10%.

Figure 6.10 (b), also shows the performance comparison between MLR and ANN models, developed using statistical texture features computed from panchromatic IKONOS data. Higher ARMSE% values were observed for the MLR models in the cases of SPHA, MTH, and volume estimations. Increased errors of 12.54%, 7.19%, and 27.96% were observed for SPHA, MTH, and volume, respectively, when comparing MLR to ANN models. However, slightly higher ARMSE% outcomes were observed for estimation of DBH (0.79%) and BA (1.10%) when applying ANN instead of MLR models.

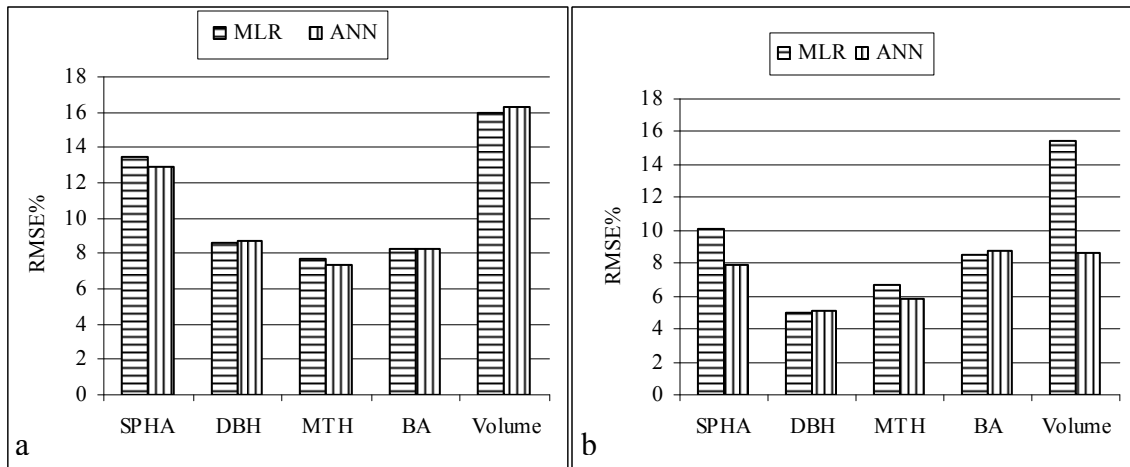


Figure 6.10 Comparison of models developed using multiple linear regression and artificial neural network statistical methods for the estimation of forest structural attributes computed from multispectral (a) and panchromatic (b) IKONOS imagery

6.5 Discussions

6.5.1 Forest attribute estimation from multispectral IKONOS imagery

Band 3 (red) and Band 4 (NIR) of IKONOS imagery provided useful information for the estimation of forest structural attributes. For example, the red band generated the most useful GLCM statistical texture features (correlation and entropy variables) for the estimation of volume from the multispectral IKONOS bands. GLCM statistical texture features (angular second moment energy and correlation), computed from the red and NIR bands, respectively, also resulted in the most suitable variables for the estimation of SPHA. Furthermore, the entropy and mean of GLCM statistical texture features computed from red and NIR bands, respectively, returned the highest coefficient of determination for the estimation of DBH. In yet another important example, GLCM statistical texture features, e.g., angular second moment, correlation, and entropy, computed from the red band and the second moment computed from NIR band, resulted in the highest coefficient of determination for the estimation of basal area. Finally, the GLCM statistical texture features of angular second moment and entropy, computed from the NIR band, and entropy and variance computed from the red band returned the highest coefficient of determination for the estimation of mean tree height. The structurally-relevant information embedded in the red and NIR spectral regions has been confirmed

results from various other studies, e.g., Foody et al. (1997), Häme et al. (1997), Eklundh and Olsson (2003), Xu et al. (2003), Lu et al. (2004), Ingram et al. (2005), Heiskanen (2006), van Aardt et al. (2007)

A key observation from this study, is that strong relationships between IKONOS-derived statistical texture features and field-measured forest structural attributes provide evidence that important plantation structural information can be extracted from remote sensing imagery using textural features. This adds to previous studies which showed that when only IKONOS spectral information was used, e.g., band reflectance and/or vegetation index data, the highest R^2 values for the estimation of forest structural attributes varied from 0.30 to 0.66 (vanAardt et al., 2007). This study contributed to the body of evidence that conclusively shows that statistical texture features can improve the estimation accuracy for forest structural attributes. Similar results on the importance of texture for estimating forest structure attributes from high spatial resolution image data have been documented in other studies, e.g., Coops and Culvenor (2000), Franklin et al. (2001), Kayitakire et al. (2006), and Johansen et al. (2007).

All five forest variables were accurately estimated when using multiple regression models. The highest R^2 value was achieved for volume, while the lowest was for SPHA; however, the RMSE% returned for volume was the highest at 16.1%. It is interesting to note that mean tree height resulted in the lowest RMSE% of 7.71%. This corresponds with results from Kayitakire et al. (2006).

6.5.2 Forest attribute estimation from panchromatic IKONOS imagery

Results from the stepwise selection algorithm indicated that the best relationships were achieved through a combination of GLOM and GLCM statistical texture features in a multi-regression model. This demonstrated that the combination of the different information sources i.e. GLOM and GLCM provided unique information towards the estimation of forest structural attributes at high levels of accuracy. However, one of the aims of this study was to provide models that had estimation errors that addressed requirements from plantation forest managers. Thus the GLOM features and GLCM

features were used collectively for developing multi-regression and ANN models for the estimation of forest structural attributes.

Sensitivity analysis also showed that GLCM variance and GLCM entropy statistical features resulted in improved relationships with forest structural attributes, when compared to alternative statistical texture features. A number of studies, including Franklin et al. (2001), Rao et al. (2002), Coburn and Roberts (2004), and Kayitakire et al. (2006), have mentioned the value that variance and entropy have when gauging forest structure using panchromatic IKONOS imagery.

6.5.3 Comparison between multispectral and panchromatic IKONOS imagery

Multiple linear regression models resulted in strong correlations between selected statistical texture features and forest structural attributes and, thus, are potentially promising for operational forest structural attribute estimation. The panchromatic data resulted in increased estimation accuracy of the SPHA, DBH, MTH, BA, and volume by 19.7%, 23.8%, 5.5%, 0.1%, and 0.2% respectively as compared with the multispectral data. Models based on the panchromatic IKONOS data provided the highest estimates of forest structural attributes (Tables 5 and Table 9). The possession of high spatial and wide wavelength range leads the potential applications of panchromatic IKONOS data for the estimation of forest structural attributes. Studies by Franklin et al. (2001) and Kayitakire et al. (2006) found that panchromatic IKONOS image effectively estimated forest variables. A study by Hyypä et al. (2000) furthermore asserted that the accuracy of forest structural variable estimations increase with an increase in the spatial resolution of the sensor used.

6.5.4 Comparison between a multiple linear regression and artificial neural network

Although the results from multiple linear regression models exhibited strong correlations between selected statistical texture features and forest structural attributes, the ANN approach was robust across all forest structural attributes and provided more estimation power than linear regression models. Using a neural network, the root mean square error

for the forest structural attribute estimation models was reduced by almost half in certain instances. The strong and significant relationships between estimated and actual field measured forest structural attributes supports the utility of ANN for the estimation of forest structural attributes from statistical texture features in this study (refer to Figure 6.10). The observed improved performance of the ANN approach over the MLR approach was attributed mainly to the ability of ANN's to capture non-linear relationships (Ingram et al. 2005). Their intrinsic non-linear structure makes them particularly suitable as fitting tools in forest structure applications.

6.6. Conclusions

Two independent investigations were conducted during the course of this study; the first investigation used statistical texture features computed from multispectral IKONOS imagery, while the second investigation used statistical texture features computed from panchromatic IKONOS imagery, both for the estimation of forest structural attributes. Multiple linear regression and artificial neural network statistical approaches were employed to measure the relationship between field measured forest structural attributes and statistical texture features computed from the multispectral and panchromatic IKONOS imagery.

The study illustrated that estimation of forest structural attributes using statistical texture features, computed from panchromatic IKONOS imagery, have significant potential. The model developed using the artificial neural network method for the prediction of stems per hectare, diameter at breast height; mean tree height, basal area, and volume were better performed for estimating forest structural attributes for the study site.

This study demonstrated the potential of remote sensing high spatial resolution imagery (IKONOS) for *Eucalyptus* plantation forest structural attribute prediction in the temperate climatic zone of South Africa. However, further research is required to document the performance of the retrieval under different environmental conditions and topographical changes, as well as for other species.

6.7 Acknowledgements

This study was conducted as part of a remote sensing cooperative program between MONDI SA, the Council for Scientific and Industrial Research (CSIR), and the University of Kwa-Zulu Natal to investigate the potential of satellite remote sensing imagery for prediction of plantation forest structural attributes. The authors would like thank Wesley Roberts, Solomon Gebremariam, Thamsanqa Mzinyane, and Wesley Naidoo for their assistance during field work. Financial support for this study was provided by the CSIR and MONDI SA.

6.8 References

Boyd, D.S. and Danson, F.M., 2005, Satellite remote sensing of forest resources: Three decades of research development. *Progress in Physical Geography*, 29: 1-26.

Boyd, D.S., Foody, G.M., and Ripple, W.J., 2002, Evaluation of approaches for forest cover estimation in the Pacific Northwest, USA, using remote sensing. *Applied Geography*, 22: 375-392.

Carvalho, L.M.T., Clevers, J.P.W., Skidmore, A.K. and De-jong, S.M., 2004, Selection of imagery data and classifiers for mapping Brazilian semi-deciduous Atlantic forests. *International Journal of Applied Earth Observation and Geoinformatics*, 5: 173-186.

Chitroub, S., 2005, Neural network model for standard PCA and its variants applied to remote sensing. *International Journal of Remote Sensing*, 26: 2197-2218.

Chubey, M.S., Franklin, S.E. and Wulder, M.A., 2006, Object based analysis of IKONOS-2 imagery for extraction of forest inventory parameters. *Photogrammetric Engineering and Remote Sensing*, 72: 383-394.

Coburn, C.A. and Roberts, A.C.B., 2004, A multiscale texture analysis procedure for improved forest stand classification. *International Journal of Remote Sensing*, 25: 4287-4308.

Coetzee, J. 1992, I: An improved method of estimating tree volume utilization of *Eucalyptus grandis*. II: A revised tree volume table for short rotation *Eucalyptus grandis* timber crops. ICFR Bulletin 9/92.

Coops, N. and Culvenor, D., 2000, Utilizing local variance of simulated high spatial resolution imagery to predict spatial pattern of forest stands. *Remote Sensing of Environment*, 71: 248–260.

Culvenor, D.S., 2002, TIDA: An algorithm for the delineation of tree crowns in high spatial resolution remotely sensed imagery. *Computers and Geosciences*, 28: 33–44.

Diamantopoulou, M.J., 2005, Artificial neural networks as an alternative tool in pine bark volume estimation. *Computers and Electronics in Agriculture*, 48: 235-244.

Eklundh, L. and OLSSON, L., 2003, Vegetation index trends for the African Sahel 1982-1999. *Geophysical Research Letters*, 30: 1430-1433.

Fauselt, L., 1994, *Fundamentals of Neural Networks*. New York: Prentice Hall.

Foody, G.M., Lucas, R.M., Curran, P.J. and Honzak, M., 1997, Mapping tropical forest fractional cover from coarse spatial resolution remote sensing imagery. *Plant Ecology*, 131: 143–154.

Franklin, S.E., Hall, R.J., Moskal, L.M., Maudie, A.J. and Lavigne, M.B., 2000, Incorporating texture into classification of forest species composition from airborne multispectral images. *International Journal of Remote Sensing*, 21: 61–79.

Franklin, S.E., Wulder, M.A. and Gerylo, G.R., 2001, Texture analysis of IKONOS panchromatic data for Douglas-fir forest age class separability in British Columbia. *International Journal of Remote Sensing*, 22: 2627–2632.

Gebreslasie, M.T., Ahmed, F.B., and van Aardt, J.A.N., 2008, Estimating plot-level forest structural attributes using high spectral resolution ASTER satellite data in even-aged Eucalyptus plantations in Southern KwaZulu-Natal, South Africa. *Southern Forests*, 70, 129-141.

Goetz, S.J., Wright, R., Smith, A.J., Zinecker, E. and Schaub, E., 2003, IKONOS imagery for resource management: Tree cover, impervious surfaces and riparian buffer analyses in the mid-Atlantic region. *Remote Sensing of Environment*, 88: 195–208.

Gougeon, F.A., Leckie, D.G., Paradine, D. and Scott, I., 1999, Individual tree crown species recognition: The Nahmint study. In Hill, D., & Leckie, D., (Eds.), *Automated interpretation of high spatial resolution digital imagery for forestry*. (pp. 209–223). Canada: Canadian Forest Service, Victoria, B.C.

Hall, R.J., Skakun, R.S., Arsenault, E.J. and Case, B.S., 2006, Modelling forest stand structure attributes using Landsat ETM+ data: application to mapping of aboveground biomass and stand volume. *Forest Ecology and Management*, 225: 378-390.

Häme, T., Salli, A., Andersson, K. and Lohi, A., 1997, A new methodology for estimation of biomass of conifer-dominated boreal forest using NOAA AVHRR data. *International Journal of Remote Sensing*, 18: 3211– 3243.

Haralick R.M., 1979, Statistical and Structural Approach to Texture. *Proceeding of the IEEE*, 67: 786-804.

Hay, G.J., Niemann, K.O. and Mclean, G.F., 1996, An objectspecific image-texture analysis of H-resolution forest imagery. *Remote Sensing of Environment*, 55: 108–122.

Haykin, S., 1994, *Neural Networks: A Comprehensive Foundation*. *The Knowledge Engineering Review*, 13: 409-412.

Heiskanen, J., 2006. Estimating aboveground tree biomass and leaf area index in a mountain birch forest using ASTER satellite data. *International Journal of Remote Sensing*, 27: 1135 – 1158.

Holmgren, P. and Thuresson, T., 1998, Satellite remote sensing for forestry planning: a review. *Scandinavian Journal of Forest Research*, 13: 90– 110.

Hyypä, H., Inkinen, M., Engdahl, M., Linko, S. and Zhu, Y.H., 2000, Accuracy comparison of various remote sensing data sources in the retrieval of forest stand attributes. *Forest Ecology and Management*, 128: 109-120.

Ingram, J.C., Dawson, T.P. and Whittaker, R.J., 2005, Mapping tropical forest structure in south-eastern Madagascar using remote sensing and artificial neural networks. *Remote Sensing of Environment*, 94: 491-507.

Jensen, J.R., Qui, F. and Ji, M., 1999, Predictive modeling of coniferous forest age using statistical and artificial neural network approaches applies to remote sensor data. *International Journal of Remote Sensing*, 20: 2805-2822.

Johansen, K., Coops, N.C., Gergel, S.E. and Stange, Y., 2007, Application of high spatial resolution satellite imagery for riparian and forest ecosystem classification. *Remote Sensing of Environment*, 110: 29-44.

Kayitakire, F., Hamle, C. and Defourny, P., 2006, Retrieving forest structure variables based on image texture analysis and IKONOS-2 imagery. *Remote Sensing of Environment*, 102: 390-401.

Lillesand, T. M., Kiefer, R. W. and Chipman, J. W., 2004, *Remote sensing and Image interpretation*. (5th ed.), Wiley, New York, pp. 785.

Lu, D., Mausel, P., Brondizio, E. and Moran, E., 2004, Relationships between forest stand parameters and Landsat TM spectral response in Brazilian Amazon Basin. *Forest Ecology and Management*, 198: 149-167.

Materka, A. and Strzelecki, M., 1998, *Texture Analysis Methods – A Review*, Technical University of Lodz, Institute of Electronics, COST B11 report, Brussels 1998.

Mcroberts, R.E. and Tomppo, E.O., 2007, Remote sensing support for national forest inventories. *Remote Sensing of Environment*, 110: 412-419.

Mihran, T. and Jain, A. K., 1998, Texture Analysis, *The Handbook of Pattern Recognition and Computer Vision* (2nd Edition), by Chen C. H., Pau, L. F., and Wang, P. S. P. (eds), pp. 207-248, World Scientific Publication Co.

Munionsen, E., Maltamo, M., Hyppanen, H. and Vainikainen, V. 2001, Forest stand characteristics estimation using a most similar neighbour approach and image spatial structure information. *Remote Sensing of Environment*, 78: 223-228.

Norris-Rogers, M., 2006, An investigation into using texture analysis and change detection techniques on medium and high spatial resolution imagery for monitoring plantation forest operations, unpublished Ph.D. thesis, University of KwaZulu-Natal.

Ojala, T., Pietikäinen, M. and Harwood, D., A 1996, comparative study of texture measures with classification based on feature distribution. *Pattern Recognition*, 29: 51-59

Pao, H. T. 2008, A comparison of neural network and multiple regression analysis in modelling capital structure. *Expert Systems with Applications*, 35: 720-727.

Patterson, D. 1996, *Artificial Neural Networks*. Singapore: Prentice Hall.

Rahman, M.M., Csaplovics, E. and Koch, B., 2005, An efficient regression strategy for extracting forest biomass information from satellite sensor data. *International Journal of Remote Sensing*, 26: 1511-1519.

Rao, P.V.N., Sai, M.V.R.S., Sreenivas, K., Rao, M.V.K., Rao, B.R.M., Dwivedi, R.S. and Venkataratnam, L. 2002, Textural analysis of IRS-1D panchromatic data for land cover classification. *International Journal of Remote Sensing*, 23: 3327–3345.

Sivanpillai, R., Smith, C.T., Srinivasan, R., Messina, M.G. and Wu, X.B., 2006, Estimation of managed loblolly pine stand age and density with Landsat ETM+ data. *Forest Ecology and Management*, 223: 247–254.

SPSS for Windows, Release 15, 2006, Chicago, SPSS Inc.

STATSOFT, Inc. 2004, STATISTICA (data analysis software system), Version 7.

St-louis, V., Pidgeon, A.M., Radeloff, V.C., Hawbaker, T.J. and Radeloff, V.C., 2006, High-resolution image as a predictor of bird species richness. *Remote Sensing of Environment*, 105: 299-312.

Tsai, F. and Chou, M.J., 2006, Texture augmented analysis of high resolution satellite imagery in detecting invasive plant species. *Journal of Chinese Institute of Engineers*, 29: 581-592.

Tuceryan, M. Jain, A.K., 1998, *Handbook of Pattern Recognition and Computer Vision*, Chapter 2: Texture Analysis, World Scientific, Singapore.

Vanaardt, J., Gebreslasie, M., Tesfamichael, S., Wesly, R., 2007, Investigating structural-spectral Interactions in managed even-aged Eucalyptus plantations using lidar and multispectral high resolution data. *Proceedings of SPIE -- Volume 6742*.

Wulder, M.A., Ledrew, E.F., Franklin, S.E. and Lavigne, M.B., 1998, Aerial Image texture information in estimation of Northern deciduous and mixed wood forest leaf area index. *Remote Sensing of Environment*, 64: 64-76.

Xu B., Gong, P. and Pu, R., 2003, Crown closure estimation of oak savanna in a dry season with Landsat TM imagery: comparison of various indices through correlation analysis. *International Journal of Remote Sensing*, 24: 1811-1822.

Zawadzki, J., Cieszewski, C.J. and Zasada, M., 2005, Semivariogram analysis of Landsat 5TM texture data for Loblly Pine forests. *Journal of Forest Science*, 51: 47-59.

CHAPTER 7

Individual tree detection based on variable and fixed window size local maxima filtering applied to IKONOS imagery for even-aged *Eucalyptus* plantation forests in KwaZulu-Natal, South Africa

* This paper based on:

Gebreslasie, M., Ahmed, F.B. and van Aardt, J., *in review* Individual tree detection based on variable and fixed window size local maxima filtering applied to IKONOS imagery for even-aged *Eucalyptus* plantation forests in KwaZulu-Natal, South Africa. *International Journal of Remote Sensing*.

Abstract. Detection of individual trees remains a challenge for forest inventory efforts in especially homogeneous, even-aged plantation scenarios. Mainly detection of individual trees using local maxima filtering was applied to airborne imagery, where point spread function and signal-to-noise ratio are smaller comparing to satellite-borne imagery. This led to the development of a novel approach to local maxima filtering for tree detection in plantation forests in KwaZulu-Natal, South Africa, using satellite remote sensing imagery. The developed approach is based on Gaussian smoothing for noise reduction and image classification, i.e. natural break classification to determine the threshold for removing pixels of extremely bright and dark areas in the imagery. These pixels are assumed to belong to the background and hinder the search for tree peaks. A semivariogram technique was applied to determine variable window sizes for local maxima filtering within a plantation stand. A fixed window size for local maxima filtering was also applied using pre-determined tree spacing. Evaluation of the various approaches was based on aggregated assessment methods. The overall accuracy using a variable window size was 85 % (RMSE = 189 trees), whereas a fixed window size resulted in an accuracy of 80 % (RMSE = 258 trees). The approach worked remarkably well in mature forest stands as compared to the young forest stands. These results are encouraging to temperate-warm climate plantation forest companies, who deals with even-aged, broadleaf plantations and forest inventory practices that require assessment at the age of eight years, or one year before harvesting.

7.1 Introduction

The structural attribute of interest in this study is stems per hectare (SPHA). SPHA forms the basis of forest inventory, e.g., scaling of tree-level volume and biomass estimates to larger areas, and as such is very important to forest management decision making (Leckie et al., 2003). The most widely used method for deriving forest structure information currently entails the utilization of sampling designs with often randomly selected plots. This leads to derivation of the final forest stand parameters based on statistical extrapolation methods (Esler, 2004). However, even though field-based approaches are effective in terms of accuracy and precision of estimates, such approaches typically are costly, which leads to infrequent assessment. Remote sensing approaches, on the other

hand, provide potential low-cost alternatives to field based assessment, but require the development of methods for accurate extraction of the required information (Wulder, 1998; Hyyppä et al., 2000; Boyd and Danson, 2005). A specific piece of the forest inventory puzzle is accurate assessment of SPHA. This has led to the extraction of individual tree locations using high spatial resolution remote sensing imagery, an alternative to remote sensing empirical approaches (Roberts et al., 2007). Research on the topic of individual tree detection, which became possible with the advent of very high spatial resolution imagery, remains a relatively new focus in the remote sensing community.

The basic theory behind tree detection techniques is that variations between image brightness values at tree crown apexes and decreasing brightness towards the crown edges can be used to delineate tree crowns (Brandtberg, 2002; Culvenor, 2002; Leckie et al., 2003; Erikson and Olofsson, 2005). Accurate estimation of individual tree location and extent ultimately can provide estimates of SPHA and spatial patterns that are in turn useful as inputs to growth modelling and merchantable volume estimation models.

A variety of approaches to tree detection exist. The template matching method, where a series of models are constructed to characterize what a tree looks like at different locations in an image, takes into consideration the tree's geometric and radiometric properties. Once this information has been developed, a moving-window correlation procedure is implemented to search for the best matching facet, i.e., where trees are most likely to occur (Pollock, 1999; Larsen and Rudemo, 1998; Quackenbush et al., 2000; Olofsson et al., 2006). The valley-following method is based on a set of predefined rules that are required before the actual crown-following takes place (Gougeon, 1995; Culvenor, 2002; Persson, et al., 2002). Tree peaks are identified by following the local upward gradient from a given pixel to the brightest local value. In contrast, the edge detection method evaluates the occurrence of edges over several image scales to define a region in which the brightness pixel value is taken as a representative location of the tree peak (Brandtberg and Walter, 1998). Finally, local maxima filtering (Wulder et al., 2000; Pouliot et al., 2002; Wang et al., 2004; Wulder and White, 2004; Korpela et al., 2006),

where the maximum pixel brightness value is assumed to represent the tree peak, applies a moving-window of a specified window size.

Promising results for detection of individual trees in plantation forests have been reported, with local maxima approaches used in Canada (Wulder et al., 2000; Wulder et al., 2002; Wulder and White, 2004) and Finland (Pitkänen, 2001). Wulder et al. (2000) used a 1 meter spatial resolution image, which was simulated from the six channels of the Multi-Detector Electro-Optical Imaging Sensor (MEIS-II), for the detection of tree location in British Columbia, Canada for Douglas fir (*pseudotsuga menziesii*) and red cedar (*Thuja plicata*) species. The local maximum filtering approach included smoothing and a fixed window-size was applied. The method showed that 64 % of trees could be correctly located, while a 22 % commission error and 36 % omission error was observed. The authors included a variable window size, defined by image spatial structure, at the same study site for the same imagery. They reported an overall accuracy of 67 % and a decrease in commission error to 11 % (Wulder et al., 2002). Wulder and White (2004) also compared airborne (MEIS-II) and satellite (IKONOS) high spatial resolution image for detection of individual trees in British Columbia, Canada. The results of the local maxima approach showed that although the IKONOS data accurately identified 85 % of individual trees in the study area, the commission error was large at 51 %. When compared to an overall accuracy of 64 % for the MEIS-II data with a commission error of 22 %, an error of 51 % may deter forest managers from using this approach. Pitkänen (2001) used aerial-image data of 75 cm spatial resolution detection of tree location in southern Finland for Scots pine (*Pinus sylvestris*) species. Gaussian image smoothing and binarization were introduced as pre-processing steps. Smoothing was used for noise reduction, while binarization was used to restrict the local maxima search to the bright areas of the images that were assumed to be tree crowns. The approach yielded acceptable results in forest stands with a low density, with 95 % of the trees being detected in these forest stands, whereas only 54 % were detected in high density forest stands.

Studies such as those described above promise well for the application of high spatial resolution remote sensing data to the detection of individual trees. However, conclusive

results are still lacking in temperate-warm climates for broadleaf, even-aged plantations scenarios. In this study we therefore investigated the local maxima filtering approach to this problem in even-aged South African *Eucalyptus* plantations. Local maxima filtering makes an assumption that the peak of the crown reflectance is located at, or very close to, the treetop and that it has relatively high spectral reflectance at this location and is surrounded by a dark background. We hypothesised that the probability of finding the peak of a tree crown could be increased by removing the extreme bright and dark pixels from the imagery before variable window local maxima filtering.

In this study, local maxima filtering methods introduced by Wulder et al. (2000) were expanded to improve tree detection using high spatial resolution satellite remote sensing imagery (panchromatic IKONOS imagery) in *Eucalyptus* plantations. The aims of this study were (i) to investigate natural break classification, which was carried out prior to the local maxima tree detection in order to eliminate non-tree crown area from the imagery and (ii) to compare the results from variable window size local maxima filtering to those obtained from fixed window size local maxima filtering. The variable window size was defined using voronoi diagrams and average semivariance range, while a priori tree spacing information was used in the case of a fixed window size.

7.2 Materials and Methods

7.2.1 Study area

The study area is located in the southern KwaZulu-Natal province of South Africa, also known as the KwaZulu-Natal Midlands. The sites chosen for this research are all managed by MONDI-SA Forest Company. Geographically, the site lies between 29° 43' 4" and 29° 56' 49" South and 30° 1' 43" and 30° 17' 26" East, as shown in Figure 5.1. The terrain in the study area ranges from gently undulating to highly dissected, strongly rolling, and hilly topography. Elevations range between 800 and 1400 m above-mean-sea-level. The geology consists of sandstone and clay formations, which have resulted in sandy clay to sandy clay loam soils. Plantation forestry is a major land use in the study area due to the suitable climate and soils. Rainfall ranges from 820 to 1300 mm, but

averages 1000 mm per annum mostly falling between October and April. Temperatures vary between 24 °C to 26 °C in summer, but drop to between 5°C and 14 °C in winter.

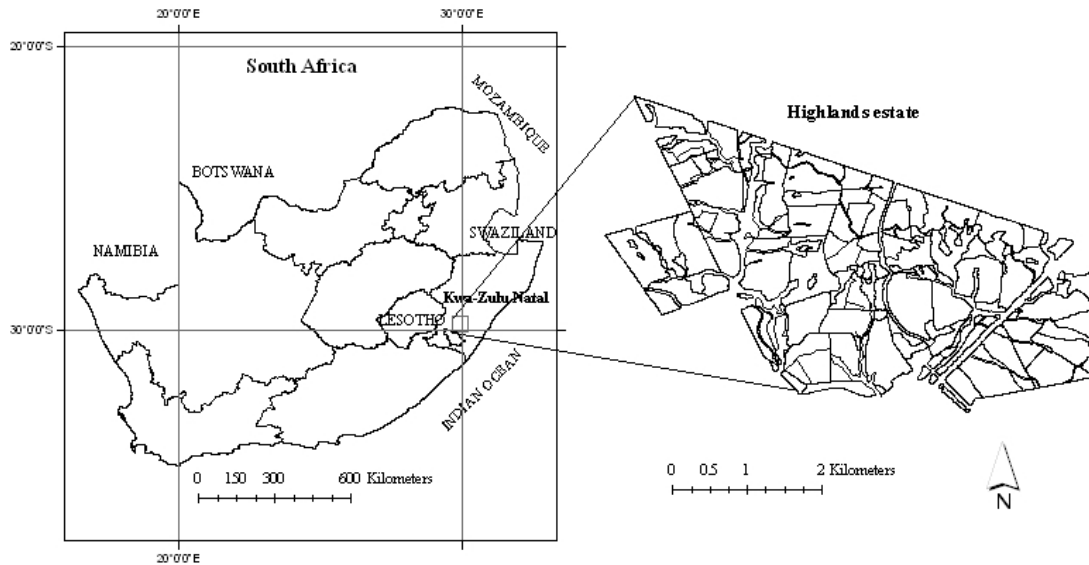


Figure 7.1 The location of the study sites in KwaZulu-Natal, South Africa

7.2.2 Field data

The study was based on data from a conventional forest inventory, carried out by MONDI-BP. The field data collection was conducted in October 2006 in 18 *Eucalyptus* plantation stands. Conventional forest inventory was based on sample plot measurements and visual estimation. The centre of each circular, 15 m radius plot was located using a compass and distance tape, relative to an accurate differentially-corrected global position systems (GPS) location external to the stand, in order to avoid within-stand GPS multi-path effects. Plot area was adjusted for slope in area of non-flat topography using a slope reading taken from a Vertex III hypsometer. Plots were subsequently mapped and spatially referenced in a Geographic Information System (GIS) using these data (i.e., GPS readings, bearings, and distance). Diameter at breast height (DBH; cm), total tree height (m), and stems per sampled plot were obtained and SPHA were computed for each stand.

The descriptive statistics from the field data are depicted in Table 7.1. The average stem per hectare was 1085 SPHA with a standard deviation of 253 SPHA. The mean tree height was 21.1 m with standard deviation of 4.3 m. The mean DBH was 17.2 cm, whereas the smallest tree had a DBH of 12.2 cm.

Table 7.1 Descriptive statistics of tree-level plantation structural attributes

Character	SPHA	DBH (cm)	Tree height (m)
Number-stands	16	16	16
Mean value	1085	17.2	21.1
Standard Deviation	253	3.1	4.3
Minimum Value	598	12.2	13.9
Maximum Value	1522	29.4	36.1

7.2.3 Remote sensing data

The panchromatic IKONOS images used in this study were acquired on October 2006. Detailed information about the acquisition configuration is reported in Table 7.2.

Table 7.2 IKONOS image characteristics

Characteristic	Specifications
Date/time(GMT)	2006-10-23/08:17
Sun angle elevation	52.875°
Sun Angle azimuth	41.4681°
Sensor angle elevation	66.99317°
Sensor angle azimuth	359.97°
Spectral bands wavelengths	0.45 - 0.9 µm

The imagery was geo- and ortho-rectified and converted to Universal Transverse Mercator (UTM; zone 36) projection and WGS 84 datum. A total of 48 ground control points were used for this purpose. A nearest neighbour re-sampling technique was used and an overall total root mean square error of less than half a pixel was obtained.

7.2.4 Tree detection procedures

Panchromatic IKONOS imagery was employed in this study for the detection of trees and subsequent estimation of stems per hectare, using local maxima filtering. The intent was not to further develop local maxima filtering, which has been well-researched in the past (Wulder et al., 2000; Wulder and White, 2004). We chose to rather focus on its application to even-aged, broadleaf *Eucalyptus* plantations, evaluate variations in algorithm inputs (window size determination), and apply local maxima filtering to high spatial resolution satellite imagery, as opposed to airborne data.

The only modification was introduced in the pre-processing stage of the imagery. Image pre-processing is a flexible stage where the user enhances the image data to maximize crown distinction from background cover types (Lillesand et al., 2004) and thereby optimizes the performance of local maximum filtering. The choice of enhancements depends on the imagery and requires some experimentation (Ju et al., 2005). We first smoothed the images using Gaussian smoothing for noise reduction. Secondly, image classification was applied using natural break classification. This was performed to determine the required threshold for cropping pixels of extreme bright and dark areas in the imagery, assumed to be background, and thus restrict the search for the local maxima. Finally, the locations of trees were extracted using two filtering window sizes. The first filtering window size was based upon the average semivariance range at each pixel. The second was based on the spacing between trees during the establishment phase of each plantation; this information is readily available from the MONDI-BP database, as it is the case for most well-managed plantations. The plantation compartments in the image were subdivided using voronoi polygon before semivariance calculation. A systematic framework of our approach is presented in Figure 7.2.

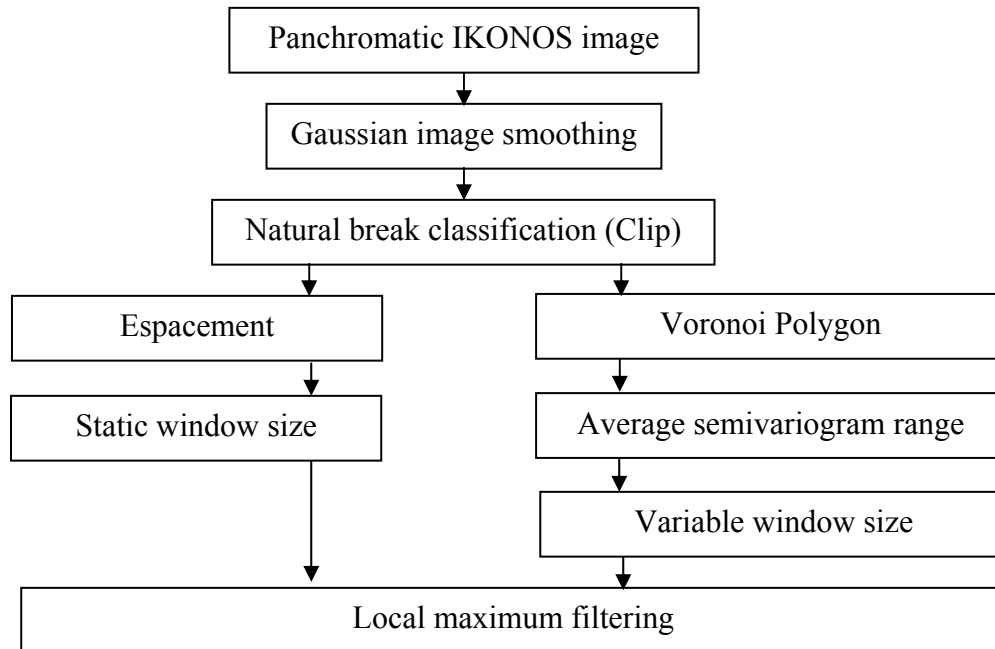


Figure 7.2 Diagram of the processing and analysis flow used in this study

7.2.4.1 Gaussian image smoothing

Image smoothing with two dimensional isotropic Gaussian kernels was applied to the panchromatic IKONOS imagery. The Gaussian smoothing filter results in a fuzzy image due to the removal of fine details and noise (Dralle and Rudemo, 1996). This filtering method uses a bell-shaped Gaussian distribution. Thus, the filter reduces the noise level in the image and also raises the radiometric values of the tree peaks, which theoretically results in reduced errors of commission (overestimation). Smoothing based on a Gaussian core is driven by two parameters, namely the standard deviation and window size (Pitkänen, 2001). In this study, standard deviation (δ) and window size were set to 1 and 3 x 3 pixels, respectively. The equation for Gaussian smoothing is:

$$G_{ij} = \frac{1}{2\pi\delta^2} e^{-\frac{i^2+j^2}{2\delta^2}} \dots\dots\dots\text{equation 1}$$

where i and j represent the distance in pixels between the centre of the core and a pixel in the 3 x 3 window, and δ is the standard deviation, which determines the form of Gaussian distribution.

7.2.4.2 Threshold definition

Major portions of the plantation stand images are comprised of tree crown, shadow, and bare soil (or under-storey vegetation). This leads to the natural break classification step that seeks to separate trees from their background. Therefore natural break classifications were used to define the threshold borderline between tree crowns and non-vegetation areas (such as shadows). This threshold was used to exclude non-tree pixels/values, or background, from the image.

Natural break classification uses an iterative algorithm to optimally assign data to classes, such that the variances within all classes are minimized, while the variances among classes are maximized. Accordingly, experimental tests were conducted on natural break classification using four, five, six, seven, and eight classes, with the intention of exploring the appropriate number of classes required to determine the threshold. This was followed by cropping the first and the last classes, which are assumed to be background (under-storey vegetation) and shadow reflection, for each experimental natural break classification test. Thus, the natural break method of classification helps to estimate a suitable “tree-no tree” threshold value.

7.2.4.3 Variable Window size

Voronoi polygons were first used to address the determination of variable window size within plantation stands for this study. Each plantation stand was divided into smaller polygon units using voronoi polygons. Semivariance was employed afterwards to determine the appropriate window size for each polygon. This approach was developed with the intention of capturing small variability within the forest stands. The window size computed using semivariance for each voronoi polygon is referred to as variable window size (VWS) in further discussions.

Semivariance is a well-known tool in geo-statistics and measures the spatial continuity of a feature over a range of space (Franklin et al., 1996; Johnston et al., 2001). For the purposes of remote sensing, Curran (1988) describes semivariance as the relationship between a pair of pixels found h pixels apart, recorded as the average squared difference

between all pixel pairs. The semivariogram (Equation 2) is a graphical representation of the average semivariance of several pixel pairs at each lag h and displays the spatial variability within the data set by capturing the variance between spatially separated pixels (Woodcock et al., 1988; Cohen et al., 1990; Wulder et al., 2000).

$$Y(h) = \frac{1}{2m} \sum_{i=1}^m [z(x_i) - z(x_i + h)]^2 \dots\dots\dots\text{equation 2}$$

where x_i is a data location, h is a vector of distance, $Z(x_i)$ is the data value of a specific attribute at location x_i , and m is the number of data pairs for a certain distance and direction of h units apart. A typical example of the semivariogram form is illustrated in Figure 7.3.

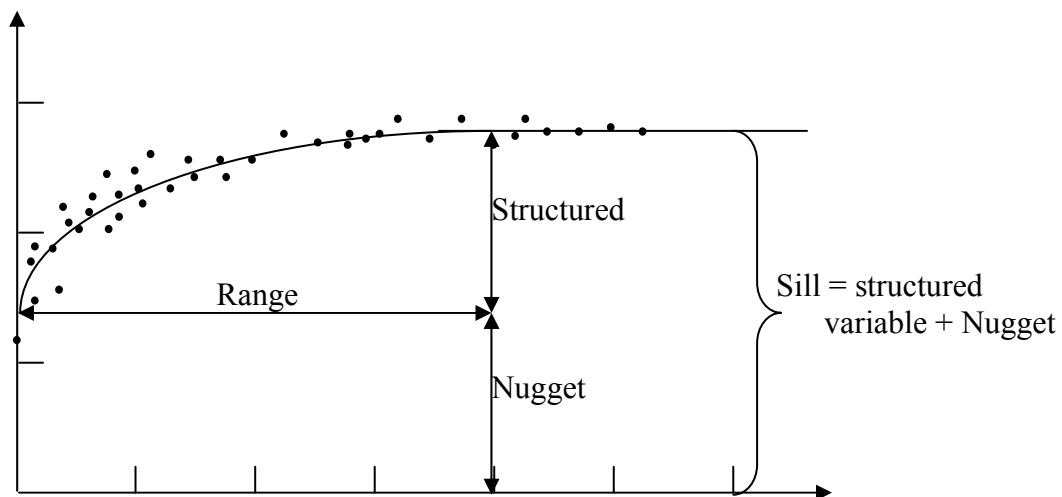


Figure 7.3 Illustration of a theoretical semivariogram diagram (Goovaert, 1997)

The *sill* is the plateau where the semivariogram levels off (slope = 0) and indicates the maximum variability between pixels. The *nugget* is the vertical discontinuity at the origin. Finally, the *range* is the distance at which the semivariogram reaches the sill, or at which two data points are uncorrelated.

We adopted the bounded semivariogram model with a maximum number of lags set to 100, or the maximum radius polygon in ArcGIS 9.1 (ESRI, 2007). The lag size was set to equal the employed image pixel size, i.e., 1 m. Curran and Atkinson (1998) stated that the reliability of semivariance $Y(h)$ degraded with increasing lag (h). Furthermore, in this

study, the effect of anisotropy was controlled by computing average omni-directional semivariance from the central pixel. Computing an average range value for each pixel in the image reduces problems that arise when attempting to select a representative single transect origin and angle (Wulder *et al.* 1998). The semivariance range values were then mapped to window size. Finally, local maxima filtering was carried out in ArcGIS 9.1 (ESRI 2007) using the average semivariance range to define the input window size parameter. A fixed window size (FWS) was also applied in this study using pre-determined spacing as an input window size parameter to the local maximum filtering algorithm.

7.2.6 Accuracy assessment of tree detection

Evaluation of classification-type approaches is typically based on aggregated assessment methods. These methods average the detected data and reference data within a given area for comparison (e.g., the number of trees detected per hectare). Accurate individual tree location results are preferred as more detailed information is provided for inventory and further analysis; however, this is difficult to achieve for a large study area. Aggregated estimates generally result in higher accuracies than individual estimates, as errors of omission and commission in tree detection tend to be averaged out during the aggregation process. Detection accuracy in this study was determined by comparing the field measured trees to those detected in the panchromatic IKONOS. Root mean square error (RMSE) and relative RMSE% were used for this purpose:

$$RMSE = \sqrt{\frac{1}{n} \sum (p_i - o_i)^2} \dots\dots\dots \text{equation 3}$$

$$RMSE\% = \frac{\sqrt{\frac{1}{n} \sum (p_i - o_i)^2}}{\bar{o}} \dots\dots\dots \text{equation 4}$$

where: n is the number of observations, p_i is the predicted value from tree detection method, o_i represents the observed values, and \bar{o} observed mean.

7.3 Results and Discussion

Natural break classification based on six classes was found to be most appropriate (Figure 7.4) during the classification assessment, even though underestimation occurred. Natural break classifications with fewer than six classes, i.e., four and five classes, were found to distinctly underestimate SPHA. The two opposite threshold values were close to the median of the histogram in these cases and resulted in a narrow range of values used for local maxima filtering. This in turn led to underestimation SPHA. On the other hand, natural break classification with more than six classes, i.e., seven and eight classes, resulted in overestimation of SPHA (Figure 7.4). In these cases, threshold values were close to the minimum and maximum values of the histogram. As a result, a wide range of values, including shadow pixel values, were computed for local maxima filtering.

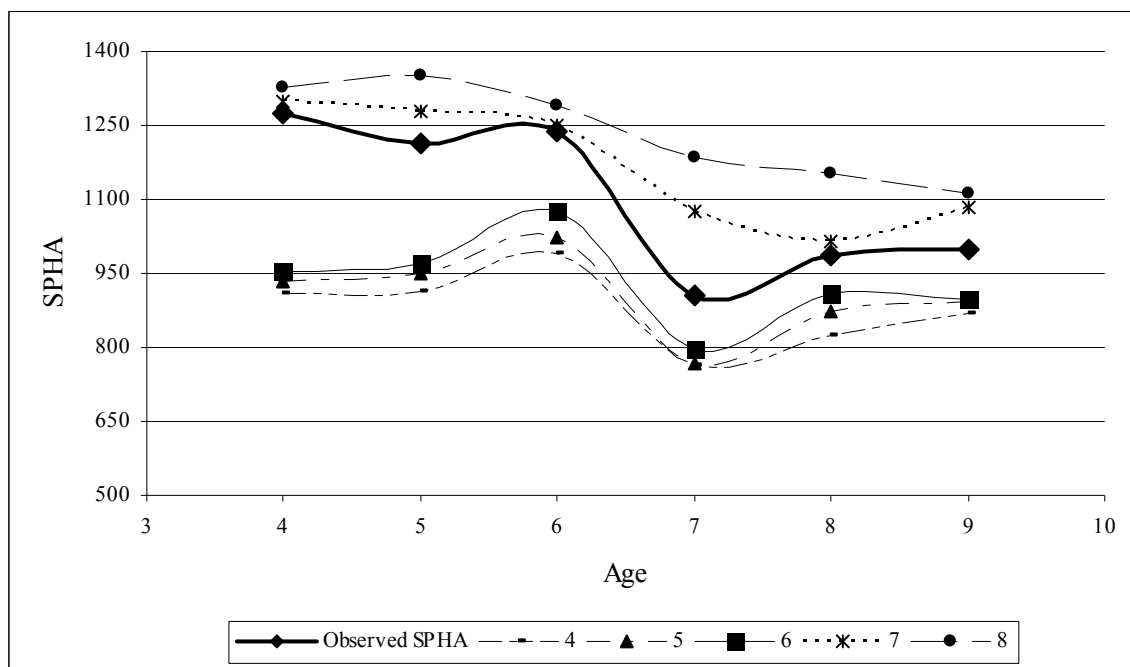


Figure 7.4 Estimated SPHA, as a function of forest stands age, at different numbers of classes for natural break classification

Results obtained from the resultant local maxima filtering, based on VWS and FWS, are summarized in Table 7.3. The accuracy of both approaches was higher for mature plantation stands as opposed to younger stands. For example, in the case of the VWS approach, the accuracy achieved for young plantation stands, defined as less than six

years old, was 75 %. This was in stark contrast to the observed 90 % accuracy achieved for mature plantation stands, defined as older than six years. The same trend was observed in the case of the FWS approach. The accuracy for the young plantation stands was 67 %, while the accuracy achieved for the mature stands was 88 %. This increase in accuracy with increasing stand age was attributed to increasing between crown gaps due to tree mortality, the result of competition for resources. This finding compared favourably with the previously published research by Wulder et al. (2000) and Pitkänen (2001). We therefore concluded that local maxima filtering methods were able to identify trees in low density forest stands (mature stands), due to the background being clearly distinguishable from the crown. This characteristic resulted in accurate estimations of SPHA using panchromatic IKONOS imagery, especially using the VWS in mature stands. This result is encouraging to the South African forest industry, since forestry inventories are usually conducted at age eight, or one year before harvesting.

Table 7.3 Results of SPHA estimation using VWS and FWS as inputs to local maxima filtering at different plantation stand ages

AGE (years)	Observed SPHA	VWS SPHA	FWS SPHA	Accuracy VWS (%)	Accuracy FWS (%)
4	1275	956	857	75	67
5	1214	972	827	80	68
6	1239	1074	1046	87	84
7	905	796	808	88	89
8	988	908	869	92	88
9	997	898	879	90	88

Plantation forest management requires that inventory errors are minimised, but still requires a choice between whether or not a small number of falsely identified trees (commission errors) or missed trees (omission errors) are allowable. We chose to optimise the filtering approach to minimise errors of commission. However, this resulted in many small trees not being identified, due to the chosen optimization strategy. Ultimately, both the VWS and FWS approaches exhibited underestimation throughout the plantation stands (Figure 7.5). The developed approach is based on the assumption

that, although both types of error are unwanted, the exclusion of a small number of relatively small trees impacted the calculation of per-hectare volume less than would the overestimation of tree numbers.

It is interesting to note from Figure 7.5, that the difference between observed and predicted stems per hectare, especially when using VWS, constantly decreased with the plantation stand age. We recommend that a correction factor is applied in such cases to achieve a 1:1 relationship between observed and predicted SPHA, which would be an interesting avenue for further research.

The underestimation of trees was attributed to a number of plantation growth dynamics. Tree gap size within a stand often reflects changes in stand age, where young stands typically have fewer gaps between trees and SPHA is equal to that at establishment of the stand. Young plantation stands are known to exhibit more homogeneous and smooth canopy surfaces and it is thus unreasonable to expect that a natural break classification and also a local maxima filtering technique from 1-meter spatial resolution would be able to accurately distinguish separate tree objects. We therefore concluded that 1 m spatial resolution panchromatic imagery is perhaps too coarse to accurately detect individual tree crowns of even-aged *Eucalyptus*-type species at young ages. The mature forest stands, with an observed accuracy level of 90%, appeared to have a more pronounced between-tree stand structure, which proved amenable to local maxima filtering based on high spatial resolution panchromatic space-borne imagery.

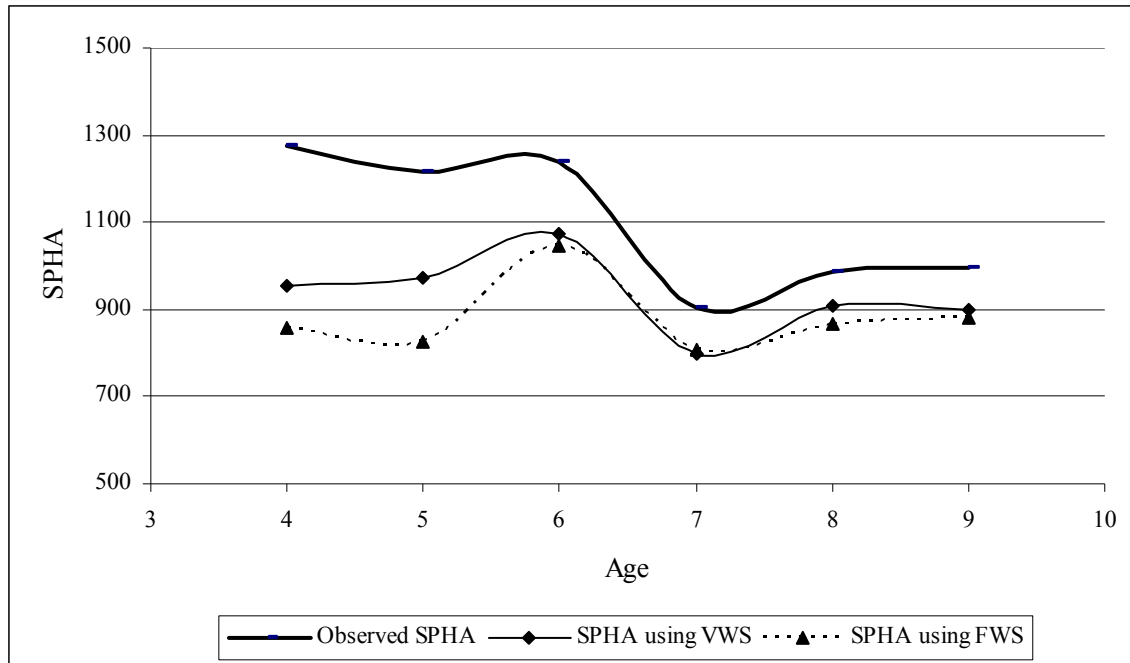


Figure 7.5 Estimated SPHA, as a function of forest stands age, using VWS and FWS window size inputs to local maxima filtering

Table 7.4 shows a summary of overall percentage accuracy results achieved using the VWS and FWS window size approaches for panchromatic IKONOS imagery. Estimation of SPHA based on the VWS approach exhibited a slightly higher accuracy of 85% (RMSE = 189 trees/ha; relative RMSE% = 17%) than that found for the FWS approach (accuracy = 80%; RMSE = 258 trees/ha; relative RMSE% = 23 %). We concluded that, overall, the adaptations to the local maxima filtering approach resulted in good accuracies for temperate-warm, even-aged, homogeneous *Eucalyptus* plantations. As comparison, Wulder and White (2004) reported an overall accuracy of 85% and an overestimation error of 51% for individual tree detection in plantation forest stands using IKONOS panchromatic imagery. These results imply that the method developed in this study could be used as a tool for SPHA estimation, especially in older pulpwood plantation stands, i.e., approximately one year before harvesting.

Table 7.4 Overall accuracies for SPHA estimation using local maxima filtering based on the VWS and FWS approaches to window size selection

	Accuracy (%)	RMSE	%RMSE
VWS	85	189	17
FWS	80	258	23

7.4 Conclusions

The methods used in this study for the estimation of SPHA constitute an amended and arguably improved approach to the complex issue of forest structural attribute estimation using satellite remote sensing imagery in plantation forestry. The approach, namely local maxima filtering based on window size determination from semivariance calculations, worked remarkably well for the detection of trees in “mature” pulpwood plantation stands. It performed slightly worse in younger plantation stands, which often have a denser, smoother canopy and resultant decrease in between-tree spectral separation.

The approach to individual tree detection consisted of first reducing noise and isolating the tree crowns from the background vegetation. This was achieved by using Gaussian smoothing and natural break classification, respectively. Secondly, the plantation stands were divided into smaller areas using voronoi polygons, prior to the application of variable window size computation within each forest stand. Finally, local maxima filtering was applied for the detection of tree peaks; the window size, required for the filtering process, was based on semivariance calculations (variable window size) and pre-determined tree spacing information (fixed window size). These approaches were tested on 1 m spatial resolution panchromatic satellite imagery.

This research has demonstrated that SPHA can be successfully estimated from panchromatic IKONOS imagery by applying the developed methodology. The level of success appeared to be dependent mainly on tree density, which is a function of plantation stand age. The between-tree spacing in young plantation stands result in limited to non-existent distinct spectral brightness valleys between trees in the panchromatic imagery. As such, the method proved to be more adept to SPHA estimation in mature plantation stands, which typically exhibit increased between-tree spacing due to

mortality and resource competition. The comparison between the VWS and FWS window size selection approaches showed that the VWS technique was superior to the FWS technique, with a reported RMSE difference of 69 trees/ha. The relative RMSE% difference was 6%, with VWS being superior at a relative RMSE% of 17%. The resultant ability of the VWS technique to produce superior tree density estimates was attributed to its aptitude to directly estimate the size of features within stands, rather than relying on a priori tree spacing information.

The main benefit of the proposed method is that estimation of SPHA would be more accurate and timely than that of conventional inventories, even being less precise. However, even though the reported relative RMSE percentages are marginally higher than acceptable values ($\pm 10\%$), these results bode well for the application of synoptic and accessible satellite imagery to forest inventory. In addition, a variety of additional management information could be synthesized from the developed approach, such as forest gap size and distribution. Variation in the image platform and spatial resolution, in addition to viewing angle and sun angle, are likely to limit the ability to achieve repeatable results in multi-temporal imagery. Thus, further research is recommended to test and extend the results of this study to a wider range of plantation forest environments.

7.5 Acknowledgements

This study was conducted as part of a remote sensing cooperative program between MONDI-BP South Africa, the Council for Scientific and Industrial Research (CSIR), and the University of KwaZulu-Natal to investigate the potential of satellite remote sensing imagery for the assessment of plantation forest structural attributes. The authors would like thank Wesley Roberts, Solomon Gebremariam, Thamsanqa Mzinyane, and Wesley Naidoo for their assistance during field work. The CSIR and MONDI-BP provided financial support for this study.

7.6 References

Boyd, D.S. and Danson, F.M., 2005, Satellite remote sensing of forest resources: Three decades of research development. *Progress in Physical Geography*, 29: 1-26.

Brandtberg, T. and Walter, F., 1998, Automated delineation of individual tree crowns in high spatial resolution aerial images by multiple-scale analysis. *Machine Vision Applications*, 11: 64-73.

Brandtberg, T., 2002, Individual tree-based species classification in high spatial resolution aerial images of forests using fuzzy sets. *Fuzzy Sets and Systems*, 132: 371 – 387.

Cohen, W., Spies, T. and Bradshaw, G., 1990, Semivariograms of digital imagery for analysis of conifer canopy structure. *Remote Sensing Environment*, 35: 167-178.

Culvenor, S. D., 2002, TIDA: an algorithm for the delineation of tree crowns in high spatial resolution remotely sensed imagery. *Computer and Geo-science*, 28: 33-44.

Curran, P., 1988, The semivariogram in remote sensing: an introduction. *Remote Sensing Environment*, 24: 493-507.

Curran, P. and Atkinson, P., 1998, Geostatistics and remote sensing. *Progress in Physical Geography*, 22: 61-78.

Dralle, K. and Rudemo, M., 1996, Stem number estimation by kernel smoothing of aerial photography. *Canadian Journal of Remote Sensing*, 26: 1228-1236.

Erikson, M. and Olofsson, K., 2005, Comparison of three individual tree crown detection methods. *Machine Vision and Applications*, 16: 1432 – 1769.

Esler, W. K., 2004, The Basics of Forest Mensuration. MONDI-SA document.

ESRI 2007, Using ArcMap™, Redlands: ESRI Press. 528 p.

Franklin, S.E., Wulder, M.A. and Lavigne, M.B., 1996, Automated derivation of geographic windows for use in remote sensing digital image texture analysis. *Computers and Geo-science*, 22: 665-673.

Goovaerts, P., 1997, *Geostatistics for Natural Resources Evaluation*. Oxford University Press, Oxford. pp. 483.

Gougeon, F., 1995, A crown following approach to the automatic delineation of individual tree crown in high spatial resolution aerial images. *Canadian Journal of remote Sensing*, 21: 274-284

Hyypä, J., Hyypä, H., Inkinen, M., Engdahl, M., Linko, S. and Zhu, Y., 2000, Accuracy comparison of various remote sensing data sources in the retrieval of forest stand attribute. *Forest Ecology and Management*, 128: 109-120.

Johnston, K., Verhoef, J., Krivoruchko, K. and Lucas N., 2001, *Using ArcGIS Geostatistical Analyst*, Environmental Systems Research Institute white paper, Redlands, CA, 2001.

Ju, J., Gopal, S. and Kolaczyk, E.D., 2005, On the choice of spatial and categorical scale in remote sensing land cover classification. *Remote Sensing of Environment*, 96: 62-77.

Korpela, I., Anttila, P. and Pitkänen, J., 2006, The performance of a local maxima method for detecting individual treetop in aerial photographs. *International Journal of Remote Sensing*, 27: 1159-1175.

Larsen, M. and Rudemo, M., 1998, Optimising templates for finding trees in aerial photographs. *Pattern Recognition Letters*, 19: 1153-1162.

Leckie, D, Gougeon, F., Walsworth, N. and Paradine, D., 2003, Stand delineation and composition estimation using semi-automated individual tree crown analysis. *Remote Sensing of Environment*, 85: 355-369.

Lillesand, T. M., Kiefer, R. W. and Chipman, J. W., 2004, Remote sensing and Image interpretation. (5th ed.), Wiley, New York, pp. 763.

Olofsson, K., Wallerman, J., Holmgren, J. and Olsson, H., 2006, Tree species discrimination using Z/I DMC imagery and template matching of single trees. *Scandinavian Journal of Forest Research*, 21: 106-110.

Persson, A., Holmgren, J. and Soderman, U., 2002, Detecting and measuring individual trees using an airborne laser scanner. *Photogrammetric Engineering and Remote Sensing*, 68: 925-932.

Pitkänen J., 2001, Individual tree detection in digital aerial images by combining locally adaptive binarization and local maxima methods. *Canada Journal of Forest Research*, 31: 832-844.

Pollock, R., 1999, Individual tree recognition based on a synthetic tree crown image model. In *Proceedings of the International Forum on Automated Interpretation of High Spatial Resolution Digital Imagery for Forestry*, Victoria, B.C., Canada, 10-12 February 1998, D. Hill and D. Leckie (Ed.) Pacific Forestry Centre, Canadian Forest Service, Natural Resources Canada, Victoria, B.C., pp. 25-34.

Pouliot, D.D., King, D.J., Bell, F.W. and Pitt, D.G., 2002, Automated tree crown detection and delineation in high-resolution digital camera imagery of coniferous forest regeneration. *Remote Sensing of Environment*, 82: 322–334.

Quackenbush, L. J., Hopkins, P. F. and Kinn, G. J., 2000, Developing forestry products from high resolution digital aerial imagery. *Photogrammetric Engineering and Remote Sensing*, 66: 1337– 1364.

Roberts, J.W., Gebreslasie, M.T., Tesfamichael, S., Van Aardt, J. N. and Ahmed, F.B., 2007, Forest Structural Assessment using Remote Sensing Technologies: An Overview of the current state of the art, *Southern Hemisphere Forestry Journal*, 69: 183-203.

Wang, L., Gong, P. and Biging, G. S., 2004, Individual tree crown delineation and treetop detection in high spatial resolution aerial imagery. *Photogrammetric Engineering and Remote Sensing*, 70: 351-357.

Woodcock, C., Strahler, A., and Jupp, D., 1988, The use of variograms in remote sensing: II. Real digital images. *Remote Sensing of Environment*, 25: 323 – 348.

Wulder, M., 1998, Optical remote sensing techniques for the assessment of forest inventory and biophysical parameters. *Progress in physical Geography*, 22: 449-476

Wulder, M.A., Niemann, K. O. and Goodenough, D.G., 2000, Local maximum filtering for the extraction of tree locations and basal area from high spatial resolution imagery. *Remote Sensing of Environment*, 73: 103-114.

Wulder, M.,A., Niemann, K.O. and Goodenough, D.G., 2002, Error reduction methods for local maximum filtering of high spatial resolution imagery for locating trees. *Canadian Journal of Remote Sensing*, 28: 621-628.

Wulder, M.A. and White, J.C., 2004, Comparison of airborne and satellite high spatial resolution data for the identification of individual trees with local maxima filtering. *International Journal of Remote Sensing*, 25: 2225-2232.

CHAPTER 8

Conclusions and Recommendations

This study examined the potential of optical remote sensing for estimating stems per hectare, diameter at breast height, tree height, basal area and volume of the even-aged *Eucalyptus* forests in the warm temperate climate of KwaZulu-Natal in South Africa. More specifically, the study focused on investigating the utility of medium spatial resolution, *viz* multispectral ASTER data for the estimation of forest structural attributes using empirical models. The study also focused on investigating the utility of high spatial resolution, *viz* multispectral and panchromatic IKONOS data for the estimation of forest structural attributes and individual tree detection. The study area were located in the warm temperate climatic zone in southern KwaZulu-Natal, South Africa.

The basic concepts and theory of relative atmospheric correction methods were discussed. The relative atmospheric correction methods, *viz* apparent reflectance model (AR), dark object subtraction model (DOS), and cosine approximation model (COST) were tested on both ASTER and IKONOS imagery. The qualitative and quantitative performances of these atmospheric correction methods were evaluated and summary results were presented. The DOS atmospheric correction method for ASTER and IKONOS imagery, within the given image and sensor parameters and for the given study area, performed relatively better than the AR and COST models. Thus it could be concluded that the image-based DOS model is better suited to atmospheric correction of ASTER and IKONOS imagery in the study area and for the purpose of forest structural assessment. It is encouraging to note that relatively simple, non-radiative transfer models could potentially be used to convert imagery to reflectance for the purposes of multi-temporal plantation forestry operations in the warm temperate climates of South Africa. It is furthermore recommended that future work could focus on the validation of the results presented here, using *in situ* measurements of surface reflectance at the time of image acquisition.

The utility of medium spatial resolution satellite imagery (ASTER) for assessment of plantation forest structural attributes *viz* stems per hectare, diameter at breast height, tree

height, basal area, and volume, was examined for the study area. The statistical relationships between plot-level field measurements of structural attributes and ASTER data were investigated using multiple linear and non-linear regression analyses as well as canonical correlation analysis. Single spectral bands and several vegetation indices were included in the analysis. Results in terms of coefficients of determination were as high as 0.64 for DBH and as low as 0.20 for volume, which indicated a need for the evaluation of high spatial resolution satellite imagery as applied to the same species and area. It could be concluded that medium spatial resolution satellite imagery on their own are not ideal for the prediction of forest structural attributes in even-aged *Eucalyptus* plantation forests as the models generally return operationally unacceptable ARMSE% values of greater than 10 %. However, one should consider that the addition of ancillary variables, *viz* age and site index, which can be accessed through forestry databases, could improve modelling abilities.

The investigations of high spatial resolution satellite imagery (multispectral and panchromatic IKONOS) for the prediction of forest structural attributes were conducted independently using their textural information. Image texture information is an important product of high resolution image analysis. Statistical texture features, *viz* grey level occurrence matrix (GLOM) and grey level co-occurrence matrix (GLOM), were extracted from the four bands of multispectral IKONOS imagery and from a panchromatic IKONOS band. Multiple linear regression and artificial neural network statistical approaches were employed to establish the relationships between field measured forest structural attributes and statistical texture features computed from the multispectral and panchromatic IKONOS imagery. The models developed using artificial neural network, which uses panchromatic IKONOS data as an input variable for the prediction of forest structural attributes returned promising results as compared to multispectral IKONOS data. This study demonstrated the potential of high spatial resolution panchromatic IKONOS imagery and artificial neural network statistical approach for the prediction of forest structural attributes in the warm temperate zones of South Africa. However, further research is required to document the performance of the

developed models under different environmental conditions as well as for other plantation forest species.

A new approach to local maxima filtering was also developed in this study for the estimation of stems per hectare in *Eucalyptus* plantation forests using panchromatic IKONOS satellite imagery. This approach was based on Gaussian smoothing for noise elimination and image classification. Natural break classification was used to determine the threshold at which to crop pixels of extreme bright and dark areas in the imagery (assumed background), to restrict the search for tree peaks. A semivariogram technique was applied to determine variable window sizes for local maxima filtering within a plantation stand. This study demonstrated that by applying this methodology, stems per hectare can be estimated with satisfactory accuracy. Variation in the sensor platform and spatial resolution, in addition to viewing angle and sun angle, are likely to limit the ability to achieve repeatable results in multi-temporal imagery. Thus, further experiments should be carried out to test and extend the results of this study to a wider range of plantation forest environments and conditions.

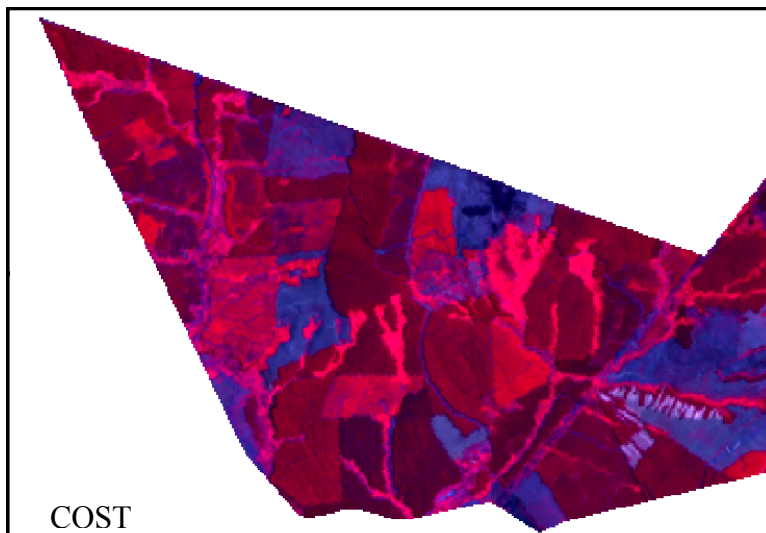
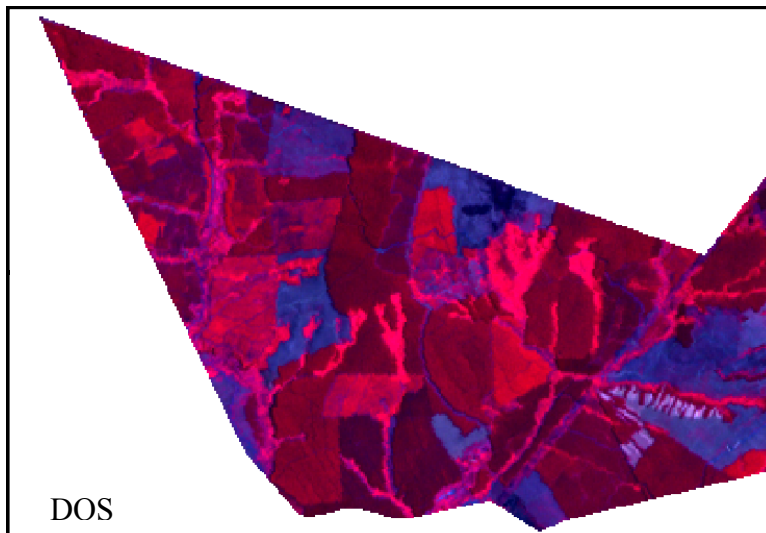
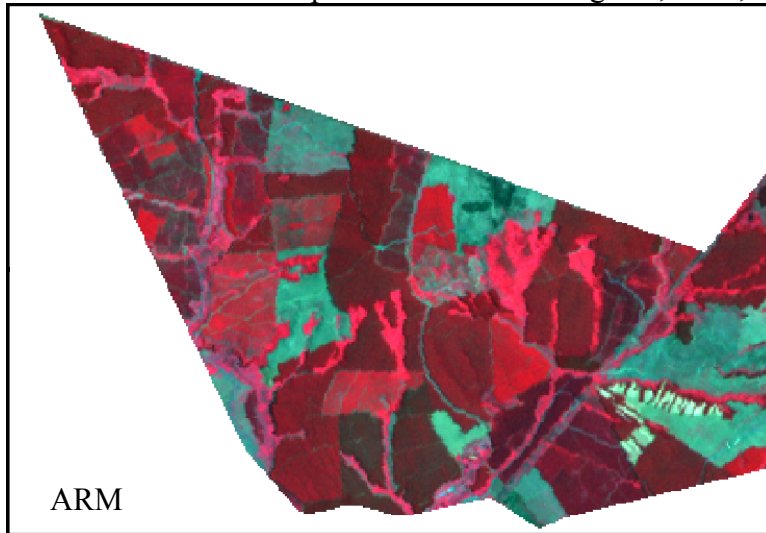
Appendix 2.1: Examples of medium resolution studies using passive optical remote sensing

Forest Type	Sensor	Variables	Methods	Results	Reference
Temperate Coniferous forests (Kansas, USA)	Landsat TM	Leaf Area Index	Adjusted R ² & Standard Error	R ² = 0.74 SEE = 0.04	Turner et al. (1999)
Boreal Forests: Spruce Pine & Aspen (Canada)	Landsat TM	Leaf Area Index	Simple ratio & bivariate regression analysis	R ² = 0.51 – 0.70	Brown et al. (2000)
Norway Spruce & Scots Pine (Sweden)	Landsat ETM+	Leaf Area Index	Correlation SR & NDVI	SR: R = 0.73; NDVI: R = 0.77	Eklundh et al. 2001
Long leaf pine, Turkey oak, Sand pine, Pond cypress, Black gum (Florida, USA)	Landsat TM	Leaf Area Index	Multiple regression ¹ & Artificial Neural Networks ²	R ² = 0.83 ¹ RMSE = 0.86 ¹ R ² = NA ² RMSE = 0.67 ²	Jensen & Binford (2004)
Boreal forest, Black spruce (North America)	Landsat ETM+	Leaf Area Index	Ordinary Least Squares Regression	R ² = 0.82 RMSE = 10.41	Cohen et al. (2003)
Pine & Broad-leaved species (Finl&)	Landsat TM	Timber Volume	<i>K</i> nearest neighbours (<i>k</i> -NN)	RMSE = 86.1 m ³ /ha	Mäkelä & Pekkariinen (2001)
Aspen, Birch, Spruce & Fir (Minnesota, USA)	Landsat TM	Timber Volume	<i>K</i> nearest neighbours (<i>k</i> -NN) with empirical bootstrapping	95 % confidence interval RMSE = 48,68 – 54,58 m ³ / ha	Franco-Lopez et al. (2001)
Lodgepole pine, white & black spruce, aspen, poplar (Alberta: Canada)	Landsat ETM+	Volume & biomass	Stand height & crown closure: inputs to BioSTRUCT model	Volume: RMSE = 4 m ³ /ha Biomass: RMSE = 4 t/ha	Hall et al. (2006)
Mixed Northern hardwood, Pine & Mixed Pine / Hardwood (Wisconsin, USA)	Landsat ETM+	Aboveground biomass	Multiple Regression	Hardwood R ² = 0.95 Pine R ² = 0.86 All R ² = 0.67	Zheng et al. (2004)
Tropical Forests (Borneo)	Landsat TM	Aboveground biomass	Artificial Neural Networks	R ² = 0.8	Foody et al. (2001)
Tropical Forests (Brazilian Amazon)	Landsat TM	Aboveground biomass	Stepwise Linear Regression Successional Forest (SF) Mature Forest (MF)	SF R ² = 0.755 MF R ² = 0.498	Lu (2005)
Conifer (Italy)	Multitemporal Landsat ETM+	Basal Area	<i>K</i> nearest neighbours (<i>k</i> -NN)	r = 0.588 RMSE = 4.02 m ² ha ⁻¹	Maselli et al. (2005)

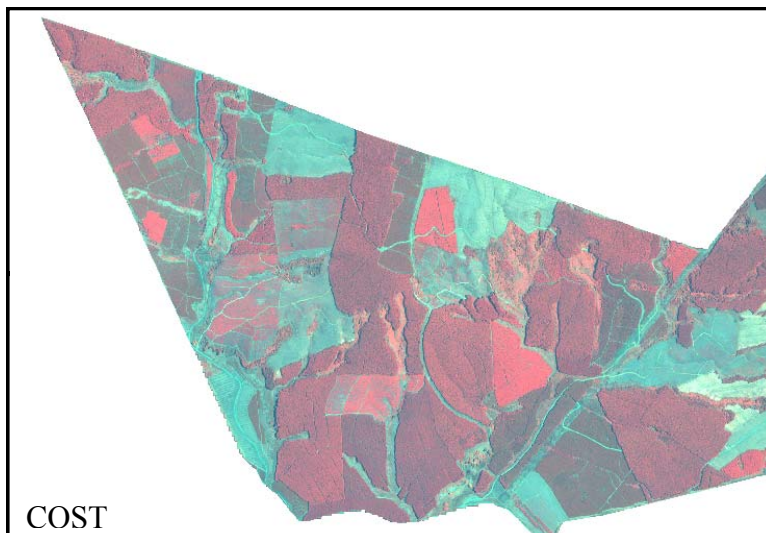
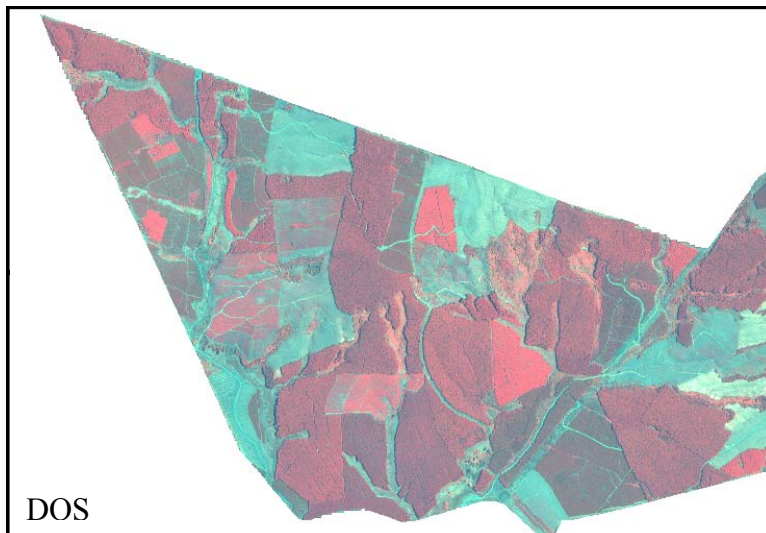
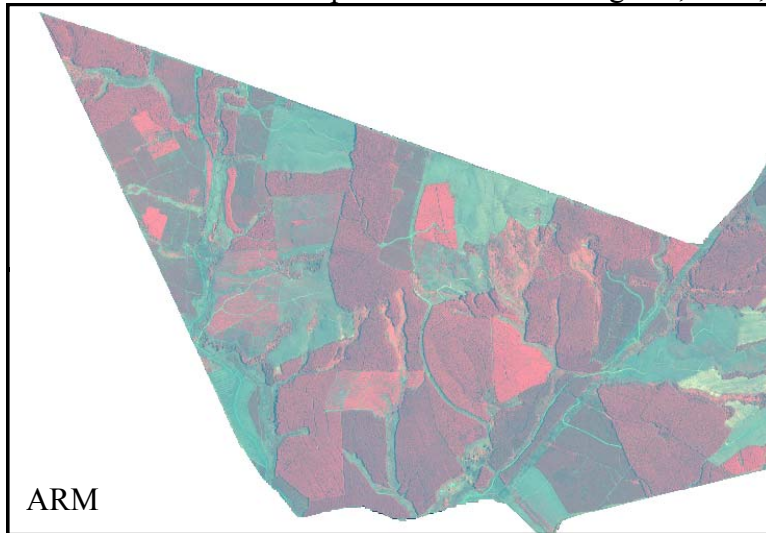
Appendix 2.2: Examples of high resolution studies using passive optical remote sensing

Forest Type	Sensor	Variables	Methods	Results	Reference
Douglas-fir (Canada)	IKONOS	Forest Age Class Separability	First- and second-order textural methods (variance and homogeneity)	Larger filters more effective at separating stands and second order texture values for age discrimination	Franklin et al. (2001)
Scots Pine, Norway Spruce, European Aspen, Grey Alder (Finland)	Compact Imaging System	Individual Tree Detection	Image smoothing and binarization	70 – 95% trees correctly identified	Pitkänen (2001)
Coniferous plantation (Vancouver, British Columbia)	MEIS-II	Individual Tree Detection	Local maximum filter	67% overall accuracy	Wulder et al. (2002)
Scots Pine, Norway Spruce, Birch and European Aspen (Sweden)	Kodak Aerochrome Infrared Film 2443	Individual Tree Crowns	Region growing supported by fuzzy rules	93% of stems correctly identified	Erikson (2003)
Coastal Coniferous Species (Canada)	CASI Imaging spectrometer	Individual Tree Crowns	Valley Following (Gougeon 1995) and Object Orientated ML classification	70 – 85% trees correctly identified Composition error = 13%	Leckie et al. (2003)
Mangroves (Panama)	IKONOS	Mangrove and Mangrove Species classification	Object- and Pixel-based classification	Pixel = 88.9% Object = 80.4% Combined = 91.4%	Wang et al. (2004)
Western Hemlock, Amabilis fir, and Western Redcedar (Canada)	CASI Imaging spectrometer	Automated Tree Recognition	Valley Following (Gougeon 1995) and Object Orientated ML classification	50 – 60% trees correctly identified Composition error = 20 – 60%	Leckie et al. (2005)
Even aged Spruce stands (Belgium)	IKONOS-2	Age, top height, crown diameter, stand density and basal area	Grey level co-occurrence matrix (Variance, contrast and correlation)	$R^2 = 0.76 - 0.82$	Kayitikare et al. (2006)

Appendix 4.1 ASTER data after atmospheric correction using AR, DOS, and COST



Appendix 4.2 IKONOS data after atmospheric correction using AR, DOS, and COST



Appendix 5.1 Correlation coefficients between plantation attributes and ASTER spectral information

	SPHA	DBH	MTH	BA	Vol.
Band-1	0.013	-0.067	0.026	-0.086	-0.085
Band-2	0.278	-0.201	-0.300	-0.346	-0.317
Band-3	0.208	0.198	0.261	0.311	0.202
Band-4	0.167	0.156	-0.074	-0.079	-0.075
Band-5	0.098	-0.108	-0.031	-0.056	-0.086
Band-6	0.044	-0.111	-0.091	-0.116	-0.118
Band-7	-0.034	0.053	0.064	0.055	0.071
Band-8	0.000	-0.158	-0.168	-0.202	-0.207
Band-9	-0.066	-0.122	-0.172	-0.227	-0.228
CCA-Bands	0.5417	0.4393	0.4931	0.4167	0.535
NDVI	0.381	0.308	0.322	0.362	0.377
MSAVI	0.381	0.084	0.315	0.339	0.350
PVI	0.334	-0.004	0.273	0.295	0.312
TSAVI	0.288	0.087	0.320	0.346	0.357
RSR	-0.078	0.223	0.168	0.171	0.173
PCA-1	0.001	-0.005	0.022	0.058	0.009
PCA-2	0.353	-0.025	0.227	0.285	0.298
PCA-3	-0.258	0.005	-0.246	-0.218	-0.247
CCA-VIs	0.4291	0.4887	0.4859	0.5454	0.4775
Log-T-Band-1	0.018	-0.086	-0.001	-0.102	-0.102
Log-T-Band-2	-0.070	-0.180	-0.206	-0.270	-0.303
Log- T-Band-3	0.306	0.053	0.307	0.317	0.321
Log- T-Band-4	0.183	-0.233	-0.117	-0.098	-0.100
Log- T-Band-5	0.119	-0.160	-0.108	-0.087	-0.131
Log- T-Band-6	0.061	-0.168	-0.166	-0.159	-0.165
Log- T-Band-7	-0.030	0.027	0.021	0.036	0.051
Log- T-Band-8	0.025	-0.240	-0.264	-0.266	-0.278
Log- T-Band-9	-0.059	-0.189	-0.271	-0.293	-0.302

Appendix 5.2 Correlation coefficients between plantation attributes and ASTER spectral information for young and mature plantation stands

	Young plantation stands (4-6 years)					Mature plantation stands (7-9 years)				
	SPHA	DBH	MTH	BA	Vol.	SPHA	DBH	MTH	BA	Vol.
Band-1	0.28	-0.28	0.10	-0.03	-0.02	-0.22	-0.01	-0.10	-0.25	-0.22
Band-2	0.65	0.55	0.48	0.39	0.49	0.59	0.43	0.32	0.43	0.42
Band-3	-0.62	-0.44	0.33	0.21	-0.25	-0.58	-0.42	-0.45	-0.32	-0.32
Band-4	0.27	-0.39	-0.06	-0.18	-0.20	0.10	-0.09	-0.48	0.06	0.02
Band-5	0.19	-0.14	0.12	0.04	0.03	0.05	-0.18	-0.29	-0.18	-0.24
Band-6	0.07	-0.07	0.09	-0.04	-0.03	0.14	-0.08	-0.11	0.03	-0.02
Band-7	-0.01	-0.11	-0.05	-0.16	-0.14	-0.03	0.12	0.09	0.21	0.17
Band-8	-0.02	-0.03	0.08	-0.08	-0.04	0.18	-0.24	-0.29	-0.16	-0.22
Band-9	-0.01	0.00	0.08	-0.03	0.00	-0.04	-0.10	-0.23	-0.20	-0.23
CCA-Bands	0.73*	0.70*	0.50**	0.52**	0.53**	0.39**	0.51**	0.60*	0.65*	0.66*
NDVI	0.55	-0.50	-0.42	-0.34	-0.40	-0.59	0.48	0.46	0.47	0.47
MSAVI	0.60	-0.54	-0.30	-0.42	-0.47	-0.56	0.36	0.41	0.39	0.39
PVI	0.66	-0.57	0.02	0.00	-0.06	0.00	0.17	0.30	0.37	0.39
TSAVI	-0.19	0.32	0.07	0.19	0.20	-0.10	0.12	0.12	-0.01	0.03
RSR	-0.09	0.23	0.07	0.18	0.18	-0.11	0.17	0.17	0.05	0.09
PCA-1	0.19	-0.37	-0.12	-0.12	-0.01	0.05	0.05	0.01	0.08	0.01

	Young plantation stands (4-6 years)					Mature plantation stands (7-9 years)				
	SPHA	DBH	MTH	BA	Vol.	SPHA	DBH	MTH	BA	Vol.
PCA-2	0.67	-0.60	-0.07	-0.02	-0.11	0.08	0.15	0.29	0.41	0.41
PCA-3	-0.59	0.57	0.03	0.06	0.10	0.01	-0.03	-0.13	-0.11	-0.16
CCA VI	0.75*	0.80*	0.60*	0.50**	0.57*	0.56*	0.51**	0.52**	0.50*	0.55**
Log-T Band1	0.29	-0.28	0.10	-0.03	-0.02	-0.22	-0.01	-0.09	-0.24	-0.22
Log-T Band2	-0.65	0.55	0.48	0.39	0.43	-0.51	-0.44	-0.32	-0.42	-0.43
Log-T Band3	0.61	-0.53	0.35	0.22	-0.33	-0.08	0.41	0.47	0.33	0.34
Log-T Band4	0.28	-0.40	-0.06	-0.18	-0.20	0.10	-0.10	-0.09	0.05	0.01
Log-T Band5	0.19	-0.14	0.13	0.04	0.04	0.05	-0.18	-0.30	-0.18	-0.24
Log-T Band6	0.05	-0.06	0.09	-0.05	-0.03	0.13	-0.08	-0.11	0.03	-0.02
Log-T Band7	-0.02	-0.10	-0.04	-0.15	-0.13	-0.04	0.13	0.10	0.21	0.17
Log-T Band8	-0.05	-0.01	0.08	-0.09	-0.05	0.17	-0.24	-0.30	-0.17	-0.23
Log-T Band9	-0.03	0.01	0.08	-0.04	0.00	-0.05	-0.09	-0.23	-0.20	-0.23
CCA-Log	0.73*	0.69*	0.51	0.52	0.53	0.39	0.53	0.61	0.64	0.66

* Correlation is significant at the 0.05 level

** Correlation is significant at the 0.01 level

Appendix 6.1 Description of the selected statistical texture features

Statistical Features	Formula		Description
	GLOM	GLCM	
Data Range	$\sum_k (k - \mu)^i p(k)$		The min-max of reflectance results
Mean	$1/2 \sum_{i=0}^{l-1} ip(i)$	$1/2 [\sum_i \sum_j i^* p(i-j) + j^* p(i,j)]$	Provides the mean of the grey levels in the window.
Variance	$\sum_{i=0}^{l-1} (i - \mu)^2 p(i)$	$\sum_i \sum_j (i - \mu)^2 p(i,j) + (j - \mu)^2 P(i,j)$	Information on how spread out the distribution of grey levels is. It is expected to be large if the grey levels of the image are spread out
Entropy	$-\sum_{k=0}^{l-1} p(i) \log_2(p(i))$	$-\sum_i \sum_j p(i,j) \log\{p(i,j)\}$	Measures the randomness of a grey level distribution. It is expected to be high if the grey levels are distributed randomly through the image
Correlation		$\frac{\sum_i \sum_j i^* jp(i,j) - \mu_i \mu_j}{\delta_i \delta_j}$	Measures the linear dependency of grey levels on those of neighbouring pixels in the GLCM
Contrast	$\sum_i i^2 P(i)$	$\sum_i \sum_j (i-j)^2 p(i,j)$	Measures the local contrast of an image. It is expected to be low if the grey levels of each pixel pair are similar
ASM	$\sum_{i=0}^{l-1} (p(i))^2$	$\sum_i \sum_j p(i,j)^2$	Measures the number of repeated pairs. It is expected to be high if the occurrence of repeated pixel pairs is high

where: k = number of gray tone values, μ = mean gray tone value, $p(i)$ is the i^{th} entry of the occurrence matrix, $p(i, j)$ is the $(i, j)^{\text{th}}$ entry of the normalized grey level co-occurrence matrix, $\mu_i = \sum_i \sum_j ip(i, j)$, $\mu_j = \sum_i \sum_j jp(i, j)$, $\delta_i^2 = \sum_i \sum_j (i - \mu_i)^2 p(i, j)$, and $\delta_j^2 = \sum_i \sum_j (i - \mu_j)^2 p(i, j)$